CFD SIMULATION OF SHELL AND TUBE HEAT EXCHANGER FILLED WITH PHASE CHANGE MATERIAL FOR SOLAR WATER HEATING SYSTEM

A Thesis Submitted
in Partial Fulfillment of the Requirements
for the Award of Degree of

DOCTOR OF PHILOSOPHY

by

SACHIN RANA

(2K18/PHDME/14)

Under the Supervision of

Dr. Mohammad Zunaid
(Assistant Professor, DTU)

Dr. Rajesh Kumar
(Professor, DTU)

Department of Mechanical Engineering
DELHI TECHNOLOGICAL UNIVERSITY
(Formerly Delhi College of Engineering)
Shahbad Daulatpur, Main Bawana Road, Delhi-110042. India
July, 2023

CANDIDATE'S DECLARATION

I hereby declare that the research work presented in this thesis entitled **"CFD Simulation of Shell and Tube Heat Exchanger Filled with Phase Change Material for Solar Water Heating System"** is original and carried out by me under the supervision of Dr. Mohammad Zunaid, Assistant Professor and Dr. Rajesh Kumar, Professor, Department of Mechanical Engineering, Delhi Technological University, Delhi, and being submitted for the award of Ph.D. degree to Delhi Technological University, Delhi, India. The content of this work has not been submitted either in part or whole to any other university or institute for the award of any degree or diploma.

SACHIN RANA

(2K18/PHDME/14)

CERTIFICATE

This is to certify that the thesis entitled **"CFD Simulation of Shell and Tube Heat Exchanger Filled with Phase Change Material for Solar Water Heating System"** being submitted by **Sachin Rana (2K18/PhD/ME/14)** to the Delhi Technological University, Delhi for the award of the degree of **Doctor of Philosophy** is a bonafide record of original research work carried out by him. He has worked under our guidance and supervision and has fulfilled the requirements for the submission of the thesis, which has reached the requisite standard. The results contained in this work have not been submitted, in part or full, to any other university or institute for the award of any degree or diploma.

24/07/2023

Dr. MOHAMMAD ZUNAID
SUPERVISOR,
Assistant Professor,
Department of Mechanical Engineering,
Delhi Technological University,
Delhi-110042,
INDIA.

24/07/2023

Dr. RAJESH KUMAR
CO-SUPERVISOR,
Professor,
Department of Mechanical Engineering,
Delhi Technological University,
Delhi-110042,
INDIA.

ACKNOWLEDGEMENTS

I want to express my gratitude to my supervisors Dr. Mohammad Zunaid and Dr. Rajesh Kumar for their valuable guidance, support, and encouragement throughout my Ph.D. program. This work could not have attained its present form without their supervision, direction, and interest in the research work. I express my gratitude to Prof. S. K. Garg, DRC Chairman and Head of Department of Mechanical Engineering for providing valuable comments and suggestions as well as giving me the opportunity to do research in the department of mechanical engineering. I am thankful to all faculty and staff members of the Mechanical, Production & Industrial, and Automobile Engineering Department for their continued valuable support. I appreciate reviewers of research papers and industry people for sparing their valuable time and constructive comments.

I wish to thank my parents, brother, sister, family members, and friends whose blessings made this work reality. I sincerely thank my wife Reetika Chauhan for her patience, support, and loving participation in accomplishing this research work. I would like to acknowledge Dr. Ashwani Kumar & Dr. Sanjeev Kumar, my friends, for their support and guidance. At last, I am thankful to God for giving me the mental and physical strength to work sincerely, diligently, and honestly.

SACHIN RANA

(2K18/PHDME/14)

ABSTRACT

Solar energy, the most promising source of energy, requires thermal energy storage (TES) due to its intermittent nature. Storage of thermal energy can take the form of sensible heat storage (SHS), latent heat storage (LHS), and thermo-chemical storage (TCS). The amount of energy that is stored in SHS depends on the specific heat of the substance, the change in temperature, and the mass of the storage material since heat energy is retained by raising the temperature of the storage material without going through a phase transition. However, LHS involves a phase transition, when heated to the constant temperature, between solid-liquid, solid-solid, and liquid-gas states and vice versa. Solid-solid phase transitions require a lower energy storage capacity than liquid-gas phase transitions which require a large increase in volume. As a result, the solid-liquid transformation is most commonly used in LHS applications because it is more efficient than other transformations.

In this study, the methods of enhancing the heat transmission in a latent heat thermal energy storage (LHTES) system with a heat exchanger of shell & tube type having a phase change material (PCM) in shell region, known as PCM heat exchanger (PCMHE), and carrying a number of tubes of circular, elliptical and square shape, to flow of a heat transfer fluid (HTF) using a two-dimension (2D) computational fluid dynamics (CFD) model has been presented. Enhancement of heat transfer in the LHTES system may be obtained either by using a suitable geometric configuration of PCMHE and/or by increasing the thermal conductivity of PCM. Heat transfer enhancements in LHTES systems can be achieved by using extended surfaces like fins and heat pipes. To enhance the heat transmission between tubes and PCM, a number of rectangular fins are attached to the outer surface of the circular, elliptical, and square tubes of the PCMHE.

Geometrical modeling of PCMHE of shell and tube type, in which a solid Gallium as a PCM is filled in the outer shell and an HTF is flowing inside tubes, has been done in Solid Works. In this

work, the outer shell of PCMHE is selected in two different shapes: square and circular. The tubes inside the outer shell of PCMHE are also selected in different shapes i.e. circular, square, and elliptical as well as in different configurations i.e. with and without fins. All the geometries of PCMHE modeled in Solid Works saves in IGES format and transported in the Ansys Fluent to convert them into finite element models by mesh generation of the geometries. Unstructured triangular elements are used for the mesh generation of all the geometries of PCMHE.

After the mesh generation is completed, the meshed model is transferred to the Ansys Fluent setup and solution mode. In the setup mode of Ansys Fluent, further operations like solver type, time dependency, gravitational acceleration, material properties, boundary conditions, etc. are selected and then the solution is executed. 2D CFD numerical investigation of heat transfer & melting of PCM in different geometries of PCMHE has been performed. After the execution of the solution of all geometries of PCMHE has been completed, viewing and postprocessing of the results are performed.

CFD investigations of heat exchanger geometries have been performed at different temperatures for liquid fraction and mean temperature of PCM as well as melting time and time for attainment of applied temperature. Results show that enhancement of heat transfer and reduction in melting time take place by employing a number of fins on tubes of PCMHE. It has also been concluded by comparing the different geometries of PCMHE that the configuration having the similar shape of shell and tubes (both shell and tubes are either square or circular) has the maximum heat transfer rate and lowest melting time compared to other geometries of PCMHE. Based on the available simulation data, the findings are validated and show good agreement, which suggests a deviation of 3.8 & 4.1 percent.

TABLE OF CONTENTS

LIST OF FIGURES

LIST OF TABLES

NOMENCLATURE

TES	Thermal Energy Storage
SHS	Sensible Heat Storage
LHS	Latent Heat Storage
TCS	Thermo-Chemical Storage
PCM	Phase Change Material
TCM	Thermo-Chemical Material
TEG	Thermo Electric Generator
TTEG	Two-stage Thermo Electric Generator
PW	Paraffin Wax
PA	Palmitic Acids
DSC	Differential Scanning Calorimetry
CAD	Computer-Aided Design
CAE	Computer-Aided Engineering
CFD	Computational Fluid Dynamics
FEM	Finite Element Model
FEA	Finite Element Analysis
LHTES	Latent Heat Thermal Energy Storage
PCMHE	Phase Change Material Heat Exchanger
STHE	Shell and Tube Heat Exchanger
HTF	Heat Transfer Fluid
STM	Source Term Method
EM	Enthalpy Method
TTM	Temperature Transforming Method
SOM	Switch-Off Method
VVM	Variable Viscosity Method
RSOM	Ramped Switch-Off Method
RSTM	Ramped Source Term Method

LIST OF SYMBOLS

Symbol	Title	Unit
Q	Heat Transfer	J
m	Mass	Kg
c_p	Specific Heat	J/kg-K
T	Temperature	K
h_L	Phase Change Enthalpy	J/kg
h_S	Sensible Enthalpy	J/kg
h_{ref}	Reference Enthalpy	J/kg
t	Time	s
LH_F	Latent Heat of Fusion	J/kg
LH_V	Latent Heat of Vaporization	J/kg
c_{ps}	Specific Heat of Solid	J/kg-K
c_{pl}	Specific Heat of Liquid	J/kg-K
c_{pv}	Specific Heat of Vapour	J/kg-K
$\vec{\mathrm{g}}$	Acceleration due to Gravity	m/s^2
k	Thermal Conductivity	W/m-K
T_S	Solidus Temperature	K
T_L	Liquidus Temperature	K
T_{ref}	Reference Temperature	K
ΔT	Difference in Temperature	K
x	Liquid Fraction	-
P	Static Pressure	Pa
$\vec{V}$	Velocity Vector	m/s
$\overrightarrow{V_p}$	Pull Velocity	m/s
S	Momentum Sink Term	-
C_{mush}	Mushy Zone Constant	-

GREEK SYMBOLS

ρ	Density	kg/m^3
β	Thermal Expansion Coefficient	/K
μ	Dynamic Viscosity	kg/m-s
ν	Kinematic Viscosity	m^2/s
τ	Viscous Stress Tensor	Pa

CHAPTER 1: INTRODUCTION AND STATEMENT OF PROBLEM

1 Introduction

Energy is an essential element required for the existence of human life on earth and plays a vital role in the development of human life. The sudden increase in global energy consumption is a result of the rapid expansion of the global economy. As the world is suffering from energy crises, the growth of civilization has largely depended on human efforts to efficiently produce, store, and convert energy into the desired form. The reasons for the energy crisis are a continuous increase in demand, population growth, and the upgradation of living standards. The major energy resources include fossil fuel-based energy sources; however, these are limited, and additionally, their increased usage is adversely affecting the ecology due to the emission of harmful gasses. It became difficult to fulfill the requirement of energy with conventional recourses as there is a scarcity in the availability of fossil fuel and increasing greenhouse-gas emissions. Thus, it is necessary to utilize various forms of natural or renewable resources [1]. Researchers over the world are working hard to overcome this situation by focusing on natural and renewable resources of energy through scientific experiments.

For steady and sure development and progress of any country, it is necessary to develop alternative resources of energy. To fulfill the increasing energy demand, renewable energy is one of the best options. There are a number of renewable energy resources, out of which solar energy is the most important form of thermal energy. Energy received by the earth from the sun is many thousand times larger than the present consumption rate of all commercial energy sources. This makes it the most promising source of energy. Fortunately, India is blessed with abundant solar radiation available almost throughout the year. In recent years, the Indian government has taken a keen interest in the solar energy sector and is continuously investing huge amounts in the utilization of solar energy [2].

Currently, when researchers around the world, are looking for solar energy to use as an alternative to fossil fuel to fulfill the energy demand, the main challenge is the continuous supply of solar energy. Solar energy though, simple to utilize, non-polluting and everlasting, is time-dependent and has intermittent character. As the availability of solar energy at night is the main challenge, one of the complementary tasks for the researchers is to develop and utilize advanced thermal energy storage (TES) systems i.e. to store solar energy in suitable forms that can be efficiently converted into the required form. TES systems, which utilize heat available from solar and other energy sources, have become one of the essential components for increasing efficiency and environmental friendliness of energy consumption in order to reduce dependence on fossil fuels. TES systems not only reduce the gap between energy supply and demand but also upsurges the performance and reliability of the systems, and contribute to energy conservation [3]. The fundamental idea of a TES system is to support energy management by storing thermal energy at periods when it is abundantly available and using it when and where it is required as shown in Figure 1.1.

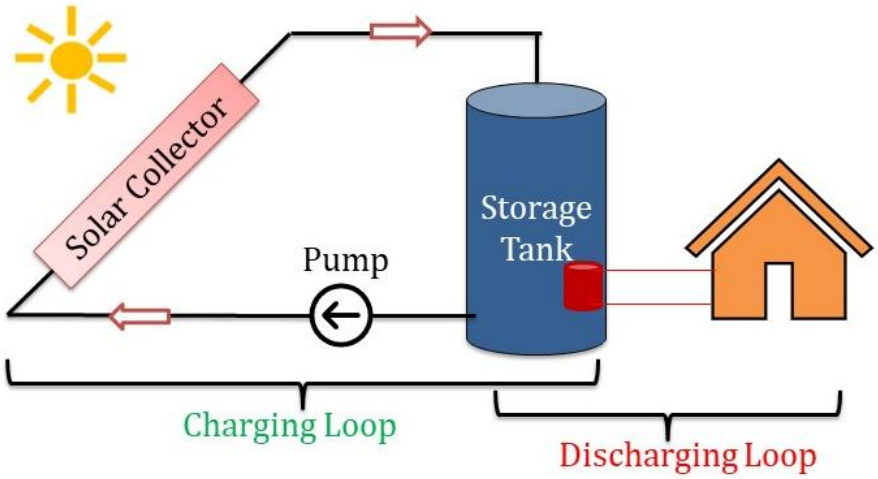

Fig 1.1 Thermal Energy Storage Cycle

Energy is transported to a TES system so that it may be utilized later. This process includes three stages: charging, storage, & discharging, creating the full storage cycle (Figure 1.2). Storage

medium with a high energy density (storage capacity), excellent transfer of thermal energy between the storage material and the HTF, the storage material's mechanical and chemical stability, compatibility between the storage substance and the material of the container, full reversibility of several cycles, minimal thermal losses throughout the duration of storage, and simplicity of control are the primary requirements for the development of a TES system.

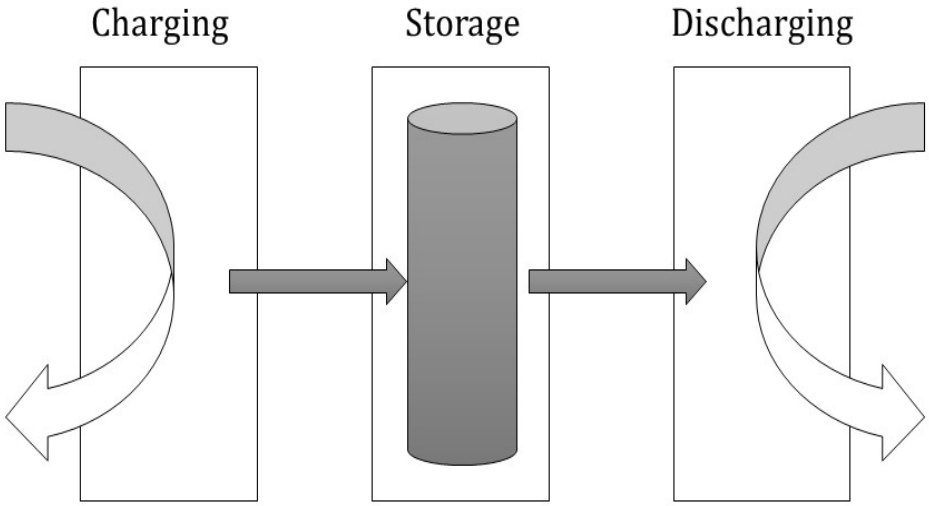

Fig 1.2 Charging & discharging in TES

1.1 Classification of Thermal Energy Storage

Sensible heat storage (SHS), latent heat storage (LHS), & thermo-chemical storage (TCS) are the three different categories of TES technologies. Table 1.1 [4] presents the three forms of the TES system's capabilities for the purpose of comparison.

Table 1.1 Comparison of the storage capacity of various storage technologies

Type of Storage Technology	**Material**	**Energy Stored (kJ/kg)**	**Temperature Range**
Sensible Heat	Granite	17	$\Delta T = 20^o C$
	Water	84	$\Delta T = 20^o C$
Latent Heat	Water	330	$T_{melting} = 0^o C$

	Paraffin Salt hydrates Salt	200 200 300-700	$T_{melting} = 5 - 130^{o}C$ $T_{melting} = 5 - 130^{o}C$ $T_{melting} = 300 - 800^{o}C$
Chemical Reactions	H_2 Gas (Oxidation) H_2 Gas (Oxidation) H_2 *Liquid* (Oxidation) Gasoline	120000 120000 120000 43200	300 K, 1 bar 300 K, 200 bar 20 K, 1 bar -

1.1.1 Sensible Heat Storage

The quantity of energy stored in SHS is a function of the mass and specific heat of the storage material in addition to the change in temperature since thermal energy is stored by raising the temperature of the storage material without going through phase transition as shown in Figure 1.3. Water, air, oil, bedrock, brick, concrete, and other materials can all be used as storage materials in SHS. While each material has its own benefits and drawbacks, they are often chosen based on their heat capacity and the storage space that is available [5]. TES materials for the SHS won't go through a phase transition procedure. The only procedure that the materials have ever gone through is a temperature change during a single phase.

The basic equation for the SHS is:

$$Q = \int_{T_1}^{T_2} m.c_p.dT \quad (1)$$

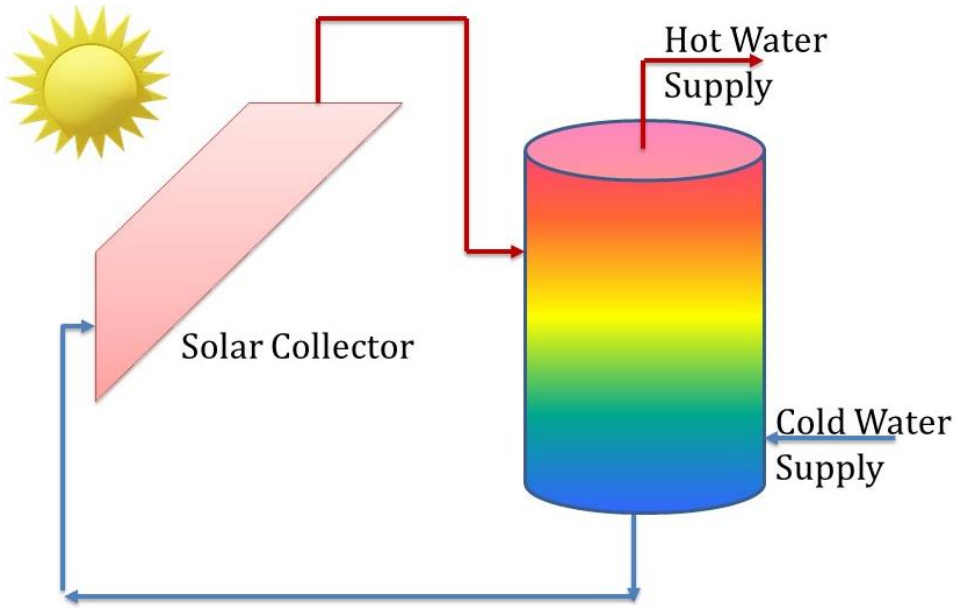

Fig 1.3 Sensible heat storage

Where Q denotes the amount of heat retained by the substance (kJ), m denotes the mas of storage substance (kg), c_p denotes the specific heat of the substance (kJ/kg-K), T_1 and T_2 are initial and final temperature (K). Since c_p depends on temperature, to get the total quantity of thermal energy stored, we may utilize equation (1). In order to account for the variation of c_p, equation (1) might be written as though the temperature range is very small.

$$Q = m.c_{p(avg)}.(T_2 - T_1) \qquad (2)$$

where the average specific heat between temperature T_1 and T_2 is represented by $c_{p(avg)}$ [6].

Based on equations (1) & (2), a large specific heat capacity c_p, may significantly impact the amount of thermal energy retained. To be employed as storage material in SHS, materials must have a large thermal capacity, be widely available, and be inexpensive [7]. After many thermal cycles, the heat storage material will not degrade much because of its long-term stability. Density, specific heat, thermal conductivity and diffusivity, vapor pressure, compatibility with container materials, and chemical stability are the factors considered when choosing an

appropriate material [8]. It is possible to store sensible heat in solid or liquid media (air storage systems are bulkier but can also be used).

Compared to LHS or TCS methods, SHS technology is easy to design. SHS can't transport or retain energy at a constant temperature and are bigger in size, which is a disadvantage. One of the main factors affecting the cost of the storage system is the compatibility with its containment, which is required for both the heat storage material and the confinement. The characteristics of the storage medium have a significant influence on the price of the SHS solution. As storage media, people typically employ water, stones, sand, and other affordable materials. Table 1.2 lists some typical components for sensible heat TES systems [5].

Table 1.2 Materials used in sensible heat storage

S. N.	Materials	Density (kg/m^3)	Specific Heat (J/kg.K)
1	Clay	1458	879
2	Brick	1800	837
3	Sandstone	2200	712
4	Wood	700	2390
5	Concrete	2000	880
6	Glass	2710	837
7	Aluminium	2710	896
8	Iron	7900	452
9	Steel	7840	465
10	Water	988	4182

1.1.2 Latent Heat Storage

The phase transition of a substance at a fixed temperature is used by the LHS system. It is based on the basic principle that when heat is applied to a substance, it changes its phase from solid to liquid and stores thermal energy as latent heat of fusion. If heat is applied to a liquid, it transforms into a vapor and stores the thermal energy as latent heat of vaporization. A solid-to-

liquid phase transformation is usually achieved by melting & solidifying a material. Liquid to vapor phase transition involves high pressure and a significant volume rise and solid to solid phase change is very slow and has very low energy density. So LHS of solid-to-liquid phase change is the only practical method of storing thermal energy. In solid to liquid phase transition, when a substance melts, heat is transmitted to it, keeping a significant amount of heat at a constant temperature, and released when the material solidifies (Figure 1.4).

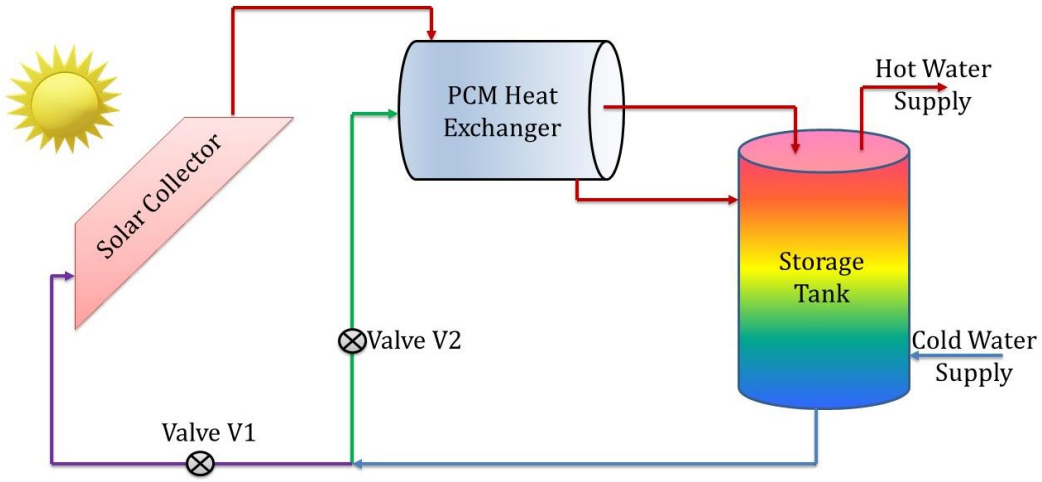

Fig 1.4 Latent heat storage

The quantity of heat stored is calculated following:

$$Q = m.h_L \tag{3}$$

where Q denotes the heat contained in the substance (in kJ), m is the mass of the substance (in kg), and h_L is the enthalpy of phase transition (in kJ/kg).

The materials used for LHS during phase transition are referred to as phase change materials (PCM). Numerous materials are investigated for PCM, but only a few numbers have found commercial success [1,3,8], primarily because issues including phase separation, subcooling, corrosion, long-term stability, and less thermal conductivity still need to be fully resolved. PCM is usually chosen based on their melting enthalpy, melting temperature, availability, and cost.

Table 1.3 [5] demonstrates the common range of melting enthalpy and melting temperature for the several types of materials utilized as PCM.

Table 1.3 Materials used in LHS systems

S.N.	Material	Melting Temperature (^{o}C)	Melting Enthalpy (kJ/kg)
1	Water	0	330
2	Water-Salt Solution	-100 – 0	200 – 300
3	Paraffin	-20 – 100	150 – 250
4	Salt Hydrates	-20 – 80	200 – 600
5	Sugar Alcohols	20 – 450	200 – 450
6	Nitrates	120 – 300	200 – 700
7	Hydroxides	150 – 400	500 – 700
8	Chlorides	350 – 750	550 – 800
9	Carbonates	400 – 800	600 – 1000
10	Fluorides	700– 900	> 1000

In the past few years, LHS techniques for solar heating and air cooling have attracted a wide variety of interest due to their ability to store enormous energy when a phase transformation occurs at a fixed temperature. The significant amount of heat that must be absorbed or released when a material transforms its phase into liquid from a solid, or vice versa, is called the latent heat of melting [9]. PCMs can be selected so that their phase change temperature optimizes the thermal gradient based on the substance with which heat is being transferred.

Figure 1.5 illustrates the rise in internal energy when heat energy is applied to a material. Temperature rises (sensible heating) or phase changes (latent heating) are the most common

consequences. When heat is supplied to a material in the solid state at point O, the solid is first sensibly heated (zone O-A) followed by a solid-to-liquid phase transformation (zone A-B), then the liquid is sensibly heated (zone B-C), then liquid changes into vapor phase (zone C-D), and finally the vapor is sensibly heated (region D-E).

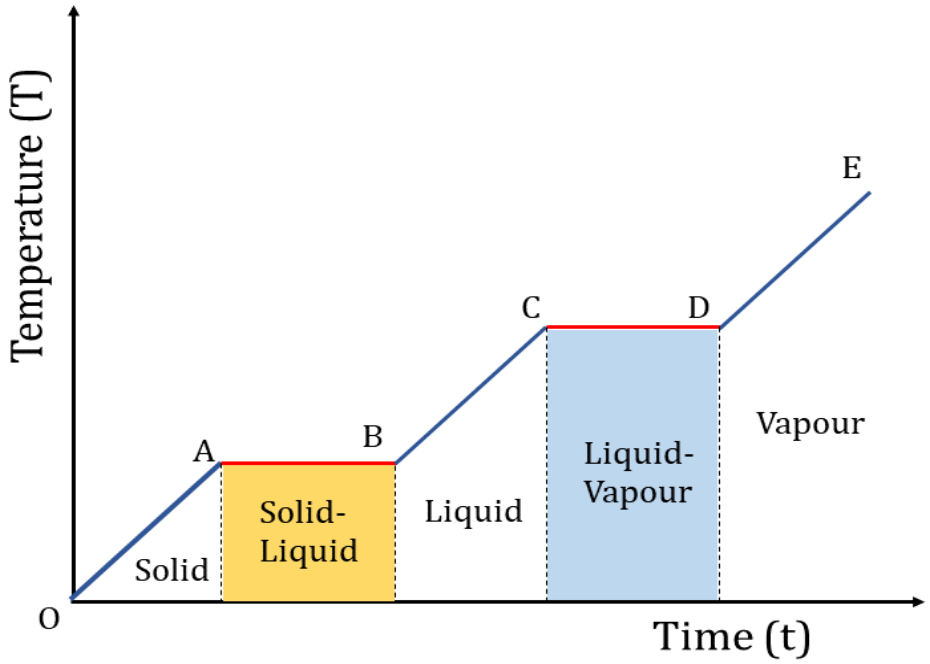

Fig 1.5 Time-Temperature diagram for heating of a storage material

The amount of heat may be expressed as follows [10]:

$$Q = m.\left[\int_{T_O}^{T_A} c_{ps}.dT + LH_F + \int_{T_B}^{T_C} c_{pl}.dT + LH_V + \int_{T_D}^{T_E} c_{pv}.dT\right] \quad (4)$$

Where c_{ps}, c_{pl}, and c_{pv} are the specific heats of the material in solid, liquid, and vapor phases, LH_F denotes the latent heat of fusion, LH_V is the latent heat of vaporization and T is the Temperature at corresponding points.

1.1.3 Thermo-Chemical Storage

When a chemical process with a lot of energy involved is employed to store energy, thermochemical heat is created as shown in Figure 1.6. When the reverse reaction occurs, the

reaction's byproducts must be able to be retained, and any heat that was independently stored during the reaction must be retrievable [5]. Therefore, this storing mechanism can only be employed with reversible reactions.

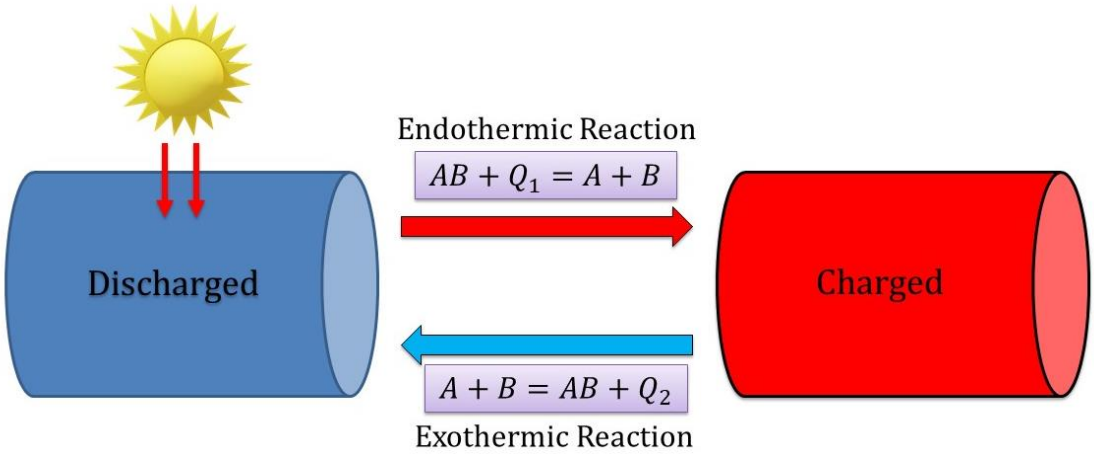

Fig 1.6 Thermo-chemical heat storage

The basic principle of the TCS has been shown in the following equations:

- Endothermic reaction:

$$AB + Q_1 = A + B \tag{5}$$

- Exothermic reaction:

$$A + B = AB + Q_2 \tag{6}$$

The compound "AB" absorbs some thermal energy during the endothermic reaction, or charging process, at significantly higher temperature circumstances, breaking down into the products of "A" and "B". In contrast, the products of "A" and "B" undergo a combination reaction during the exothermic reaction, or the discharge process, creating the compound "AB" while releasing a certain amount of thermal energy.

Results "A" and "B" should be gathered separately in order to prevent a simultaneous reverse reaction during the charging procedure. Therefore, the corresponding reversible reaction will be more practical for the implementation of TCS, if "A" and "B" are in different phases, such as one

is gas and the other is in solid phase. The stable storage of the reactants is ensured by the well-defined separation of resultants "A" and "B," which is a crucial aspect of long-term thermal energy storage.

TCS is separated into sorption systems and chemical processes. High TES density and reversibility are needed in the substances for chemical reactions. The performance efficiency of chemical energy conversion is often higher than that of physical approaches for energy storage (SHS and LHS). Finding the right reversible chemical reaction for the TES being used is the biggest challenge [11].

Thermochemical processes, whose enthalpy is in the high range, are employed as Thermo Chemical Material (TCM) at high temperatures (greater than 400°C). Additionally, systems that employ TCM to store thermal energy can be used as seasonal storage systems since the reaction's products must be kept separate from one another. [12]. The ineffective heat and mass transport in the reactive bed & the low thermal performance of the fundamental cycle are the primary problems in solid-gas chemical reactions [13].

The following prerequisites must be satisfied for a thermochemical process to be taken into consideration for energy storage:

- The reactants must be inexpensive.
- The reaction has to be reversible and run close to equilibrium.
- The energy that is stored in the TCS needs to be sufficient.
- The reactant should be able to utilize as much of the solar spectrum in the terrestrial atmosphere as feasible, with or without the inclusion of a photosensitizer.

While sensible heat storage loses the stored heat to the environment and necessitates isolation, storage methods based on chemical processes suffer from minimal losses.

1.2 Comparison of TES Types

The design of SHS systems is less complex than that of LHS or TCS systems, but SHS has the negative effects of being larger and unable to store or supply energy at a constant temperature. The charging process results in energy losses due to the storage of sensible heat. These losses depend on the thermal characteristics of the storage material, storage time, temperature, volume, and shape. The characteristics of the storage medium have a significant influence on the price of the SHS solution. It is highly usual to use very inexpensive materials as the storage medium for solids like rocks, sand, and refractory as well as liquids like oils, water, and some inorganic molten salts [14].

SHS method with water as a storage medium appears to be the most advantageous from a thermodynamic standpoint because of the high specific heat of the water and the potential for high capacity rates for charging and discharging. Corrosion from prolonged operation is the major issue with water storage systems. The volume of the storage may be extremely big for significant heat capacities, making the system as a whole very heavy. This is another drawback of water storage systems. Controls are necessary since stratification is an issue with big storage facilities as well. There are no issues with corrosion or scale formation when using rock storage, although the system's volume may grow as the cost rises.

On the other hand, the high quantities needed by the other two kinds are avoided through the employment of phase change storage systems. After some time, a storage material loses its ability to store energy due to the interaction of its bonds with the container.

When taking into account TCS, this technique makes use of reversible chemical processes during the charging and discharging phases. The benefit of this method is that the storage media will be extremely stable and suited for long-term preservation if the reaction's by products can be effectively segregated. To yet, though, there hasn't been much evidence of a reversible chemical

reaction occurring within the temperature ranges used for domestic hot water heating applications.

comparatively, the volume occupied by a water storage system is 80 times greater than that of a phase change system, and its amortization period is four times longer than that of phase change systems. PCMs are either enclosed as self-contained grains or packed in specific containers as tubes, shells, etc. The most costly but also the most compact forms are phase change systems, and because of their compactness, their initial cost is quite low.

When taking into account SHS solutions, theoretical and technical research as well as applications for the liquids and solids form have reached a pretty advanced degree of development. SHS systems utilize both temperature changes and the material's heat capacity to store energy since heat may be stored by raising the temperature of a material. The quantity of heat stored in the SHS system relies on the specific heat, temperature differential, and amount of material, hence, it requires a considerable large quantity of materials. Considering the thermo chemical energy storage, there are known to be essentially no reversible chemical reactions within the temperature range of domestic hot water heating applications. LHS systems, on the other hand, are often based on the quantity of heat absorbed or emitted during a material's phase transformation.

LHS is a particularly effective heat storage system among those previously discussed. Its ability to store a large amount of energy in an isothermal process is a special characteristic [15]. Phase change systems will be the most promising ones if the issues with them are resolved. Therefore, LHS systems have been selected for technological research in this work.

1.3 Phase Change Materials

Latent heat thermal energy storage (LHTES) devices use PCMs as storage substances to store heat energy. In this instance, a material changes its state by absorbing heat energy from the surrounding area during the phase transition, and when reverse operation is needed, the stored energy is released back into the environment. As the temperature rises, PCMs initially act similarly to other conventional materials, but when heated at higher temperatures and close to the phase transition, energy is absorbed. PCMs are composed of materials that absorb or release thermal energy at constant temperatures, unlike traditional materials. In contrast to conventional storage materials like water or rock, a PCM typically absorbs and releases thermal energy 5 to 14 times more quickly [16].

Solid-solid, solid-liquid, solid-gas and liquid-gas phase transformations are all possible ways for PCMs to store thermal energy. When a solid substance absorbs heat, it transforms from one solid structure that is crystalline, semi crystalline, or amorphous to another solid structure, and vice versa [17]. Compared to other varieties, this form of phase transition often contains less latent heat and a lower volume change. Recently, nonvolatile memory has utilized this kind of phase transition of PCM [18].

A typical commercial kind of phase transition in PCMs is a solid-liquid phase change. In this kind of phase transition, when the temperature approaches the melting point, PCM absorbs thermal energy to transform from a crystalline molecular arrangement to a disordered one. Solid-liquid PCMs have greater latent heat and sensible volumetric change than solid-solid PCMs. Solid-gas and liquid-gas phase shifts have larger latent heat contents, but they are also accompanied by significant volumetric changes that are problematic for LHTES systems [19]. Despite having a lower latent heat of fusion than liquid-gas, solid-liquids have a far lower

volumetric change (about 10 percent or less). Therefore, it would be more practical from an economic standpoint to use PCMs based on solid-liquid phase transition in LHTES systems.

1.4 Classification of PCMs

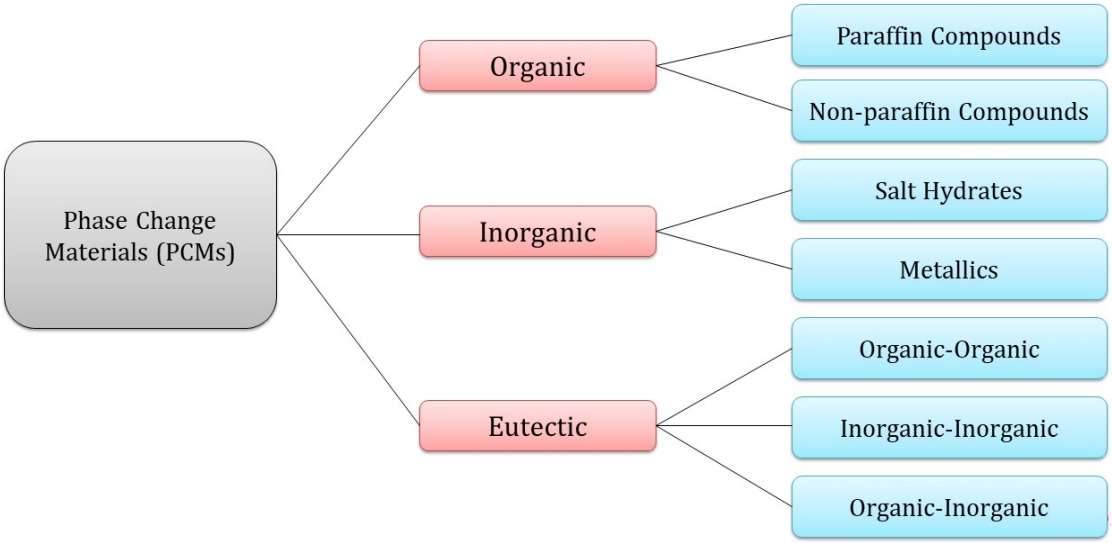

Fig 1.7 Classification of PCM

PCMs in liquid-gas and solid-gas transformations show incredibly large volume changes despite being a significant thermal energy storage capability, as was described in the preceding section. On the other hand, the capacity for thermal energy storage in solid-solid PCMs is also smaller. Therefore, the above-mentioned PCMs have not received much attention to commercialization, with the exception of a few circumstances. Solid-liquid PCMs are now the most popular transition type that has been widely commercialized. The three main types of solid-liquid PCMs are eutectics, inorganics, and organics [20] as schematically given in Figure 1.7.

1.4.1 Organic PCMs

Organic PCMs are possibly the most crucial element. Over several phase change cycles, organic PCMs display no modification in performance structure additionally, organic PCMs do not exhibit supercooling phenomena. It is distinct how organic PCMs are categorized. Their

application contexts serve as the major basis for this classification. They are often divided into two main groups, namely paraffin and non-paraffin parts.

Paraffin is one of the most common PCMs. Waxy solid paraffin is the common name for PCMs made of paraffin. Usually, paraffin has a large latent heat capacity. Paraffin waxes may typically be obtained in a wide variety of temperatures and are generally considered to be secure, trustworthy, affordable, and non-irritating chemicals. The majority of technical grade waxes may be utilized as PCMs in LHTES systems, which is advantageous economically. Paraffin waxes are stable and inactive from a chemical perspective. Although they have low vapor pressure, they have moderate volume changes during melting. The PCMs made of paraffin are typically highly stable over a large number of solidification-melting cycles.

In addition to their advantageous characteristics, paraffin also exhibits several unfavorable traits, such as limited heat conductivity, low melting points, and moderate to severe flammability. By using additives or paraffin composites, some of these drawbacks, most notably heat conductivity, and flammability, can be partially eliminated.

The most popular families of organic PCMs are also known to be non-paraffinic PCMs. They differ from paraffin in terms of their characteristics, but they are also extremely similar to one another. Different kinds of ether, fatty acids, alcohol, and glycol have been used by researchers as TES materials. These substances often burn easily and have weaker oxidation resistance [21,22]. The latent heat capability of non-paraffin organic PCMs is large, but they also exhibit short-term toxicity, flammability, and poor thermal conductivity.

1.4.2 Inorganic PCMs

The key advantages of inorganic PCMs are their greater thermal conductivity and high thermal energy storage capacity. They are frequently categorized as metals and salt hydrates.

The most significant class of inorganic PCMs that are frequently used in LHTES systems is salt hydrates. Inorganic salts and water are combined to form salt hydrates. In reality, salt hydrates undergo a phase transition that entails the loss of all or most of their water, which is essentially analogous to the thermodynamic melting of other materials.

The anhydrous salt and water are separated from the hydrate crystals at the phase transition. Salt hydrates provide a number of benefits, but they also have significant drawbacks that limit where they may be used. The inconsistent melting behavior of salt hydrates is one of these issues. In this case, the amount of water produced during the dehydration process is insufficient to completely dissolve the salts. In this instance, phase separation happens as a result of the salts precipitating. Salt hydrates are supplemented with a different substance, such as a thickening agent, to avoid this issue. The phenomena of supercooling present salt hydrates with yet another significant issue. Because the development of the nucleus is delayed during the crystallization process in this phenomenon, the substance remains liquid even at temperatures below freezing [23].

Overall, salt hydrate's high melting temperature, reasonably high thermal conductivity (nearly two to five times greater than paraffin), and little volume changes while melting are its most alluring features. They are also sufficiently affordable to be used, highly non-toxic, and compatible with plastic packaging [24].

The inorganic PCMs also include metals. The great heat conductivity and high mechanical characteristics of metals are their most noticeable benefits. There are a variety of metals with different melting points. Additionally, they serve as high-temperature PCMs.

Indium, Cesium, and Gallium, among other metals, are employed for low-temperature PCMs, whereas Zn, Mg, and Al are utilized for high-temperature applications. For systems that operate

at extremely high temperatures, several metal alloys with high melting points have been employed. These metal alloys can be utilized in the field of solar power systems as high-temperature PCMs [25]. They may also be employed in fields where maintaining temperature in furnaces or reactors that operate at high temperatures is necessary.

1.4.3 Eutectics

At least two different kinds of phase change materials are present in a eutectic PCM. Eutectic PCMs are mixtures of phase change materials that are either organic-organic, organic-inorganic, or inorganic-inorganic. Eutectics has unique qualities. Eutectics do not undergo phase separation into their constituent parts since the melting-solidification temperatures are often lower than those of the constituents. As a result, these materials do not exhibit phase separation or supercooling phenomena.

Compared to salt hydrates, eutectics often have a higher thermal cycle. They are most frequently found as inorganic-inorganic eutectics. However, organic-inorganic and organic-organic variations have gotten increasing attention in recent research. Eutectics' widespread commercialization is one of their biggest issues. They often cost two to three times as much as commercial PCMs [26].

1.5 Selection of PCM

PCMs come in a variety of desirable temperature ranges. Obviously, a PCM might not possess all the characteristics necessary to store heat energy in a perfect material. Therefore, to obtain the desired properties, combining such substances with either more PCMs or other additives would be preferable. However, when employing PCMs as latent heat storage materials, it is important to take into account their thermodynamic, kinetic, and chemical characteristics as well as their cost and availability. The ideal phase change temperature must be present in the used PCMs. On

the other hand, a material's physical size decreases as its latent heat increases. High thermal conductivity also aids in energy release and conservation. The phase stability of PCMs during melting and solidification, from a physical and kinetic perspective, leads to the best possible TES. Additionally, its high density allows for greater storage capacity with small material quantities. Smaller volume changes and lower vapor pressures are suitable for continuous applications during phase transition.

Physical, thermal, chemical, and kinetic properties of the materials, as well as cost, ease of access, product safety, adaptability, and dependability, are all taken into consideration when choosing PCMs for a certain TES application. Environmental and social implications are taken into account as part of the assessment criteria for PCMs-based TES in addition to its technical features. Determining a PCM's thermophysical qualities is essential for assessing its appropriateness for a given application and temperature range. One of the main criteria for choosing PCM for a certain TES application is that its phase transition temperature falls within the operating temperature range. For the PCMs to function at their best, further desirable thermal qualities include desirable latent heat, greater thermal conductivity, energy density, and heat capacity. The quantity of energy that a particular PCM is capable of storing or releasing is related to the values of latent heat and heat capacity. Higher latent heat and heat capacity indicate a PCM's ability to store and release energy, whereas higher thermal conductivity guarantees a PCM's ability to do so more quickly. Ideal PCMs must have the following physical characteristics: low vapor pressure during operation, favorable phase equilibrium, small volumetric changes during phase transitions, and desirable density [3]. Additionally, the elimination of supercooling, a higher nucleation rate, and a sufficient crystallization rate are required kinetic properties for the efficient use of PCMs for TES, while the appropriate chemical

properties include high chemical stability, a reversible solidification/melting cycle, and the non-corrosive, non-toxic, non-explosive, and non-flammable nature of PCMs [27,28].

Due to the enormous number of PCMs that are now available and/or being developed in the field of TES, the selection process for the best suitable PCM for a given application is extremely complicated and time-consuming. The majority of the materials in the literature have very little information on their thermophysical characteristics, making the selection process extremely difficult. This method includes a number of drawbacks, such as limited information available on the pricing and the effects of the PCMs on the surroundings. The comparison is undertaken after getting details of the investigated PCMs [29].

1.6 Applications of PCM

1.6.1 Solar Water Heating

As solar energy is the most abundant, cleanest, sustainable energy available, the use of PCMs as thermal energy storage in domestic solar water heating is a subject of great interest in research literature in order to bridge the gap between available solar energy and the demand for hot water. Conventional solar energy storage system uses sensible heat of the water for energy storage in the form of an increase in its temperature. PCM heat exchanger-based solar heating system uses latent heat of fusion as an energy storage medium which offers greater energy storage compared to conventional solar heating systems. In a PCM heat exchange-based solar heating system, energy is stored as latent heat of fusion of PCM in the day time when solar energy is available which can be used later in the night time depending upon the need as shown in Figure 1.8.

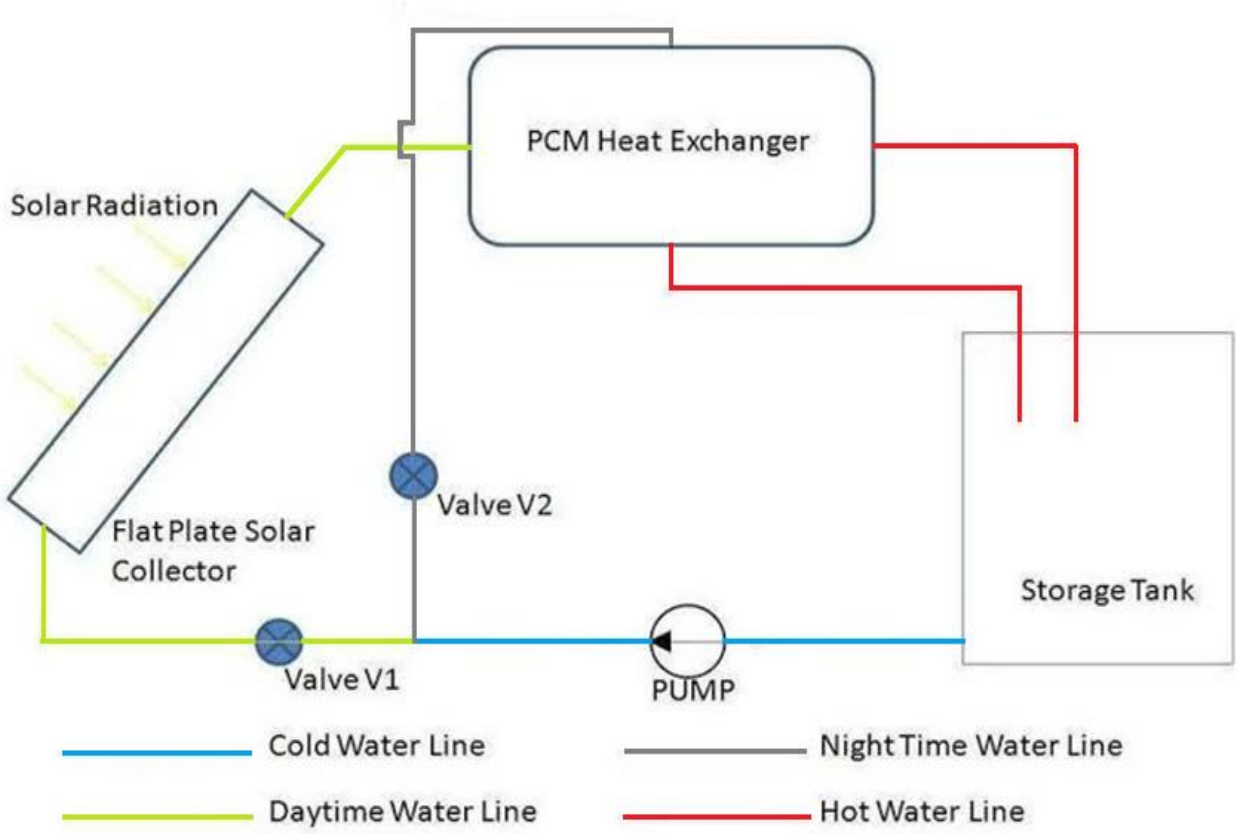

Fig 1.8 PCM Heat Exchanger used in solar water heating

1.6.2 Building Materials

In buildings that need a restricted temperature range, PCMs can be employed for heat or cold storage with great storage density and thermal comfort. So, if solar energy is stored efficiently in the daytime, it may be used to combat nighttime cold. It can also assist in storing the energy that is accessible during the day and maintaining a comfortable interior temperature. Encasing PCM inside the surfaces of the building may improve energy storage in the walls or other parts of the building structure. The latent heat capacity of the PCM can be utilized used to capture solar energy and decrease the temperature changes in the building. It also maintains the temperature closer to the desired temperature throughout the day.

Yan T. et. al. [30] proposes a self-activated heat removal using a pipe-encapsulated PCM wall model for cooling of building in summer. In this model, the PCM encapsulated between the inner pipe and the outer pipe can absorb the heat from the wall body and store it as latent heat in the daytime, and the stored heat in the PCM can be transferred into outer space in the nighttime using the gravity heat pipe. Results show that the pipe-encapsulated PCM wall with active heat removal can reduce internal surface heat flux significantly and effectively for building envelopes in hot climates.

1.6.3 Refrigerated Vehicles

Refrigerated trucks are regulated by small refrigeration units in order to maintain the truck's interior at a steady temperature and humidity level. The refrigerated unit is operated by engine power hence the cost of shipment is highly affected by the temperature to be maintained in the truck. PCM can be used in order to reduce peak heat transfer rates and total heat flows into a refrigerated truck.

Ahmed M. et. al. [31], in order to limit heat transmission into the vehicle, paraffin-based PCM was used in place of the standard form of insulation for refrigerated trucks. Peak heat transfer rates were reduced by 29.1 percent on average when all walls were considered, however, the maximum heat transmission rate was reduced from 11.3% to 43.8% for individual walls. There had been a 16.3% decrease in the transmission of heat on average inside the refrigerated truck compartments. These findings may lead to energy savings, reduced emissions from diesel-powered refrigeration units, smaller refrigeration equipment, and longer equipment lifespans.

1.6.4 Li-ion Battery

Li-ion batteries have been widely used in electronic devices for a long time (cell-phones, laptops, and portable devices). Several researches have been done on the possibility of using Li-ion

batteries for transportation applications in order to reduce emissions from vehicles. Li-ion battery modules can be connected in order to meet the nominal voltage to run the vehicle in electric mode. However, due to exothermic electrochemical reactions, Li-ion batteries release energy in the form of heat during discharge. The generated heat should be transferred from the body of the battery to the atmosphere. If the rate of heat transfer is not sufficient, some of the gelled phase materials turn into the gas phase and increase the internal pressure of the cell. Therefore, the energy should be released from the cell as soon as possible or the temperature of the cell should not be increased.

Ping P. et. al. [32] proposed a PCM fin structure-based temperature management method for batteries. A study is conducted on a battery module with five cells to see the influence of pure PCM under different melting temperatures, fin thickness, fin spacing, and PCM thickness on thermal performance in order to optimize the battery thermal management system. The maximum temperature on the battery surface and temperature difference within the battery module was monitored during 5 continuous charging-discharging cycles to study the effect of PCM-fin structure. Decreasing fin thickness reduces the maximum temperature and temperature difference of the battery module by increasing the heat exchange area with PCM. Increasing the PCM thickness improves the thermal performance other than other factors. By using a PCM-fin structure, the latent heat of PCM fully utilizes due to improved heat conduction and natural convection. Compared with pure PCM, the PCM-fin structure can increase the PCM liquid fraction by 29% and reduces the maximum surface temperature of the battery module by 36.4% as a result it reduces the failure risk of the battery thermal management system.

1.6.5 Thermoelectric Generator

A thermoelectric generator is a solid-state device that directly converts heat into electricity through a phenomenon called the Seebeck effect. Despite having various advantages like environment-friendly, silent operation, compactness, and long operational life, its low conversion efficiency is the main challenge. In recent times, a number of high-performance thermoelectric materials with enhanced performance have been developed. In the thermoelectric generation system, the main focus should be on the optimization of the heat sink and heat source design simultaneously. PCM as a heat sink is a novel idea for the cooling purpose of a thermoelectric generator.

Atouei et. al. [33] fabricated and tested a model of a two-stage thermoelectric generator (TTEG) system integrated with PCM. In the first stage, a thermoelectric generator module is installed between an electric heater and a PCM. In the second stage, five modules are installed between PCM and the heat sink. A comparison between TTEG and the common TEG system is made to analyze the performance of the TTEG. The results show that the TTEG generates 27% more net power than the common TEG system. Also, when the heater is off, TTEG supplies voltage for about 7900s, while a common TEG system supplies the voltage for the 2100s.

1.7 Organization of Thesis

The present thesis "**CFD Simulation of Shell and Tube Heat Exchanger Filled with Phase Change Material for Solar Water Heating System**" is described in the form of chapters. It consists of total 6 chapters. The brief details about each chapter are as follows.

Chapter 1: This chapter deals with the introduction of the thesis, starting with the energy resources to solar energy and then narrowing down to TES. Further discussion is carried out on PCM and the selection of PCM in solar water heaters.

Chapter 2: Critical literature review and general discussion was performed in this chapter to find the research gaps. PCM with LHTES, solar water heating systems with PCM, CFD simulation of PCM heat exchangers, and methods of enhancing the capacity of TES are discussed in this chapter.

Chapter 3: This chapter includes the selection of heat exchanger geometry with and without fins to enhance heat transfer and physical modeling of the selected configurations of heat exchangers. The meshing of the CAD model, to convert it into a finite element model, is also performed in this chapter along with the grid independency test.

Chapter 4: This chapter deals with the study of mass, momentum, and energy equation for the melting phenomenon of PCM. The numerical analysis of the melting of PCM in all geometries of the heat exchanger is explained in this chapter. To validate the result, a validation graph is also presented in chapter 4.

Chapter 5: This chapter deals with the CFD simulation study of the melting rate of PCM with and without fins, followed by results and discussion.

Chapter 6: This chapter describes important conclusions from each part of the present work and also discussion has been carried out on potential aspects for future work.

CHAPTER 2: LITERATURE SURVEY AND GENERAL CONSIDERATION

2 Literature Survey

In this chapter, a comprehensive literature survey on the enhancement of heat transmission of PCM-based materials and TES systems is presented in four distinct parts.

Part 1 considers the use of PCM in LHTES with its characteristics for different applications.

Part 2 deals with the study of solar water heating systems with PCM, their construction, and the different influencing characteristics.

Part 3 survey is made on the limitations of LHTES and techniques used to improve its performance of it with PCMs.

Part 4 surveys the different works carried out to simulate LHTES systems with PCM filled in an outer shell using CFD analysis.

As the solar energy is abundantly available it can be stored and used whenever required. It is clear that solar energy is an important source of energy however to utilize it efficiently, it is necessary to develop TES devices that are reliable and economical [1]. TES can take the form of sensible heat storage or latent heat storage. Atul Sharma et al. [3] reported on aspects of PCMs with their classification, types, and applications in which PCM is used.

The TES could be of sensible, latent heat type, or a combination of both. With the sensible heat type, the temperature of the material changes as energy is stored while with the latent heat type, energy is stored as material changes from one phase to another. To store an equal quantity of energy, significantly larger quantities of storage material are required for sensible heat storage in comparison with latent heat storage. In comparison with SHS, the LHTES technique has potential due to its advantages like large energy storage per unit volume, constant energy supply/storage, isothermal nature, compactness, etc [34].

PCM as LHTES has given a prominent choice for the storage of energy due to its characteristic and high storage density to store energy at a constant temperature. Phase change occurs in one of the forms: solid to solid, solid to liquid, solid to gas, liquid to gas, and vice versa. PCMs can be organic, inorganic, eutectic, etc. PCMs are very frequently used because of their low vapor pressure, large latent heat, non-toxicity, good thermal and chemical stability, and low price [35–37]. However, most of the PCMs exhibit low thermal conductivity which hinders its large applicability to various systems. The effect of the lower conductivity is reflected during energy withdrawal or retrieval with an appreciable temperature drop during the process. This drastically affects the performance of the system and leads to the increasing period of melting & solidification (charging & discharging period of the system).

Belen Zalba et al. [38] reported the review of thermal energy storage with PCM is an important research topic. He explained the history of TES with the phase change process. More than 150 materials as PCM listed with 45 commercially available PCMs are used and he also focused on analysis of heat transfer with applications.

2.1 Use of PCM in LHTES

The effectiveness of LHTES can be enhanced by selecting the proper PCM. The selection of PCM is done so as to match the phase change temperature with the temperature of the application with which the heat is being exchanged. There are also several characteristics of PCMs such as melting point, latent heat of fusion, density, thermal conductivity, etc. which will make them suitable for a number of applications. Several studies have been performed to examine the overall thermal behavior and performance of LHTES with PCM. These studies focus on the different characteristics of PCMs such as their suitability for applications,

geometrical aspects, melting and freezing characteristics, and consequently the heat storage and retrieval rate.

Phase change materials find applications in greenhouses to store solar energy for curing, drying, and the egg incubation process. PCM is employed in space heating and cooling of building structures for maintaining the desired thermal comfort. PCMs also widely used in solar applications namely solar water heaters, solar air heaters, and solar cookers, because during sunshine hours solar energy is abundantly available and can be stored easily. During off-sunshine hours PCM retrieves this stored energy back to the material to be heated [39,40].

PCMs were applied in different geometry such as cylindrical, spherical, square, etc. Numerous numerical and experimental studies were carried out on different geometries with PCM. A. Felix Regin et al. [41] reported on the melting characteristics of paraffin wax contained in cylindrical capsules. Studies have been carried out with the parameters namely, natural convection, contact melting, and phase change temperature and their effects on heat transfer characteristics.

Results show that magnitude of Stefan's number governs the melting process. The PCMs are also used with spherical geometry which has a number of advantages over other geometries. It has a favorable ratio between the volume of energy stored and the area for heat transfer. J. P. Bedecarrats et al. [42] reported on the performance of PCM encapsulated in spherical containers during the charging and discharging process. In this study water with nucleating agent was used as PCM. Results show faster heat storage for lower inlet temperature and larger flow of heat transfer fluid.

Determination of a feasible heat storage material was carried out by, M. Veerappan et.al. [43] with 35 mol% lauric acid and 65 mol% capric acid, calcium chloride hexahydrate, n-octadecane, n-hexadecane, and n-eicosane inside spherical enclosures. Results were validated with the model

developed for melting and solidification in a sphere with conduction, natural convection, and heat generation. The investigation shows that calcium chloride hexahydrate has excellent characteristics for solar latent heat storage applications. The parametric study shows that during solidification higher heat flux is released at lower fluid temperature and thereafter drastic decrement in the heat flux was observed. Numerical and experimental studies for constrained and unconstrained melting in the spherical capsule were carried out to understand the buoyancy-driven convection for the constrained melting process [44,45]. Levent Bilir and Zafer Ilken [46] numerically formulated the inward solidification problem of PCM encapsulated in a spherical/cylindrical container. A dimensionless total solidification time of PCM was set in terms of the Biot number, Stefan number, and superheat parameter.

PCMs can be used for various applications and storage of solar energy is one of them. However, this source is diluted and scattered which depends upon the day-night cycle and weather conditions. Due to its uneven nature, it is difficult to apply it effectively in domestic use, particularly in solar water heating systems. In solar water heaters, energy is stored during day time, and hot water is consumed in the evening and in the morning. Therefore, it is necessary to store the energy which is available during day time. The use of PCMs is the valid solution to this complexity because of their isothermal behavior, small unit size, and high heat storage capacity during charging and discharging [47]. The next part of the review gives different methods which are applicable for enhancing the performance of solar water heaters by applying different kinds of PCMs.

G. Murali et al. [48] Examined the performance of PCM-incorporated thermosyphon solar water heating system. PCM cylinders are used in water tank charging to carry out charging and

discharging experiments. The discharging experiments with and without PCM are validated by CFD simulation.

H. M. Teamah, et al. [49] studied multi-tank thermal storage systems for multi-residential solar domestic hot water applications. The thermal storage system includes phase change materials of different melting temperatures incorporated in the tanks. The hybrid tank model was linked with the collector performance. The multi-tank hybrid system thus allowed for over 50% reduction in the required storage volume. It was found that cascading four 75 L tanks containing PCMs of melting temperatures 54°C, 42°C, 32°C and 16°C gives a similar solar fraction to that for a 630 L water-only tank. A thorough economic analysis requires a detailed optimization study for the hybrid system and is planned for future research.

Yaxue Lin, et al. [50] studied thermal conductivity enhancement, thermal properties, and applications of PCMs in TES. It is found that the addition of thermal conductivity enhancement fillers is a more effective method to improve the thermal conductivity of PCMs. The methods for enhancing the thermal conductivity of PCMs, which include adding additives with high thermal conductivity and encapsulating phase change materials are reviewed. The applications of PCMs in solar energy systems, buildings, cooling systems, textiles, and heat recovery systems are introduced as well. It is said that both carbon-based additives and metal-based ones possess excellent thermal conductivity; however, carbon-based additives are better than metal-based additives in terms of density and stability.

Kandasamy Hariharan, et al. [51] investigated the phase change behavior of paraffin phase change material in a spherical capsule for solar thermal storage units. The melting and solidification behavior of paraffin phase change material encapsulated in a stainless-steel spherical container has been studied. In the melting process, the hot air, used as the heat transfer

fluid enters the test section and flows over the spherical capsule resulting in the melting of PCM. In the solidification process, the ambient air flows over the capsule and received heat from phase change material resulting in the solidification of phase change material. A computational fluid dynamics analysis has also been performed for the encapsulated PCM during the phase transition process. The reasons for the deviation between the results are analyzed. The CFD results show that the time needed for solidification is 33% more and the time needed for melting is 30% more compared to the respective experimental results.

2.2 Solar Water Heating Systems with PCM

Solar water heater with PCMs such as LHTES is getting popularity since they are simple to fabricate, easy to maintain, and relatively inexpensive. Internationally the demand for solar water heaters is increasing significantly in the last decade. Solar water heating system is generally very simple using only sunlight to heat the water. Working fluid water is brought in contact with a dark surface which is exposed to sunlight, causing the rise in temperature of the fluid. They can be classified into two main categories: (a) Active systems in which pumps are used to circulate the water or a heat transfer fluid, (b) Passive systems (or thermosyphon systems) in which the water or a heat transfer fluid is circulated by natural convection. The solar water heater performance is improved by connecting the solar water heater in series or by adding energy storage material into the storage tank.

Various methods are attempted to improve the functionality of solar water heaters by adding PCMs to the tank. Some of these techniques are (i) To get hot water in off sunshine period; the solar water heater containing the layer of PCM-filled capsules is used. (ii) A system having a double rectangular enclosure in which water is filled in the bottom enclosure and paraffin wax is

filled in the top enclosure. (iii) Identical eight typical solar water heaters were connected serially with the PCM, and small aluminum cylindrical containers containing paraffin wax [52–54].

Abdul Jabbar N. Khalifa et al. [55] used solar collectors integrated with the back layer of paraffin wax for their experimental investigation. Evaluation of various parameters regarding the collector plate shows the plate temperature is increased up to a certain distance after which it is nearly constant which clearly shows the storage of the energy in the PCM.

Pasam Bhagyalaxmi et al. [56] selected paraffin wax and palmitic acid as PCM mixed in different proportions (40-60%, 50-50%, and 60-40% PW-PA) and investigated their thermal behavior through DSC and further similar studies were also conducted by mixing copper oxide Nano-powder with paraffin wax.

Murali G., et al. [57] investigated the effect of stratification in the solar water heater tank providing latent thermal energy storage with the ratio of improved surface to volume and compared the stratification caused by in-flow from the open side inlet and open bottom inlet attained with a diffuser.

Al-Hinti I., et al. [58] investigated experimentally, the performance of water as a phase change material to store thermal energy for use with conventional solar water heating systems. The forced convection used for a short time shows the minimum effect on the performance of the system. The performance of the system was analyzed under an open-loop operation pattern, simulated with the daily used pattern.

2.3 Limitations of LHTES and Enhancement Techniques Used to Improve Performance

In order to augment the performance of PCMs, many efforts have been attempted and various methods are recommended. It includes the use of extended surfaces, the use of multiple PCMs, micro-encapsulation of PCM, and the addition of high-conducting materials [59]. In multiple

PCM systems PCMs with their decreasing melting points are arranged which maintains the temperature difference between heat transfer fluid and PCMs. This kind of arrangement allows sufficient driving force for energy storage along the flow direction. The numerical study of Yuwen Zhang and A. Faghri [60] shows enhancement in the LHTES system by using internal fins in the shell and tube-type heat exchanger. Results show an increment in melt volume fraction with an increase in the number of fins which clearly shows the boost in the heat transfer.

R. Velraj et al. [37] Proposed three enhancement methods namely, the use of internal fins, the addition of lessing rings, and bubble agitation. The experimental study has revealed that the first two methods of enhancement are suitable for solidification and the last one is for melting. In recent studies, Jundika C. Kurnia et al. [61], numerically verified the different configurations, e. g. U-tube, U-tube with in-line fins, and a novel festoon design of PCM in thermal energy storage. It indicates that the novel festoon design gives the highest heat transfer performance. Although the improvement occurs by applying the above-mentioned methods, they have the limitation of volume occupancy. Therefore, it is necessary to find out a way that gives better enhancement with less volume utilization.

Enhancements using fins were shown to be the most practicable option among the alternative methods of heat transfer enhancement resulting in their more conventional design, easier production, cheaper cost, and greater efficiency [62]. Experimental comparisons of the PCM heat transfer increases with circular and longitudinal fins were also conducted. Following that, the PCM with longitudinal fins performed better, as the addition of longitudinal fins resulted in a 12.5 percent reduction in time to melt for an intake heat transfer fluid temperature of 80°C [63]. On the other hand, triplex tube heat exchangers are used with various fin designs, indicating that the size, quantity, and pitch of the fins had a significant impact on PCM's melting time [64,65].

PCM heat exchanger systems having a variety of shapes and sizes were used in some of the relevant investigations and concluded that the efficacy of enhancement of heat exchange for a certain application is also influenced by other factors such as design configurations, heat transfer fluid and type of PCM [66,67]. The total heat transfer coefficient of the twin-pipe heat exchanger having PCM integrated into graphite matrices was the highest, while the compact heat exchanger could deliver the most thermal power due to its biggest percentage of heat transmission area to exterior volume, according to the experimental studies. As a result, the PCM heat transfer improvements can be affected by a variety of design and operational variables. It is therefore necessary to find out an efficient approach for evaluating, comparing, and optimizing these possibilities. For a PCM cylinder-shaped thermal storage reservoir with solar assistance, dynamic models based on the enthalpy technique were constructed [68,69]. The models were then evaluated and validated against the findings of the experiments. The findings of the study revealed that several critical design and operational characteristics might have a major impact on the PCM thermal storage tank's performance. These included storage tank architectures, PCM kinds, and heat transfer fluid flow rate and temperature, among other things [70].

CFD modeling, which numerically solves the mass, energy, and momentum partial differential equation of Navier-Stokes, can be an effective simulation technique for predicting the melting/solidification behavior of PCM among the available design and assessment approaches [71]. The enthalpy technique, which finds the enthalpy value in the energy equation, can be used to do this. The overall enthalpy value includes both sensible and latent components, with latent enthalpy expressed as a percentage of PCM's latent heat in the liquid phase. This proportion is often referred to as the liquid fraction of PCM [72]. When compared to experimental research, CFD modeling methodologies offer a variety of benefits, including reduced time and more

planned possibilities for analysis. Some substantial and thorough simulation results can be achieved using a verified CFD model. Among other things, these include the dynamical characteristics of PCM temperature, melting/solidification rate, heat transmission rate, and stored/released energy. However, several critical characteristics must be included to set up an appropriate CFD PCM heat exchanger (PCMHE) model, when different heat transfer enhancing materials are added with the PCM, for example, the effective thermal conductivity. In addition, in the CFD model to describe the PCM phase transition characteristics, an appropriate phase change model should be used, with the "volume of fluid" model being the most widely used [73,74].

2.4 CFD Simulations LHTES Systems with PCM Filled in an Outer Shell

A number of CFD numerical analysis has been employed to improve heat transmission in TES systems. It has been investigated from the study that heat transmission can be increased either by using the suitable geometric configuration of the heat exchanger or by increasing the PCM's thermal conductivity. Methods used to improve heat transmission are the use of fins, elliptical tubes, heat pipes, etc. [75]. A 2D CFD simulation is implemented to look into the melting and solidification of Gallium in the form of PCM in a circular shell, with the shape of a heating source placed into the shell optimized. To maximize PCM melting time, a constant temperature boundary condition was given to a cylindrical heating source without a fin, and a four-finned heating source placed inside a circular shell packed with PCM and liquid fraction was explored. It has been seen from the simulation that the geometry with four fins increases the heat transmission in PCM and the time to melt decreased from 18.35 minutes to 13.35 minutes [62]. To enhance the heat transfer, a 3D CFD study of a heat exchanger of fin and tube type has been performed in which tubes are elliptical having different ellipticity ratios and orientation

from horizontal to anticipate the phenomenon of heat transmission and friction characteristics. For the tubes having an ellipticity ratio of 0.6, the friction factor is 52.9 percent lower than that of circular tubes. The predicted CFD results are validated with results obtained from the literature [76].

The methods utilized to enhance the thermal conductivity are using porous materials, composites of greater thermal conductivity, inclusion of nanoparticles, etc [77]. A CFD study to enhance the heat transmission of a shell and tube heat storage device having air as the heat transmission fluid in the tube and a PCM in the shell divided into multiple segments of metal foam. This work has been done due to the realization that temperature variation in the shell during the process of phase change decreases in the direction of the flow of heat thus reducing the rate of heat transmission. This study shows that the solidification and melting times of PCM are being lowered by making use of multiple segments of metal foam [78]. Also, a PCM heat exchanger with tubes having spiral wires in its circumference may be utilized to improve heat transmission due to the lower thermal conductivity of studied PCM as well as inside the tubes, a liquid for heat transmission is circulating. CFD analysis of PCM heat exchanger has been done and compared with experimental data and found that the time taken in melting of PCM is less than the time taken in solidification of PCM as a result of convective heat transfer and buoyancy effect in the PCM [79].

Although energy storage by latent heat can be utilized by changing of phase from liquid to gas, the transition from liquid to gaseous phase requires a significant pressure and volume rise [80,81]. Because of its large capacity to absorb thermal energy, the use of PCM in STHEs is a creative approach in the domain of investigation to bridge the difference between actual energy demand and energy supply. In the research area of PCM and its usage in shell and tube heat

exchangers (STHE), there is a lot of scope for research. In the last 15 years, only a few research articles on improving the performance of PCMs in STHEs have been conducted.

The installation of PCMs in the walls of buildings can be used to absorb solar energy during the day and then use for space heating and other uses at night. A design of constructing a building structure is created along with PCM within an encased heat pipe that is self-enabled to remove thermal energy for building summertime cooling. This installation incorporates two pipelines in a circle into the building structure, with a liquid moving through the internal pipeline. Between the external and internal pipes, PCM is introduced. Heat is captured from the building structure by PCM and circulating fluid during the daytime and discharges into the atmosphere at night using a heat pipe with gravity [82]. Diarce et. al. [83] have conducted a 2D CFD study of a building structure with PCM placed in the external wall as well as the analysis has been done to determine whether it is appropriate to utilize PCM as a single-stage material accepting its temperature-dependent change in specific heat rather than expecting to be a melting/solidification approach and dismissing heat hysteresis and convection impacts to limit the time for simulation. A CFD approach is utilized to investigate the behavior of characterized PCM because of thermal hysteresis. As a shell material, natural PCM n-octadecane is combined with an inorganic component called silica to evaluate the measure of change of phase where the majority of thermal energy is moved via conduction as well as the impact of embodiment along with the thermodynamic conduct of PCM is demonstrated [84]. Experimental data is utilized to create and evaluate CFD numerical modeling of a PCM-enabled system. The model is investigated using two numerical simulations. The results indicate that if a reliable simulation technique and proper fundamental thermal parameters are used, equivalent results may be achieved by comparing simulation results with experimental data [85].

Mohammadnejad F and Hossainpour S [86] used COMSOL multi-physics software to conduct a CFD simulation to examine the discharged behavior of a fixed bed with multiple layers of elevated temperature-encased PCMs. The effect of each layer's height and porosity, as well as other PCM topologies based on their phase-change temperatures, is investigated. Increases in working fluid inflow rate and the permeability of PCM layers in the fixed bed have identical effects and cause the fixed bed to decline more quickly. Many studies focus on internal phase transition material optimization, such as employing shape-stabilized technologies and adding additives.

2.5 Research Gaps

As solar energy is the most abundant, cleanest, renewable energy source available, it is widely used in domestic solar water heating systems. Its main drawback is that it is available only in the daytime. To bridge the gap between available solar energy and the demand for hot water, an effective TES system is required. Conventional solar water heaters store energy by increasing the temperature of water in the form of sensible heat. LHTES system store thermal energy as latent heat by changing the phase from solid to liquid, therefore, offers greater energy storage compared to conventional solar water heating system. PCM is a material used in LHTES systems to store thermal energy by transforming its phase from solid to liquid or vice-versa. Change of phase from liquid to vapor involves a large change in volume and high pressure, therefore it is not a good practice. In PCMHE-based solar water heating systems, energy can be stored in the daytime when solar energy is available and used later in the nighttime.

In conventional heat exchangers, the heat transfer phenomenon is well understood. Therefore, experimental or simulation studies available in the literature are in abundance. On the other hand, PCMHE is a new field of study and limited research work has been done so far. A survey on

PCMs as LHTES is done which is very useful for better utilization of solar energy in solar water heating systems when it is abundantly available. On the other hand, the observations of different researchers were shows lower thermal response of PCMs due to their lower heat transfer capabilities. Improvement in the heat transmission capabilities of PCM is the key objective of the researchers.

Researchers presented a number of experimental and CFD numerical investigations having heat transfer enhancement approaches for PCMs to advance the thermal performance of LHTES. It has been investigated from the study that the heat transmission capabilities of PCM can be increased either by using the suitable geometric configuration of PCMHE or by increasing the PCM's thermal conductivity. Many of the solutions proposed the use of extended surfaces (fins), elliptical tubes, and heat pipes, however, some suggested mixing the PCM with the particles having greater thermal conductivity like carbon fiber and metal beads at random [75,76,87]. Enhancements using fins were shown to be the most practicable option among these alternative heat transfer enhancement methods resulting in their more conventional design, easier production, cheaper cost, and greater efficiency. Hence the addition of fins to the tubes of a PCMHE is a promising technique used to enhance the performance of solar water heaters.

Work commenced in this study examining the performance of pure PCM filled the shell region of a PCMHE of circular and square shape having a number of circular, elliptical, and square geometry with and without fins for solar water heating system which is considered as LHTES has been done by CFD analysis. Different geometries of PCMHE have been investigated and compared for maximum heat transmission into the PCM by using fins on the tubes of the heat exchanger. Attempts are also done to assess the melting behavior of pure PCM by CFD analysis.

It has been investigated from studies that the heat transfer capability of PCM can be increased either by:

- ❑ Using the suitable geometric configuration of PCMHE
- ❑ Increasing the PCM's thermal conductivity

- ➢ Previous studies have addressed the need for methods for improving the heat transfer capabilities of LHTES systems having circular tubes and have not compared different shapes of the tubes in shell & tube heat exchangers.
- ➢ Studies reported in the literature dealt with the use of fins for heat transfer enhancement without using the variation of the number of fins on the circumference of the tubes.
- ➢ In literature, some of the investigations present the use of elliptical tubes with different ellipticity ratios but have not made an attempt to use the fins on elliptical tubes.

Design, CFD simulation, and cost-effectiveness analysis will be the main motivation to undergo an in-depth study of PCMHE. This could be helpful for maximizing the heat transfer effects.

2.6 Research Objectives

The main objective of this research is to enhance the performance of a PCMHE by employing a suitable geometric configuration that gives maximum heat transmission from tubes to PCM and has a minimum melting time of PCM. Keeping in view the gaps in the literature, the following objectives have been formulated for carrying out the present research work.

(i) CFD Modeling and simulation of PCM Heat exchanger of Shell & tube type filled with PCM having circular tubes.

(ii) CFD Modeling and simulation of PCM Heat exchanger of Shell & tube type filled with PCM having elliptical tubes.

(iii) CFD Modeling and simulation of PCM Heat exchanger of Shell & tube type filled with PCM having circular tubes with fins.

(iv) A comparison of the results of the circular tubes, elliptical tubes, and circular tubes with fins and the best-suited configuration of the PCM Heat Exchanger is selected.

2.7 Research Methodology

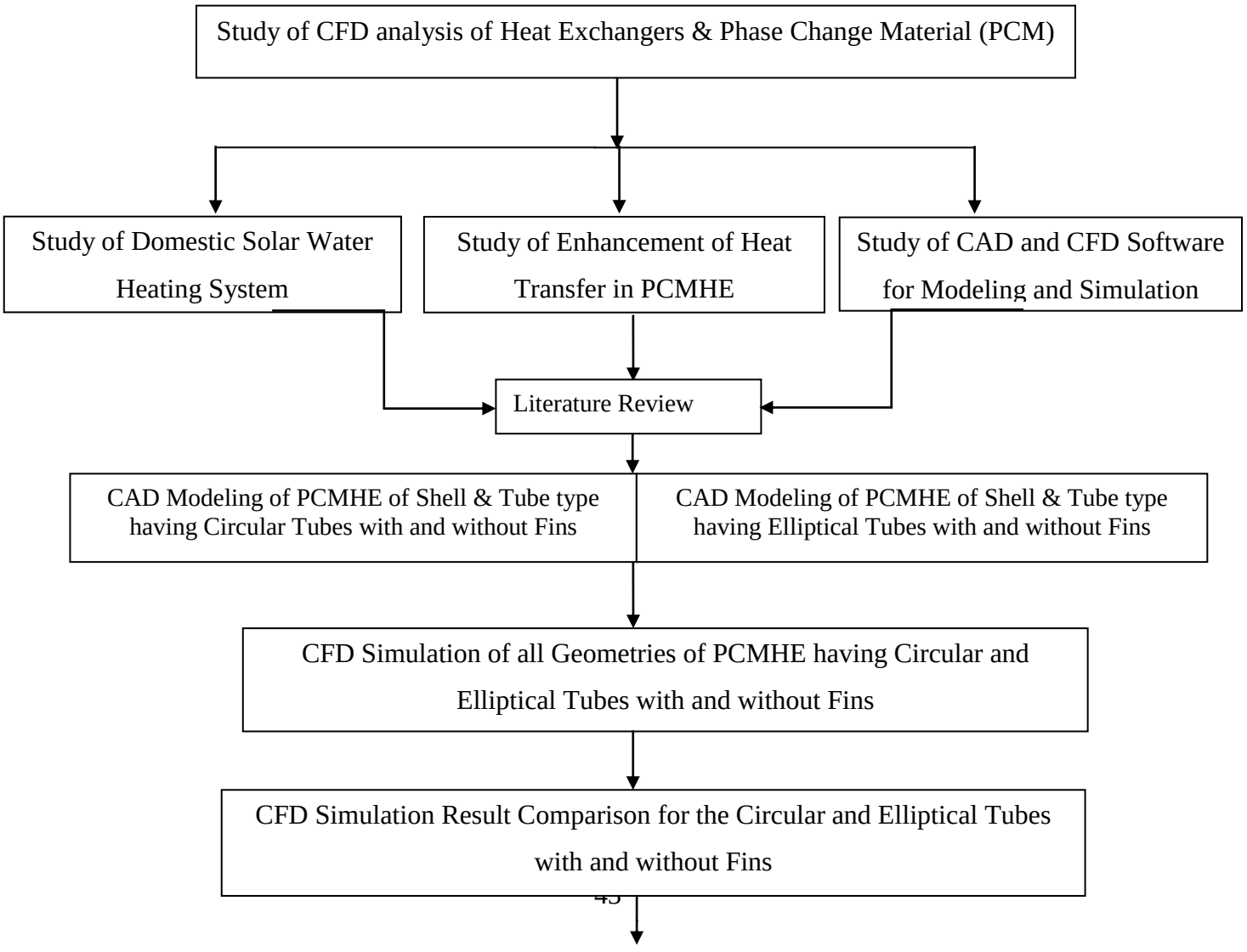

Selection of Best suited PCMHE Geometry for Solar Water Heating System

Conclusion and Future Scope

2D CAD models have been developed and investigated in Ansys Fluent for heat transfer analysis in circular and square shell PCMHE. The equations of conservation of mass, momentum, and energy for the current model have been developed and solved using CFD in Ansys Fluent. To fulfill identified research objective following research methodology will be adopted.

(i) Literature study of PCMs in LHTES for solar water heating systems for domestic applications.

(ii) Study of CAD (Solid Works) and CFD software (Ansys Fluent) for modeling and simulation of geometries of PCMHE.

(iii) 2D Modelling of all geometries of PCMHE of circular and square shells having circular and elliptical tubes with and without fins.

(iv) CFD simulation of all geometries of PCMHE of circular and square shells having circular and elliptical tubes with and without fins.

(v) CFD Simulation result comparison of all geometries of PCMHE of circular and elliptical tubes with and without fins.

(vi) Selection of best-suited PCMHE geometry for solar water heating system.

(vii) Conclusion and future scope.

CHAPTER 3: MODELLING AND MESHING

3 Introduction

In this chapter, different geometries of STHE have been modeled. STHE is a non-contact type heat exchanger which is used for transferring thermal energy from one fluid to another fluid by virtue of temperature difference. It consists of a large shell and a number of tubes are inserted in this shell. In STHE, one fluid is filled in the outer shell, and the other fluid is filled in the inner tubes. If one fluid in an STHE is a PCM, which is filled in the outer shell, it is known as a PCMHE. In this chapter, different configurations of PCMHE with some modifications have been modeled and meshed to investigate the melting phenomenon of PCM.

The main challenge with PCMHE is the low heat transfer rate due to the lower thermal conductivity of PCMs. To overcome this problem, a different configuration of PCMHE with & without fins & different shapes of the tubes are modeled in this chapter. To accelerate heat transmission and to reduce PCM's melting time, a number of fins are incorporated into the tubes of different shapes.

The CFD simulation of all the geometries of PCMHE has been done in Ansys Fluent after creating a finite element model (FEM) by meshing the physical model. A 3D model of PCMHE has a very large number of elements in FEM and takes a very long computational time to solve the mass, momentum, and energy equations. Also, the results are much better in 2D analysis compared to 3D analysis [88]. Hence a 2D CAD model of PCMHE is selected for this study.

3.1 About Solid Works

Solid Works is selected to model all the geometries of the PCMHE in this work. Solid Works is a solid modeling computer-aided design (CAD) and computer-aided engineering (CAE) application. It is a powerful CAD software and product design tool for the modern-day designing of solid products. It is a very user-friendly tool to create a CAD model in two and three-

dimensional. A parametric feature-based design process is used by the solid modeler Solid Works to produce models and assemblies.

The shape or geometry of the model or assembly is determined by the values of the parameters, which are constraints. Parameters might be geometrical terms like tangent, parallel, concentric, horizontal, or vertical, or they can be numerical terms like line lengths or circle diameters. In order to represent design intent, relations can be used to link together numerical parameters. Design intent refers to how the part's designer intends to react to updates and modifications. For instance, you would like the hole at the top of a beverage can to remain there no matter how tall or large the container is. If the user tells SolidWorks that the hole is a feature on the top surface, the software will respect their design intent regardless of the height they eventually give the can.

In Solid Works, creating a model often begins with a 2D drawing. Geometry elements including points, lines, arcs, conics, and splines are included in the sketch. To specify the size and placement of the geometry, dimensions are added to the sketch. Attributes like tangency, parallelism, perpendicularity, and concentricity are defined through relations. Because Solid Works is parametric, the dimensions and relationships determine the geometry rather than the other way around. The drawing's dimensions can be managed independently or in connection to other characteristics that are either within or outside the sketch.

The component's building blocks are referred to as features. They are the procedures and forms that create the component. For shape-based features, a 2D drawing of forms like bosses, holes, slots, etc. is usually the first step. Following that, the part's form is either cut or extruded to add or subtract material. Operation-based features, which do not rely on sketches, include things like fillets, chamfers, shells, applying drafts to a part's faces, etc.

In an assembly, mates are the equivalent of sketch relations. Assembly mates establish analogous relations with regard to the individual parts or components, enabling the simple creation of assemblies, just as sketch relations describe sketch geometry's connection to requirements like tangency, parallelism, and concentricity. With the aid of sophisticated mating features like gear and cam follower mates, modeling gear assemblies may precisely reproduce the rotating motion of a real gear train. These characteristics are included in Solid Works.

And last, drawings may be made from both components and assemblies. Views are created automatically from the solid model, and when needed, annotations, measurements, and tolerances may then be added to the drawing effortlessly. The majority of paper sizes and standards are included in the drawing module.

Solid Works allows saving 2D and 3D model information in *. iges format, It enables the model's modification and presentation across several platforms. The 2D CAD model, created in Solid Works, can be easily transported and modified in the ANSYS Design Modeler in IGES format.

3.2 Geometrical Modeling

Geometrical modeling of PCMHE of shell and tube type, in which a solid PCM is filled in the outer shell and four tubes of different shapes has been done in Solid Works in 2D. In this work, the outer shell of PCMHE is selected in two different shapes: square and circular. The tubes inside the outer shell of PCMHE are also selected in different shapes i.e. circular, square, and elliptical as well as in different configurations i.e. with and without fins.

3.2.1 Square Shell Geometries

In square shell geometries, the outer shell of PCMHE is kept in a square shape and the shape of the inside tubes is varied. The shape of the tubes inside the shell is kept circular, square, and

elliptical and a comparison is made based on the liquid fraction and melting time of PCM for the best-suited geometry. The dimensions of the square shell in all configurations of PCMHE are taken to be 200×200 mm. The dimensions of the tubes of circular, square, and elliptical shapes are set in such a way that the surface area of the shell should be uniform in all configurations. To keep the surface area constant in all configurations of PCMHE the dimensions of circular tubes are taken to be Ø 30 mm, the dimensions of the square tubes are taken to be 26.5×26.5 mm and the dimensions of the elliptical tubes with the ellipticity ratio of 0.6 are taken to be 38.7×23.2 mm. For maximal heat transmission, the ellipticity ratio for the heat exchanger with elliptical tubes has been set to 0.6 [14]. The center point of all the tubes in every configuration is kept at a distance of 50 mm from the center of the heat exchanger horizontally as well as vertically as shown in Figure 3.1. The surface area and the dimensions of the tubes in all configurations are shown in Table 3.1.

Table 3.1 Geometrical characteristics of square shell PCMHE having circular, square, and elliptical tubes

S.N.	**Parameter**	**Configuration of Heat Exchangers**		
1	Geometry	Circular Tube	Square Tube	Elliptical Tube
2	Surface Area	37173 mm^2	37191 mm^2	37179 mm^2
3	Dimensions of tubes	Ø 30 mm	26.5 mm ×26.5 mm	38.7 mm ×23.2 mm

A 2D CFD computational investigation is then performed on the PCMHE having a square shell filled with solid PCM and an HTF fluid flows at a higher temperature compared to the starting temperature of the PCM in the circular, square, and elliptical tubes. The heat transmission between the HTF and PCM is investigated using three distinct geometries of PCMHE. To

achieve mass conservation across all designs, all configurations are employed with a uniform surface area.

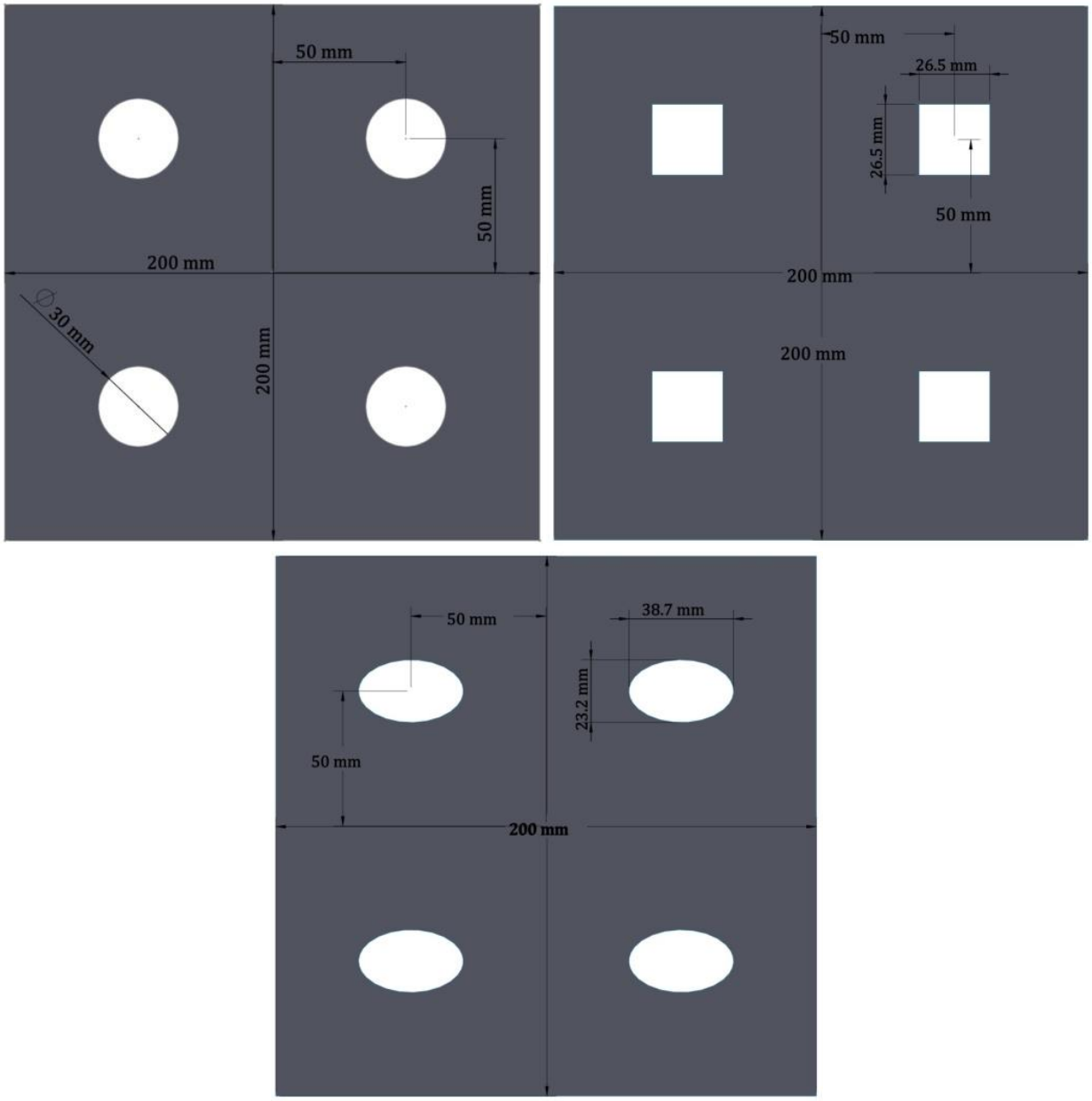

Fig 3.1 Physical modeling and geometrical dimensions of the square shell PCMHE having circular, square, and elliptical tubes

A different investigation has also been made in a square shell geometry having square tubes. To enhance the heat transmission and to reduce the PCM's melting time, four fins are inserted on the outer surface of the square tubes. Two configurations of PCMHE with square shell geometry,

square tubes without fin and square tubes with four fins, have been modeled in this study. The dimensions of the square shell in both configurations of PCMHE are taken to be 160×160 mm. The size of the square tubes in the square shell is taken as 20×20 mm and the distance of the center of the tubes from the center of the square shell is kept at a distance of 40 mm horizontally as well as vertically for the uniform melting of PCM. Four rectangular fins are mounted on the square tubes and the dimension of the fins are 7×2 mm.

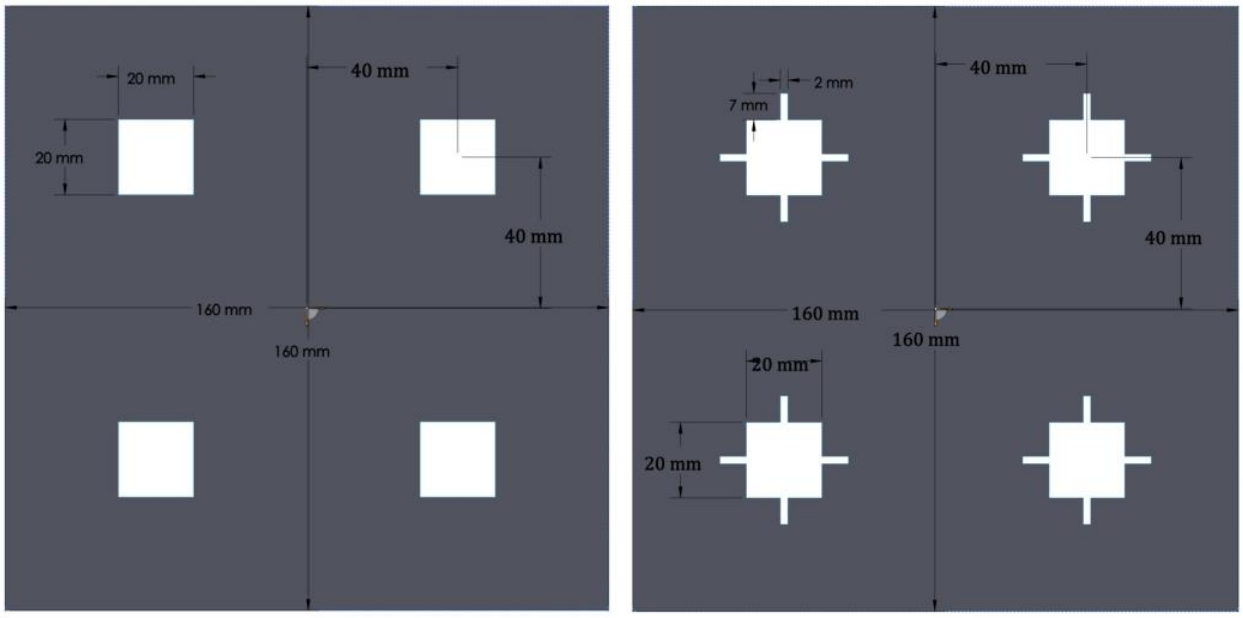

Fig 3.2 Physical modeling and geometrical dimensions of the square shell PCMHE having square tubes with and without fins

In this work, two different configurations of PCMHE have been investigated to analyze the heat transfer rate from the square tubes to PCM. Both the geometries have been utilized with a fixed surface area to make sure mass conservation among all configurations. The dimensions of the geometries of PCMHE with and without fins are presented in Figure 3.2.

3.2.2 Circular Shell Geometries

In these geometries, the shape of the outer shell of PCMHE is taken as circular and the shape of the inside tubes is also taken as circular. A PCM is filled in the circular shell and a HTF is

flowing in the tubes. In this study, a comparison has been made among the circular shell geometries of PCMHE to see the effect of the number of fins incorporated into the circular tubes on the heat transfer rate into the PCM. The three geometries of PCMHE include circular tubes without fins, circular tubes with three fins, and circular tubes with six fins.

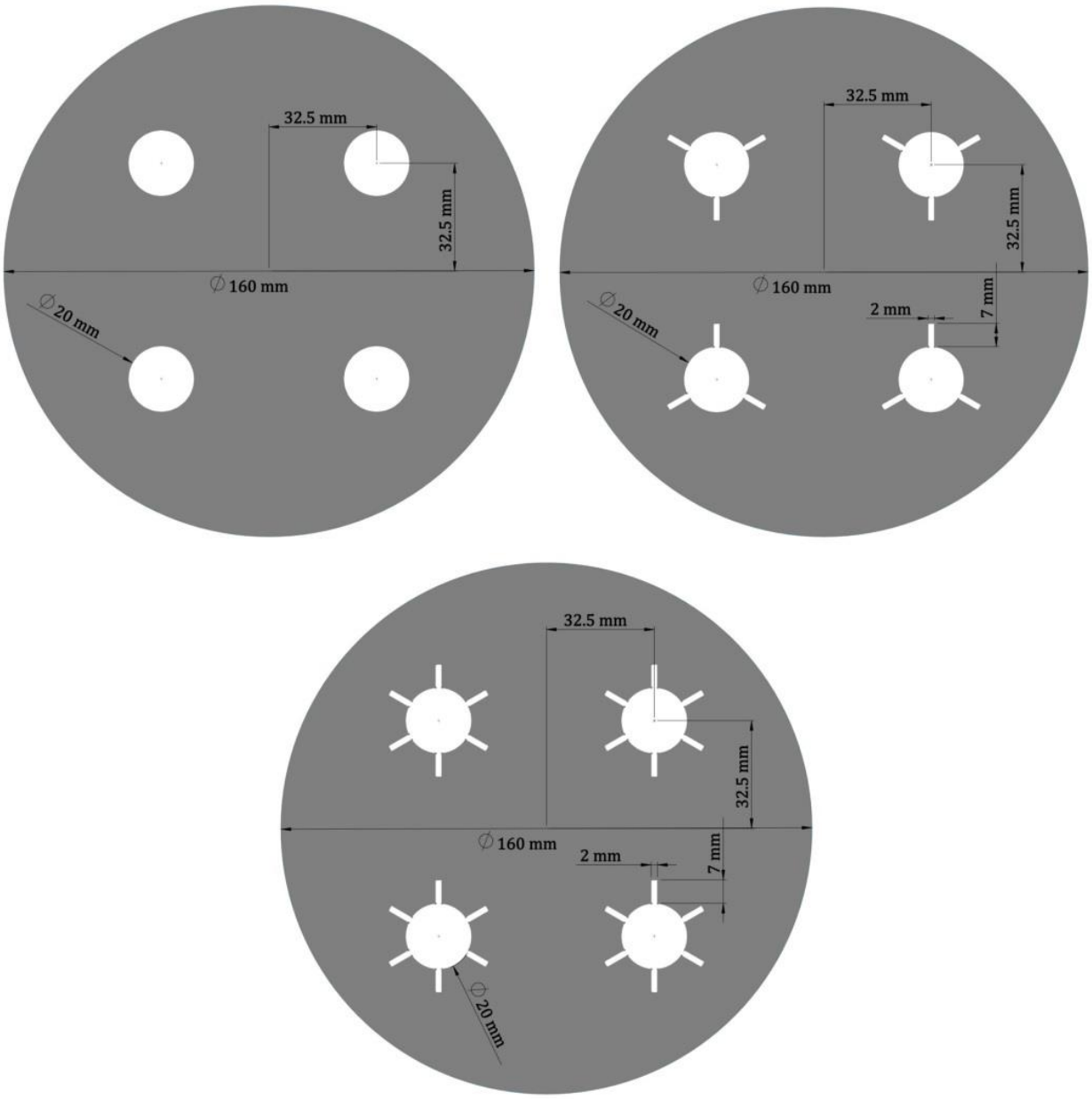

Fig 3.3 Geometrical dimensions of the circular shell PCMHE having circular tubes with 3, 6, and without fins

The dimension of the circular shell is taken as ∅ 160 mm and the dimension of circular tubes is taken as ∅ 20 mm in all configurations of PCMHE. The distance of the center of the tubes from the center of the circular shell is kept at a distance of 32.5 mm horizontally as well as vertically for the uniform melting of PCM and the dimension of the fins are 7×2 mm. All the geometries have been utilized with a fixed surface area to make sure mass conservation among all configurations. The dimensions of the geometries of PCMHE with and without fins are presented in Figure 3.3.

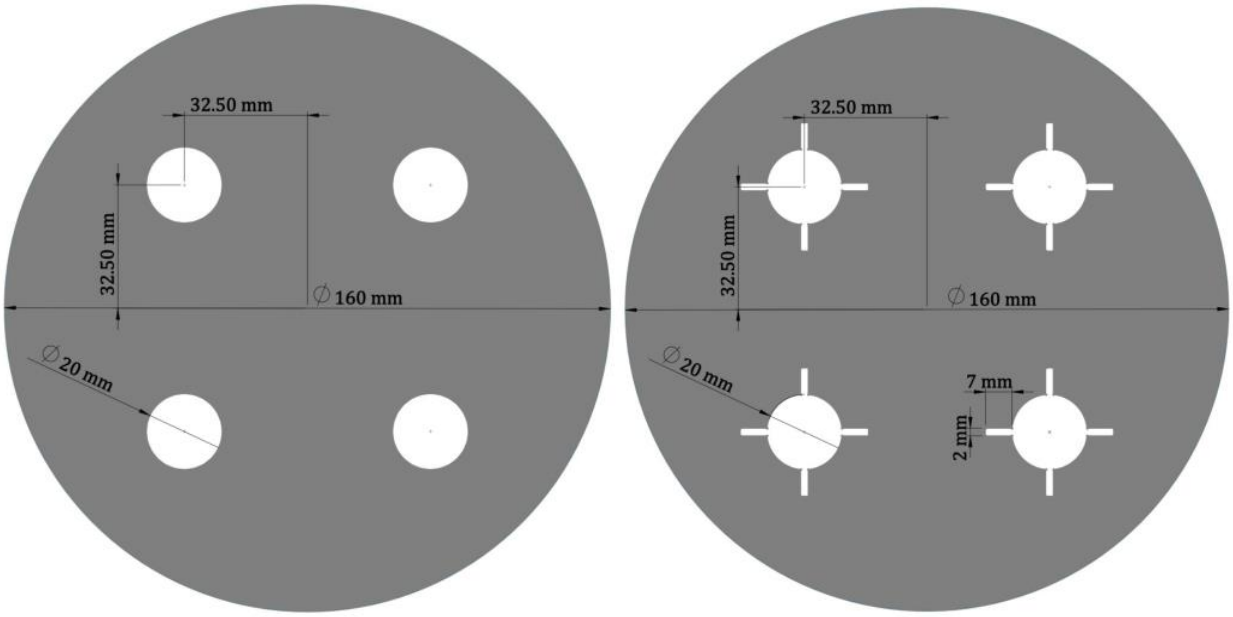

Fig 3.4 Geometrical dimensions of the circular shell PCMHE having circular tubes with 4 and without fins

A different investigation has also been made with circular shell geometries having circular and elliptical tubes. To enhance the heat transmission rate and to reduce the PCM's melting duration, rectangular fins are inserted on the outer surface of the circular and elliptical tubes. The number of fins is also varied to investigate the effect of the number of fins on the circular and elliptical tubes. Six configurations of PCMHE with circular shell geometry are modeled in this geometry. The geometries of PCMHE include circular tubes without a fin, circular tubes with two fins, and

circular tubes with four fins as well as elliptical tubes without a fin, elliptical tubes with two fins, and elliptical tubes with four fins.

The dimensions of the circular shell in all the configurations of PCMHE are taken to be ∅ 160 mm. The dimensions of the tubes of circular, and elliptical shapes are set in such a way that the surface area of the shell should be uniform in all configurations. To keep the surface area constant in all configurations of PCMHE, the dimension of circular tubes is taken as ∅ 20 mm and the dimensions of the elliptical tubes with an ellipticity ratio of 0.6 is taken as 12.91×7.75 mm. The distance of the center of the tubes from the center of the circular shell is kept at a distance of 32.5 mm horizontally as well as vertically for the uniform melting of PCM and the dimension of the rectangular fins is taken as 7×2 mm. All the geometries have been utilized with a fixed surface area to make sure mass conservation among all configurations. The dimensions of the geometries of PCMHE having circular tubes with and without fins are presented in Figure 3.4 and geometries having elliptical tubes with and without fins are presented in Figure 3.5.

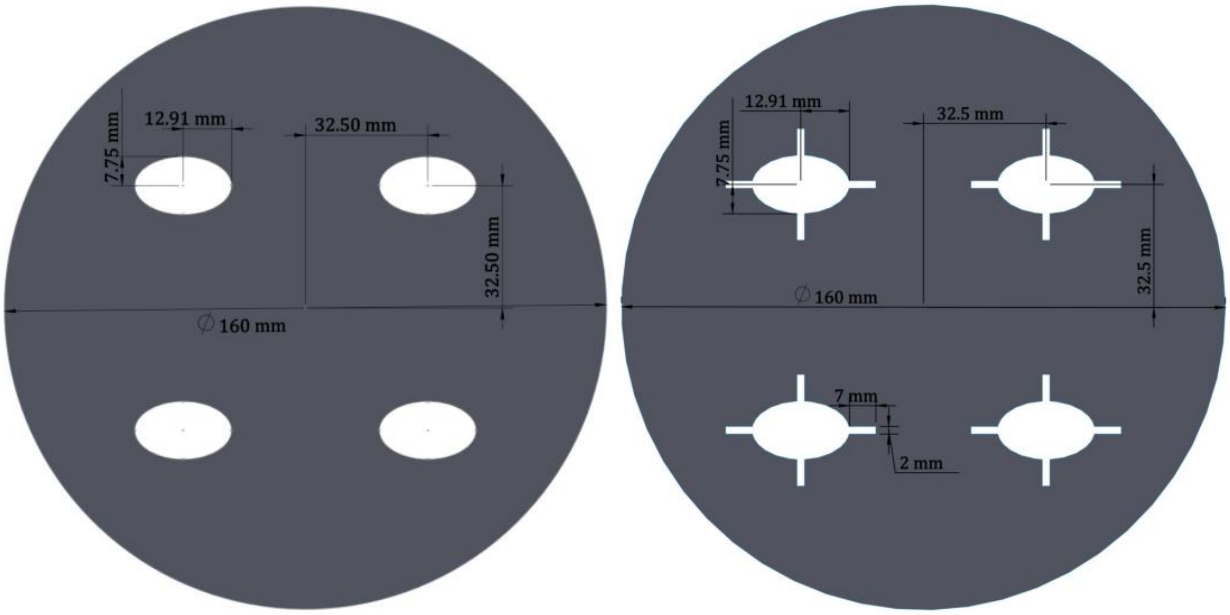

Fig 3.5 Geometrical dimensions of the circular shell PCMHE having elliptical tubes with 4 and without fins

All the geometries of PCMHE modeled in Solid Works saves in IGES format, which lets the model be displayed and modified in Ansys design modeler. The 2D CAD models now be transported in the Ansys Fluent to convert them into FEM by mesh generation of the geometries.

3.3 Mesh Generation

Mesh generation or meshing is an integral part of the engineering simulation process where complex geometries are divided into simple elements that can be used as discrete local approximations of the larger domain. Since meshing typically consumes a significant portion of the time it takes to get simulation results, the better and more automated the meshing tools, the faster and more accurate the solution.

Meshing has a significant role when it comes to the engineering simulation process. Creating a high-quality mesh is one of the most critical factors that should be considered to ensure simulation accuracy. Creating the most appropriate mesh is the foundation of engineering simulations because the mesh influences the accuracy, convergence, and speed of the simulation.

Computers cannot solve simulations on the CAD model's actual geometry shape as the governing equations cannot be applied to an arbitrary shape. Mesh elements allow governing equations to be solved on predictably shaped and mathematically defined volumes. Typically, the equations solved on these meshes are partial differential equations. Due to the iterative nature of these calculations, obtaining a solution to these equations is not practical by hand, so computational methods such as Computational Fluid Dynamics (CFD) and Finite Element Analysis (FEA) are employed.

Generally, finer meshes with smaller elements produce more accurate results. However, adding more elements to a Finite Element Model adds computational expense in two ways:

- More elements mean that more equations need to be solved at each time step, increasing both solution time and memory requirements.
- The results files from these analyses take more disk space to store.

Consequently, areas of high mesh density are restricted to areas of interest in the analysis. ANSYS provides a general-purpose, high-performance, automated, intelligent meshing tool which produces the most appropriate mesh for accurate and efficient solutions.

3.4 Types of Mesh

There are two main element shapes used in structural analysis in Ansys Mechanical, hexahedral (hex) or tetrahedral (tet) elements in 3D as well as triangular (tri) and quadrilateral (quad) in 2D. In 3D, other element shapes such as pyramid or wedge-shaped elements also exist, mainly as transitional elements between tet and hex elements as shown in Figure 3.6.

The ideal element shape for analysis is usually determined by the geometry that is represented in the analysis. In general, it is easier to use tri elements than quad elements in 2D geometries. However, it is up to the user to best judge which element shape will be best for analysis. In this

research work, tri elements are used for the mesh generation of all 2D geometries of PCMHE [62].

Fig 3.6 Common types of mesh

3.5 Meshing of Square Shell Geometries

2D CAD models of square shell PCMHE having circular, square, and elliptical tubes are imported into Ansys Mechanical. After importing into Ansys mechanical, before mesh generation, name selection of the different sections of PCMHE has been done to provide boundary conditions during numerical solution in Ansys Fluent.

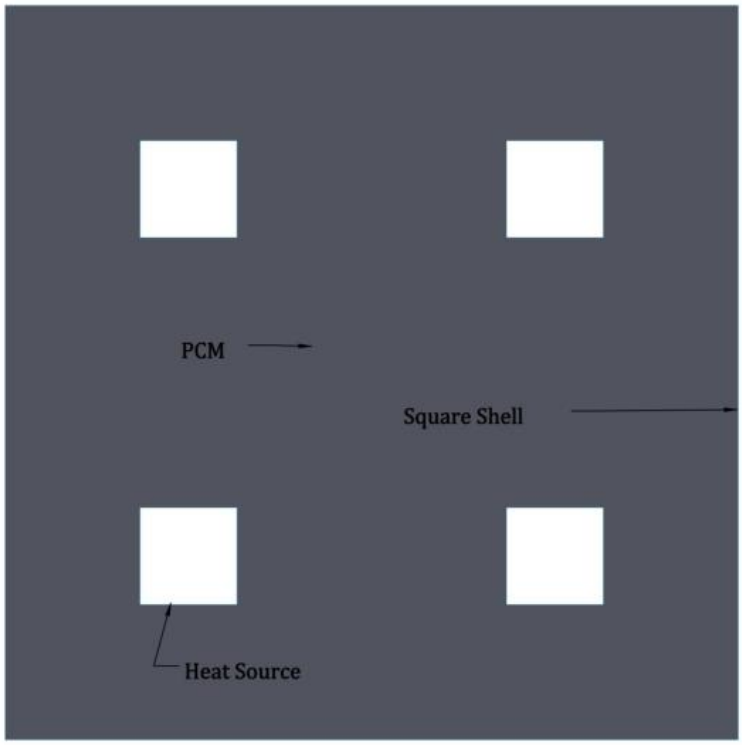

Fig 3.7 Name selection of square shell PCMHE

The outer wall of the heat exchanger is named a square shell to provide adiabatic wall condition, the circular, square, and elliptical tubes are named as a heat source to provide a constant temperature condition, and the area between the outer wall and tubes are named as PCM to provide material properties as shown in Figure 3.7.

After giving the name selection in the Ansys mechanical, mesh generation of the CAD model has been done. Square shell walls and tube walls of the geometries are provided with edge sizing and the area covered by PCM is provided with face sizing. Unstructured triangular elements are used for the mesh generation of all the configurations of the square shell heat exchanger as shown in Figure 3.8. The final mesh of the circular tube geometry of the heat exchanger has 77856 elements, square tube geometry has 76782 elements and elliptical tube geometry has 78066 elements.

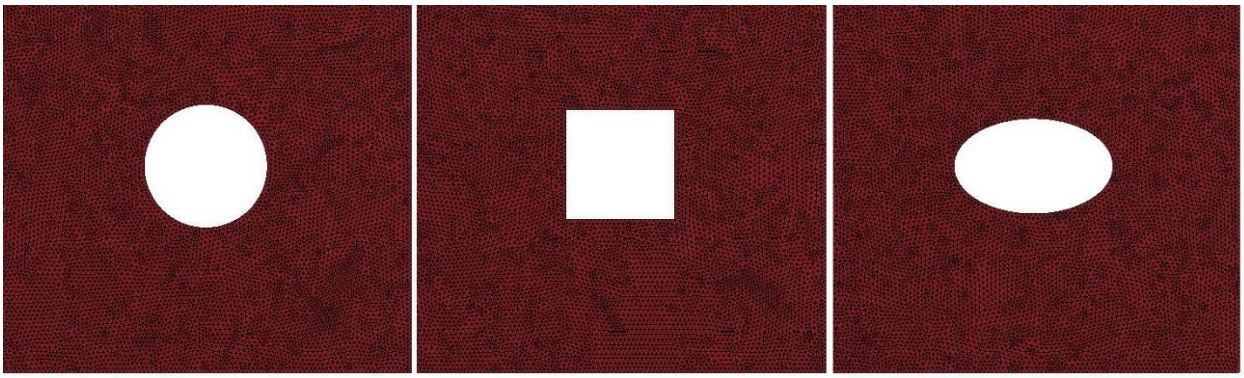

Fig 3.8 Mesh generation of the circular, square, and elliptical tube geometries

The mesh generation of other geometries of square shell PCMHE, which include square tubes without fins and square tubes with four rectangular fins, has also been done after importing into Ansys Mechanical. The name selection of these configurations is the same as in previous geometries. Square shell and square tubes with and without fins are provided with edge sizing and PCM is provided with face sizing with triangular elements for mesh generation of the heat exchanger geometries. The resulting mesh of the square tubes without fin geometry of the heat

exchanger has 73208 elements and square tubes with four fins geometry has 155208 elements as shown in Figure 3.9.

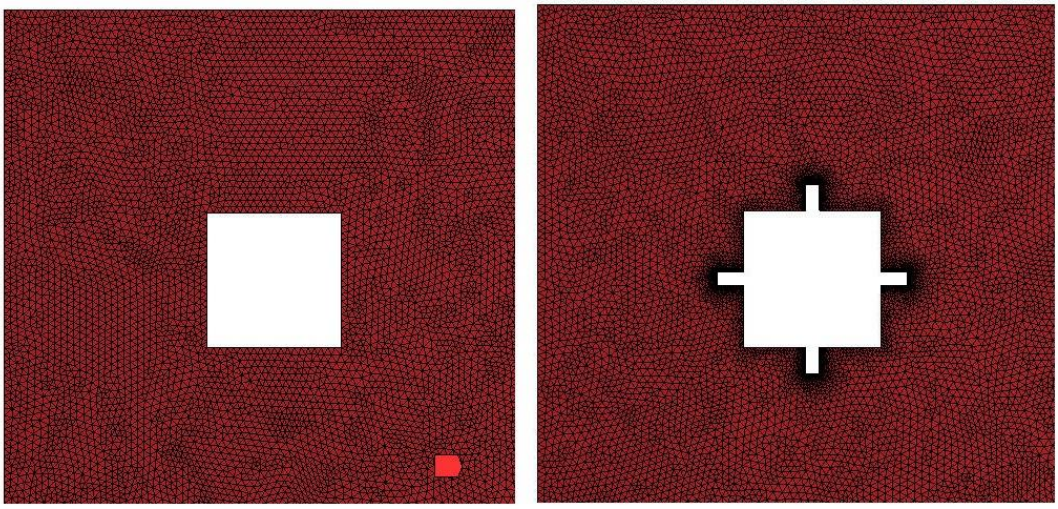

Fig 3.9 Mesh generation of the square tubes without fin and with fins geometries

3.6 Meshing of Circular Shell Geometries

After importing the 2D CAD models of circular shell PCMHE geometries having circular tubes without fins, with three fins, and with six fins into the Ansys mechanical, name selection of the heat exchanger models has been done. The outer wall of the heat exchanger is named a circular shell, the circular tubes are named as a heat source and the area between the outer wall and tubes is named PCM.

After giving the name selection, mesh generation of the heat exchanger geometries has been done. Edge sizing is provided to the circular shell and heat source and face sizing is provided to PCM. Unstructured triangular elements are used for mesh generation of all the geometries of the circular shell heat exchanger as shown in Figure 3.10. The final mesh of the circular tubes without fin geometry of heat exchanger has 39367 elements, circular tubes with three fins geometry has 42942 elements and circular tubes with six fin geometry has 46778 elements. A

well-designed solution adaptive mesh refinement was employed for better prediction of the interior flow field behavior, resulting in a finer for properly anticipating the flow characteristics.

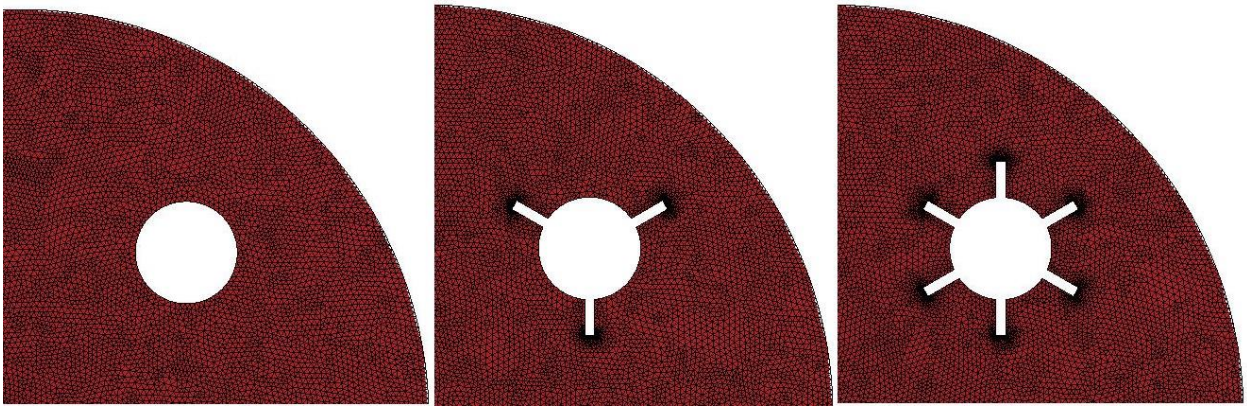

Fig 3.10 Mesh generation of the circular tubes without fin and with fins geometries

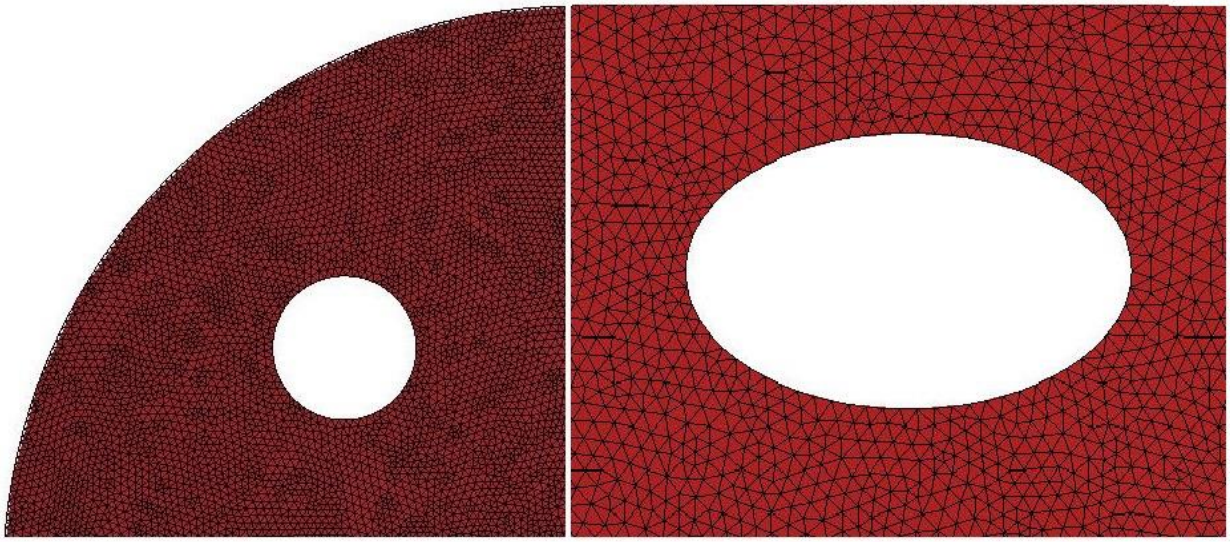

Fig 3.11 Mesh generation of the circular and elliptical tubes without fin geometries

The mesh generation of other geometries of circular shell PCMHE, which include circular tubes without fins, with two fins, and with four fins as well as elliptical tubes without fins, with two fins, and with four fins, has also been done after importing into Ansys mechanical. The name selection of these configurations is the same as in previous geometries. Circular shell and tubes with and without fins are provided with edge sizing and PCM is provided with face sizing with triangular elements for mesh generation of the heat exchanger geometries as shown in Figure

3.11. The resulting mesh of the circular tubes without fin geometry of heat exchanger has 39367 elements, circular tubes with two fins geometry has 42002 elements and circular tubes with four fins geometry has 44182 elements as well as the resulting mesh of the elliptical tubes without fin geometry of heat exchanger has 40001 elements, elliptical tubes with two fins geometry has 42166 elements and elliptical tubes with four fins geometry has 44164 elements.

3.7 Grid Independence Study

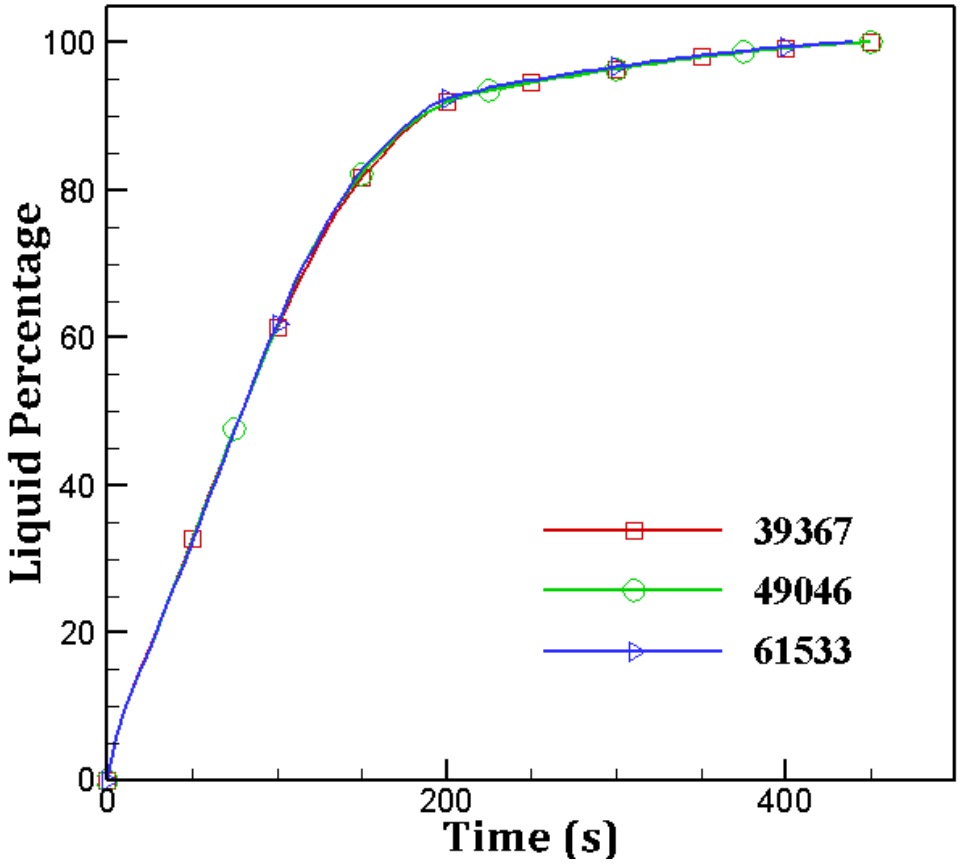

Fig 3.12 Grid independence study of circular tubes without fin geometry

The simulation results were grid-independent due to the use of an unstructured triangular grid, as shown in Figure 3.12. In practice, the accepted grid caused the temperature and liquid percentage measurements to converge regardless of the mesh. The number of elements in the geometry of circular shell PCMHE having circular tubes without fin has been increased from 39,367 to

61533. Furthermore, the mesh refinement of cylindrical tubes with a fixed temperature boundary condition has more focus.

The goal of this meshing approach is to more accurately reflect the physical processes that occur around circular tubes. In terms of the liquid percentage development in the cylindrical shell region, no substantial change has been detected for the configuration of circular tubes without fin as shown in Figure 3.12, maintaining the authenticity of the utilized mesh. As a result, it was discovered that the number of elements 39,367 for the configuration having circular tubes without fins accurately describes the simulation results.

When the mesh generation is completed, the meshed model is transferred to the solution mode using the Mode toolbar. The remaining operations like establishing boundary constraints, describing the properties of fluids, performing the solution, and viewing and postprocessing the results are performed in solution mode.

CHAPTER 4: NUMERICAL ANALYSIS

4 Numerical Analysis

After the mesh generation is completed, the meshed model is transferred to the Ansys Fluent setup and solution mode. In the setup mode of Ansys Fluent, further operations like solver type, time dependency, gravitational acceleration, material properties, boundary conditions, etc. are selected and then the solution is executed.

4.1 General Setups

Pressure-based solver is used in the numerical simulation of all PCMHE geometries. There are two types of solvers in Ansys Fluent (i) Pressure based and (ii) density based. The pressure-based approach was developed for low-speed incompressible flows, while the density-based approach was mainly used for high-speed compressible flows. The pressure-based solver is the widely used solver and it is more suitable for incompressible flows.

Two pressure-based solver algorithms are available in Ansys Fluent, a segregated algorithm, and a coupled algorithm. In the pressure-based solver, the governing equations are solved sequentially i.e. governing equations for the variables are solved one after another. Unlike sequential pressure-based solvers, there is another pressure-based solver which is called coupled solver. In coupled pressure-based solver the momentum and continuity equations are solved simultaneously, as the governing equations are solved in the coupled manner and other scalar equations are solved in a segregated manner. The solution convergence rate is greatly enhanced when compared to the sequential pressure algorithm. But in terms of memory, the coupled needs more memory requirement than the sequential. In a density-based solver, the energy, momentum, continuity, and species transport equations are solved simultaneously.

Steady-state models are based on the assumption that all flow conditions and properties of the system are constant with respect to time. Transient models, however, can handle conditions that

change with time and assess the time-dependent impact on thermal and flow predictions. In the current study, a transient model is selected to see the effect of heat transfer rate on the melting time of PCM.

A 2D numerical simulation has been conducted in this research work, hence gravitational acceleration is given as -9.81 m/s2 in the y-direction which means the gravitational acceleration will work in a negative y-direction (downward direction).

4.2 Selection of Fluent models

Ansys Fluent consists of the following models to provide the solution to the specified problems.

- Multiphase
- Energy
- Viscous
- Radiation
- Heat Exchanger
- Species
- Discrete Phase
- Solidification & Melting
- Acoustics
- Structure
- Potential/Li-ion Battery

4.2.1 Viscous Models

Ansys Fluent consists of the following viscous models based on the characteristics of the fluid flow. The inviscid model specifies the inviscid flow assuming negligible viscosity of the fluid and the laminar model specifies the laminar flow or streamline flow of the fluid characterized by a low Reynold number in which the fluid travels smoothly or in regular paths. All the remaining viscous models in Ansys Fluent specify turbulent flow to be calculated using one of the remaining models according to the flow conditions.

- Inviscid
- Laminar
- Spalart - Allmaras
- k-epsilon
- k-omega
- Transition k-kl-omega
- Transition SST
- Reynolds Stress
- Scale-Adaptive Simulation (SAS)
- Detached Eddy Simulation
- Large Eddy Simulation

In this research work, the movement of the fluid is assumed only during the melting process of PCM due to density difference and so the velocity of PCM is very low. The PCM has a considerable amount of viscosity and has a specific role in the analysis, hence inviscid model cannot be assumed. Due to the very low velocity and considerable viscosity of PCM, Laminar flow is considered for this instigation.

4.2.2 Numerical Models for Solidification & Melting

Fixed grid or continuum model and variable grid or two-phase model are the two main types of computational phase transition models that have been documented in the literature [89]. The foundation of variable grid models is the use of distinct computational fields for solids and liquids or a different set of equations that are connected by transferring terms between stages [90]. The variable grid model was implemented by Ismail et al. [91] and by Gupta and Kumar [92].

The fixed grid model employs an individual computational domain and a set of continuity, energy conservation, and momentum equations that are applied to the whole domain. As a result, fixed grid models are easier to implement and produce reliable results than variable grid models [93]. Therefore, in the literature, fixed grid models are presented more frequently. In the fixed grid mathematical model, the conventional equations are usually revised to account for the latent

heat & velocity transition between liquid & solid states, which are two physical phenomena connected to phase change. The change in velocity happens because liquids behave according to the fluid mechanics equations whereas solids remain static. Modeling of latent heat and modeling of velocity transitions are used to categorize fixed grid models.

The energy equation uses latent heat models that might be based on source term (E-STM), enthalpy (E-EM), or temperature transforming model (E-TTM) [94]. Similarly, there are three basic categories for velocity transition models: switch-off method (SOM), source term method (STM), and variable viscosity method (VVM). The ramped switch-off method (RSOM), the ramped source term method (RSTM), and the Darcy STM are smoother variations of the SOM and STM groups, respectively [93]. Figure 4.1 demonstrate the fixed grid phase transition models, according to the classification of Hu and Argyropoulos [89] as well as Ma and Zhang [93].

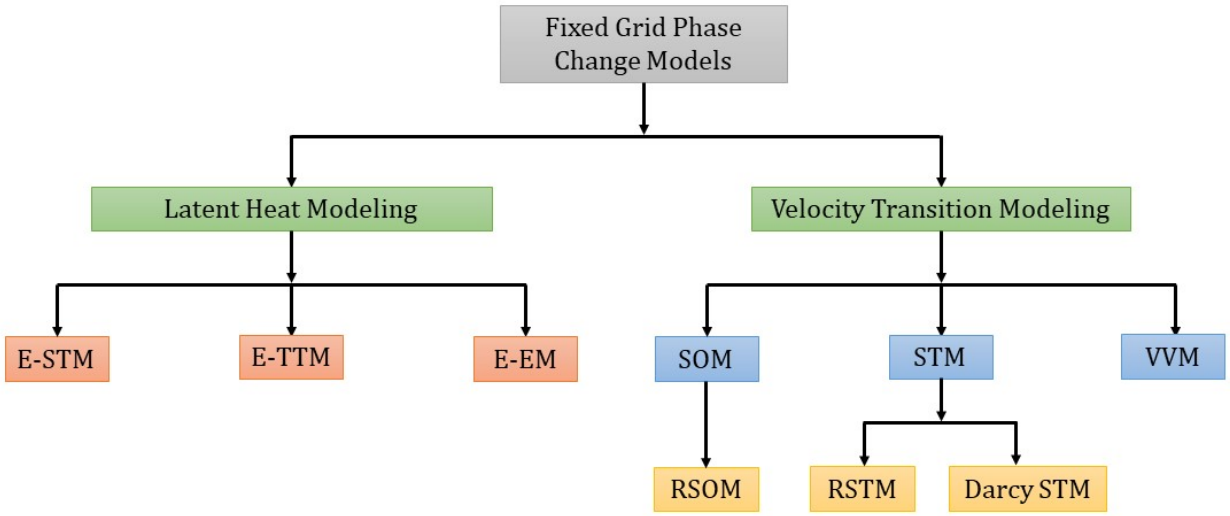

Fig 4.1 Classification of fixed grid phase change models

4.2.2.1 Latent Heat Modeling

Modifications to the energy equation are used to simulate latent heat. Energy equations depending on the temperature as well as specific heat (E-TTM), the use of a source term (E-

STM), and the enthalpy-based energy equation (E-EM) are classified as a result of the equation's modification. The equation for energy conservation can be summarized as follows:

$$\rho c_p \left(\frac{\partial T}{\partial t} + \overrightarrow{V} \nabla . T \right) = \nabla . (k \, \nabla T) \tag{7}$$

where ρ denotes density, c_p denotes specific heat, T denotes temperature, t denotes time, $\vec{V}$ denotes velocity vector, and k denotes thermal conductivity.

Source Term Method (E-STM)

Modeling the latent heat in various ways is made possible by the addition of a source term to the energy equation. According to this approach, the energy equation has an extra source term that is comparable to the latent heat. For illustration, the source term (F) organized by Voller and Swaminathan [95] is displayed in Equation (8)

$$F = -\rho h_L \frac{\partial x}{\partial t} \tag{8}$$

where h_L denotes the latent heat and x denotes the liquid fraction, which ranges between zero (solid phase) and one (liquid phase). When the influence of the component's composition and solubility is taken into account during the phase change analysis, this method can be helpful in the research of metallic alloys [95].

Temperature Transforming Method (E-TTM)

Regarding the temperature method, provided by Morgan [96], the energy equation takes on the fundamental representation depicted in equation (7). A rise in specific heat within the phase transition temperature range is modeled as latent heat. Because E-TTM requires a range of temperatures to simulate the latent heat in the energy equation, the results' precision is constrained when used with isothermal phase transition [97].

Enthalpy Based Method (E-EM)

In enthalpy based method [98,99], the equation for energy conservation takes the form represented in the following equation:

$$\frac{\partial(\rho h)}{\partial t} + \nabla.\left(\rho h\vec{V}\right) = \nabla.\left(k\,\nabla T\right) \tag{9}$$

where h denotes the total enthalpy, which is created by sensible and latent parts. Phase change properties may be simulated using enthalpy-based approaches, including isothermal or continuous properties.

4.2.2.2 Velocity Transition Modeling

The goal of modeling the velocity transition is to explain how the flow of the liquid phase and the static behavior of the solid vary over time. The modifications to the momentum equation can be used to characterize the velocity change. SOM, STM, and VVM are the three primary categories for such modifications. Equation (10) illustrates the momentum equation in its unaltered fundamental form.

$$\frac{\partial\rho\vec{V}}{\partial t} + \nabla.\left(\rho\vec{V}\vec{V}\right) = -\nabla P + \nabla(\mu\,\nabla\vec{V}) + \rho\vec{g} \tag{10}$$

where P denotes the pressure, μ denotes the dynamic viscosity, and $\vec{g}$ denotes the acceleration due to gravity.

Switch-Off Method (SOM)

SOM is based on a relatively easy method to simulate the velocity change between solids and liquids since, in the solid phase, there is no velocity [100]. The velocity modulation function might be executed effectively in the computational code for setting the value of velocity in the control volume to zero with a temperature lower than the phase transition temperature [96]. As

the velocity change occurs as a function of temperature in such approaches, the momentum equation is unaltered. The velocity field may become irregular as a result of SOM, though, and the outcomes may become inconsistent. Through functions to smooth the transition, the ramped switch-off method (RSOM) has been designed to decrease such discontinuities. In order to suppress the solid motion, the functions often utilize numerical coefficients of high value [101].

Source Term Method (STM)

The traditional momentum equation is given a source term (S) in the STM, which assumes a high value whenever the substance becomes solid [93]. In order to achieve equilibrium with the high value of the source term, there is a suppression of velocity in the solid zone in order to solve the momentum equation. It is important to note that velocity field discontinuities can be created using techniques similar to SOM. Similar to RSOM, a method called the Ramped Source Term Method (RSTM) has been created to help with discontinuity issues [101]. Darcy STM suggested by Voller and Prakash [98] is a variation of the RSTM that is commonly regarded as a separate approach because it is primarily used to study phase transition processes. In this approach, the source term depends on Darcy's law to facilitate flow in a porous medium is represented by the equation (11).

$$S = \frac{(1-x)^2}{(x^3+\varepsilon)} C_{mush}(\vec{V} - \overrightarrow{V_p}) \tag{11}$$

where ε is a tiny value (0.001) to avoid dividing by zero, C_{mush} denotes mushy zone constant, and $\overrightarrow{V_p}$ is solid velocity due to the pulling of solidified material out of the domain (also known as pull velocity). C must have a big enough value to both reduce the velocity in the solid phase and enable significant flow in the mushy zone [98].

Variable Viscosity Method (VVM)

The VVM, suggested by Gartling [102] uses the fundamental form of the momentum equation. The main component of it is a rise in the viscosity of the solid phase. Through an increase in the diffusive components in the momentum equation, a solid's higher viscosity causes a drop in velocity. Compared to SOM or STM groups, there is less research utilizing VVM in the literature. Despite the delivery of precise results [100,103], as the solid viscosity value rises, VVM often requires longer computation times [104], posing some potential discretization challenges [100].

4.2.2.3 Numerical Models Used in Literature Regarding PCMs

An appropriate numerical approach combines at least one of each group of approaches outlined in the preceding sections since the solidification & melting process contains latent heat and velocity transition in between stages. The complete phase change models are obtained through the combination of one mathematical approach to latent heat for the energy conservation equation and one mathematical approach for velocity transition for the momentum equation. The most frequent numerical technique combinations are displayed in Table 4.1 among the numerous feasible combinations [105].

Table 4.1 Numerical formulations used in literature for PCMs

		Latent Heat Formulations		
		E-STM	**E-TTM**	**E-EM**
Velocity Transition Formulations	**SOM/RSOM**	[106]	[96]	-
	STM/RSTM	-	-	[107]
	Darcy STM	[98,108,109]	[110]	[16,111-135]

	VVM	[103,104,136,137]	[138–140]	[141,142]

While no literature was discovered that discusses the combination of E-STM and STM, E-TTM and STM, or E-EM and SOM, various research is founded on the pairing of E-EM with Darcy STM. The formulation known as "enthalpy-porosity," which combines E-EM with Darcy STM, has proven to be the most widely applied. However, a number of approach combinations were little investigated, therefore, such combinations represent a large area to be explored.

4.2.2.4 Ansys Solidification & Melting Model

Ansys Fluent may be used to resolve fluid flow issues whether melting and/or solidification occur at a single temperature (for example, in pure metals) or across a wide temperature range (e.g., in binary alloys). Ansys Fluent makes use of an enthalpy-porosity formulation rather than directly following the liquid-solid front. In order to account for the decrease in pressure brought on by the presence of solid material, the solid-liquid mushy zone is considered a porous zone with a porosity equal to the liquid percentage, and the corresponding momentum source factor is added to the momentum equation.

Ansys Fluent models the solidification/melting process using the enthalpy-porosity method in which, the melt interface is not tracked explicitly. Instead, each cell in the domain has a value known as the liquid fraction that represents the portion of the cell volume that is in liquid form. At each iteration, the liquid fraction is calculated using an enthalpy balance.

The liquid percentage ranges from 0 to 1 in the region known as the "mushy zone". The mushy zone is modeled as a "pseudo" porous medium with a porosity that goes from 1 to 0 when the substance solidifies. The porosity is zero when the material has entirely solidified in a cell, which causes the velocities to equally be zero.

The solidification/melting approach is only usable with the pressure-based solver; the density-based solvers do not support it. The solidification/melting model cannot be used for compressible flows.

4.3 Material Properties

After selecting the suitable viscous model and solidification/melting model, material properties have to be defined. The **Materials** task page allows you to set the properties for any fluid or solid materials in the Ansys Fluent simulation. The **Create/Edit Materials** dialog box is used to create and modify materials. Materials can also be downloaded from the global database into the current solver or defined locally. After copying the materials into the current solver, input fields for the properties of the material are set that are required for the active physical models. Input fields are set to define material properties, the physical equations used to compute material properties, and the methods used for each property input. An important step in the setup of the model is to define the materials and their physical properties.

Gallium has been suggested as a PCM because of its higher thermal storage capability and favorable melting temperature for application in a household solar water heating system. Gallium as a PCM also has the advantages of being inexpensive, noncorrosive, and stable across a high number of heat cycles.

The following material properties as well as the physical equation used to compute material properties are defined for Gallium as a PCM in the active physical model of the current solver.

4.3.1 Density

ANSYS Fluent provides several options for definition of the fluid density. The Boussinesq approximation model is selected for defining the density and a constant value of density is

specified. In the Boussinesq approximation model, it is also necessary to set the **Thermal Expansion Coefficient**, as well as relevant operating conditions.

A buoyancy-driven flow is induced due to the force of gravity acting on the density variations. When the density variation is caused by temperature, such buoyancy-driven flows are termed natural convection flows. For many natural-convection flows, the Boussinesq approximation model is used to get faster convergence. Excluding the buoyancy element in the momentum equation, the Boussinesq approximation approach considers density as an unaltered quantity across all calculations.

$$(\rho - \rho_0)\, g \approx -\rho_0 \beta (T - T_0) g \tag{12}$$

where ρ_0 denotes the (constant) density of the fluid, T_0 denotes the operating temperature, and β denotes the thermal expansion coefficient. This expression is created by applying the Boussinesq approximation $\rho = \rho_0(1 - \beta \Delta T)$ to remove ρ from the buoyancy term. This approach is accurate as long as the variations in actual density are minimal; specifically, the Boussinesq approach remains correct if $\beta(T - T_0) \ll 1$. The Boussinesq model should not be used if the temperature differences in the domain are large.

4.3.2 Thermal Conductivity

The thermal conductivity must be defined when heat transfer is active. It is mandatory to define thermal conductivity when modeling energy and viscous flow. ANSYS Fluent provides several options for definition of the thermal conductivity. A constant value of thermal conductivity is provided in this investigation. Thermal conductivity is defined in units of W/m-K.

4.3.3 Specific Heat

The specific heat must be defined when the energy equation is active. ANSYS Fluent provides several options for the definition of the specific heat capacity. A constant value of specific heat is provided in this investigation. Specific heat capacity is input in units of J/kg-K.

4.3.4 Viscosity

As laminar flow is considered in the viscous model, the value of viscosity must be defined in the physical properties of PCM. A constant value of PCM viscosity is provided in the active physical model. Viscosities are input as dynamic viscosity (μ) in units of kg/m-s. ANSYS Fluent does not ask for the input of the kinematic viscosity (ν).

4.3.5 Pure Solvent Melting Heat

Pure solvent melting heat specifies the latent heat for the melting and solidification model. A constant value of latent heat for PCM is provided in this investigation in J/kg.

4.3.6 Solidus & Liquidus Temperature

The solidus temperature is the highest temperature at which an alloy is solid – where melting begins. The liquidus temperature is the temperature at which an alloy is completely melted. At temperatures between the solidus and liquidus, the alloy is part solid, part liquid. The solidification and melting in pure metals take place at one temperature and in binary alloys it takes place over a range of temperatures. As PCM in this investigation is a pure metal, the solidus & liquidus temperatures will be the same. Hence a single and common value is provided for solidus and liquidus temperature in this investigation.

Table 4.2 Thermo-physical properties of pure Gallium

S.N.	Thermophysical Properties	Value
1	Density (ρ)	6093 kg-m^{-3}
2	Coefficient of Thermal Expansion (β)	0.00012 K^{-1}
3	Thermal Conductivity (k)	32 W-m^{-1}-K^{-1}
4	Specific Heat (c_P)	381.5 J-kg^{-1}-K^{-1}
5	Dynamic Viscosity (μ)	0.00181 kg-m^{-1}-s^{-1}
6	Pure Solvent Melting Heat (LH_F)	80,160 J-kg^{-1}
7	Solidus Temperature (T_S)	29.8^{o}C
8	Liquidus Temperature (T_L)	29.8^{o}C

4.4 Mathematical and Numerical Methodology

Simplifying assumptions are commonly employed in computational models to accelerate convergence and enable the solution within a reasonable amount of time. These simplifying assumptions may be applied to boundary constraints, geometry, and materials characteristics.

The implementation of a lesser-sized domain (1D or 2D) and the use of symmetries constraints are two examples of geometrical simplifications that are significant. The first approach requires lesser equations to be addressed, while the latter decreases the size of the domain being solved and subsequently the number of cells. Consequently, by using the mentioned Simplifying assumptions, the cost of computation is greatly reduced [105].

In terms of material characteristics, modifications comprise the assumption that properties are constant in every phase, irrespective of temperature, or even constant in both phases, i.e., there are no differences in properties between solids and liquids. The widely recognized Boussinesq method, which takes into account the density constant throughout all calculations excluding the

body forces component of the momentum equation, is an additional helpful simplification assumption [98]. Convective movements are minimally processed into the model under this assumption.

Usually, boundary constraints are imposed on the PCM container's heat-transferring areas. These conditions include: (i) ignoring the effect of a container's wall thickness; (ii) applying constant temperature throughout time; and (iii) neglecting the impacts of fluid flow outside of the container [105].

4.4.1 Boundary Conditions

Figure 4.2 represents the assumptions taken in this research as well as boundary conditions that apply to all configurations of the physical models.

- The outer surface of the tubes in all of the geometries investigated in this research are kept at a constant temperature. The temperature of 50^{o}C, 60^{o}C and 80^{o}C is selected for PCMHE because practically this range is suitable for domestic solar water heating system.
- The outside wall of the circular and square shell in all configurations is maintained adiabatic. It is assumed that there will no heat transfer from the outer surface of the shell to the surroundings.
- The inner tubes are assumed to be static, as well as PCM motion at the external wall of the tube is assumed to be zero, implying that the tubes' exterior wall is not slipping.
- PCM's initial temperature remained constant at 27°C in all configurations investigated in this research.

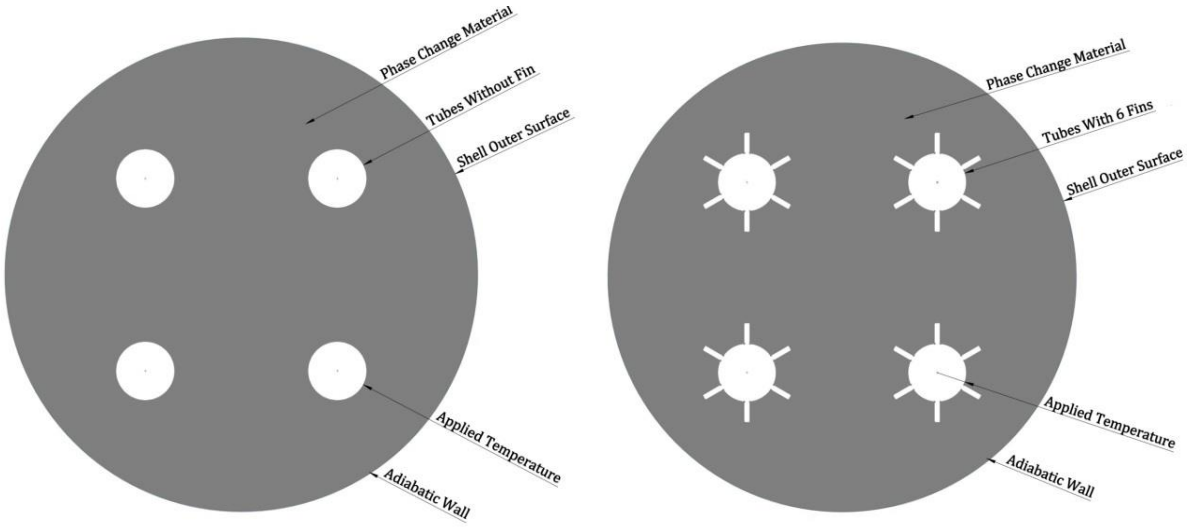

Fig 4.2 Assumptions and Boundary Conditions

4.4.2 Assumptions

When investigating a 2D unsteady modeling, the phenomenon of energy transfer in all configurations of PCMHE includes the following assumptions.

- PCM thermo-physical properties are considered to be constant except for density variations with temperature.
- The PCM has been considered to be incompressible.
- In the buoyancy-driven region, the Boussinesq approximation has been utilized to examine density fluctuations with temperature.
- PCM flows in a two-dimensional and laminar motion in the melting area.
- The effect of the tube wall thickness has been assumed to be negligible.

4.4.3 Mathematical Formulation

The two-dimensional transient velocity field and temperature field of heat exchanger configurations undergoing PCM melting are investigated using continuity, momentum, and

energy equations. Considering the above-said assumptions and taking into account the gravity effect, the resulting equations can be written as follows.

4.4.3.1 Continuity Equation

The equation for continuity is described as follows [79].

$$\frac{\partial \rho}{\partial t} + \nabla.(\rho \vec{V}) = 0 \tag{13}$$

Where ρ is the PCM density and $\vec{V}$ is the two-dimensional velocity vector.

4.4.3.2 Momentum Equation

The momentum expression in a two-dimensional vector form is stated using body force as that of the buoyancy force [79].

$$\frac{\partial \rho \vec{V}}{\partial t} + \nabla.\left(\rho \vec{V} \vec{V}\right) = -\vec{\nabla} P + \nabla.\bar{\bar{\tau}} + \rho \beta \Delta T \vec{g} + S \tag{14}$$

where P is static pressure, ΔT denotes the difference in temperature of PCM, β is the coefficient of volumetric thermal expansion, $\vec{g}$ is the gravity vector's acceleration, and τ is the viscous stress tensor.

Because of the decreased porosity in the mushy region, S stands for momentum source term [79]. In the enthalpy-porosity technique, the mushy zone (partially solidified section) is considered a porous medium. The porosity of each cell is determined by the proportion of liquid in that cell. Because porosity in completely solid zones is zero, velocity in all of these locations is zero.

4.4.3.3 Energy Equation

A representation of the energy equation for PCM melting is shown below [79].

$$\frac{\partial (\rho h)}{\partial t} + \nabla.\left(\rho h \vec{V}\right) = \nabla.(k \nabla T) \tag{15}$$

Where k denotes the thermal conductivity of fluid and h is the enthalpy of fluid per unit mass and is defined as:

$$h = h_S + h_L \tag{16}$$

$$h_S = h_{ref} + \int_{T_{ref}}^{T} c_P dT \tag{17}$$

where h_S denotes the sensible enthalpy, h_{ref} denotes reference enthalpy at the reference temperature T_{ref} and c_P is specific heat.

$$h_L = x \times LH_F \tag{18}$$

where h_L represents the phase change enthalpy that changes during solidification and melting and x is the fraction of liquid that may vary between zero (for a solid) and one (for a liquid). In terms of temperatures, the liquid fraction may be stated as:

$$x = \begin{cases} 0 & if \quad T < T_S \\ 1 & if \quad T > T_L \\ \dfrac{T - T_S}{T_L - T_S} & if \;\; T_S < T < T_L \end{cases} \tag{19}$$

4.4.4 Numerical Formulation

The mathematical CAD models of all configurations of PCMHE in this research have been constructed and utilized to solve the equation that comprises the phase change model. After calculating the temperature and enthalpy field, an enthalpy porosity technique is used to define the phase transformation interface. The CFD code has been designed to account for two-dimensional effects. The development of a 2D model was chosen to minimize computational time and to better simulate the PCM melting process. Instead of directly following the formation of a liquid-solid front, an enthalpy porosity technique is used to describe the phase transformation surface after obtaining the enthalpy field and temperature.

The solidification & melting model is utilized using the Ansys Fluent software together with the PISO method for the pressure-velocity coupling to evaluate the governing equations of the heat exchanger and phase change process. The tube's wall in all geometries is subject to a no-slip condition, assuming that the PCM's velocity at the tube's wall is zero. Additionally, the momentum and energy equations were solved using the QUICK differencing approach, while the pressure correction equations were solved using the PRESTO scheme. Pressure, density, momentum, energy, and liquid fraction all have under-relaxation value factors of 0.3, 1, 0.7, 1, and 0.9, respectively. The convergence requirements are set at 10^{-3}, 10^{-3}, and 10^{-6} for the continuity, momentum, and energy equations, respectively.

4.5 Time Step Independence Study

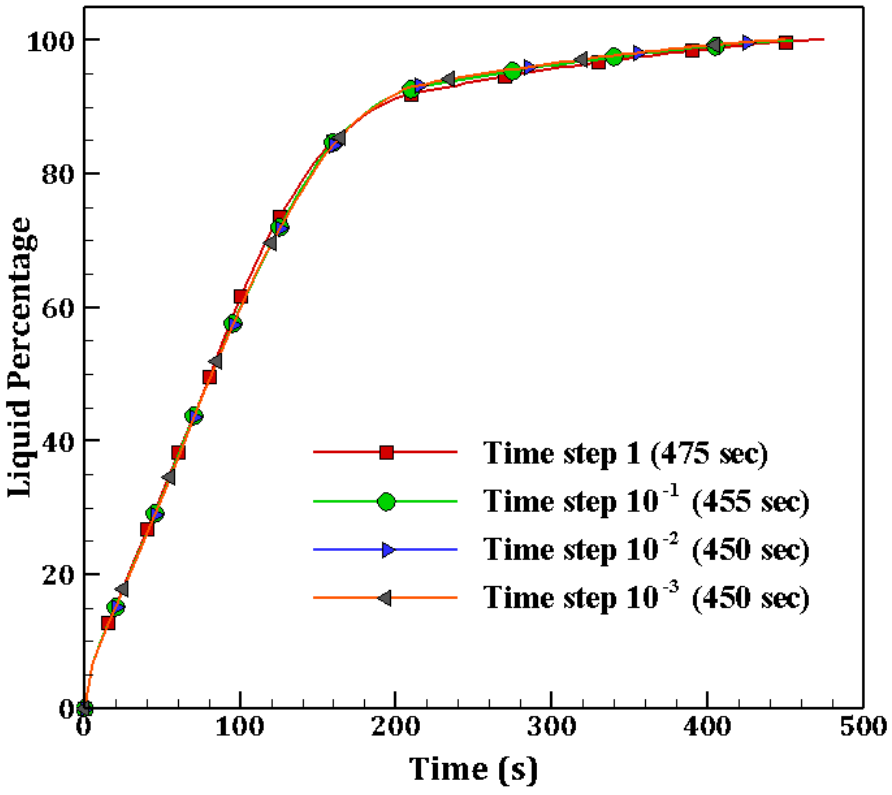

Fig 4.3 Evolution of liquid percentage for different time step sizes

Figure 4.3 illustrates the variation of liquid percentage for different sizes of time step for the selected grid for the geometry having elliptical tubes without fins and Figure 4.4 shows the percentage of PCM converted into liquid for different time step sizes after 200 seconds.

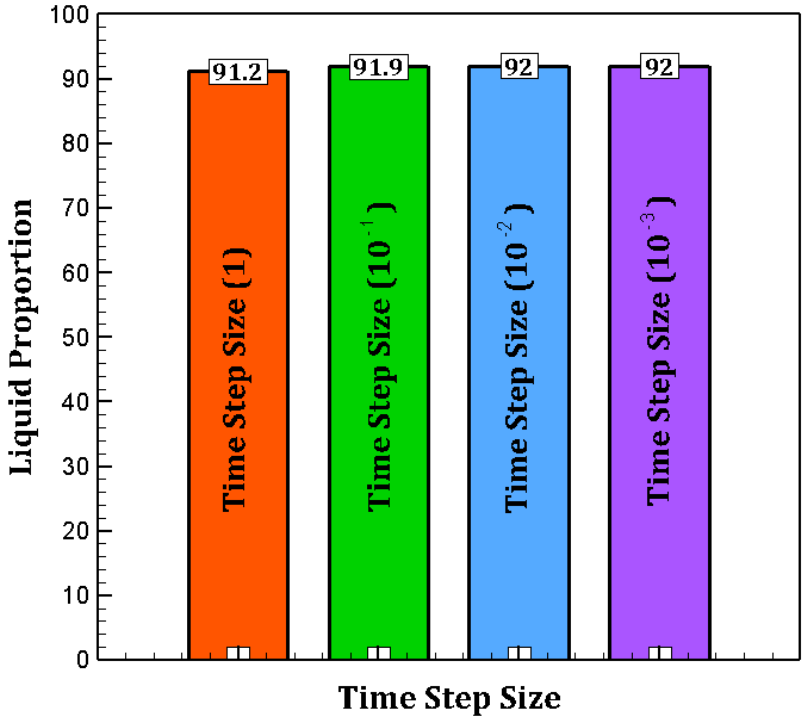

Fig 4.4 Liquid percentage for different time step sizes at 200s

The liquid percentage after 200 seconds is 91.2% for the time step size of 1, 91.9% for the time step size of 10^{-1}, 92% for the time step size of $10^{-2,}$ and 92% for the time step size of 10^{-3}. As shown, the results are almost not changed for the considered time step sizes of 10^{-2} and 10^{-3}. Therefore, 10^{-2} is selected for the size of the time step in this study.

4.6 Validation of Results

The work of Bouhal T. et al. [62], who numerically assessed a 2D CFD simulation to investigate the melting process of Gallium as a PCM filled in a cylindrical cavity having heat sources without fin as well as with four fins and utilizing a fixed temperature of 40^{o}C applied on heat sources, is being utilized to test the validity of the current numerical investigation.

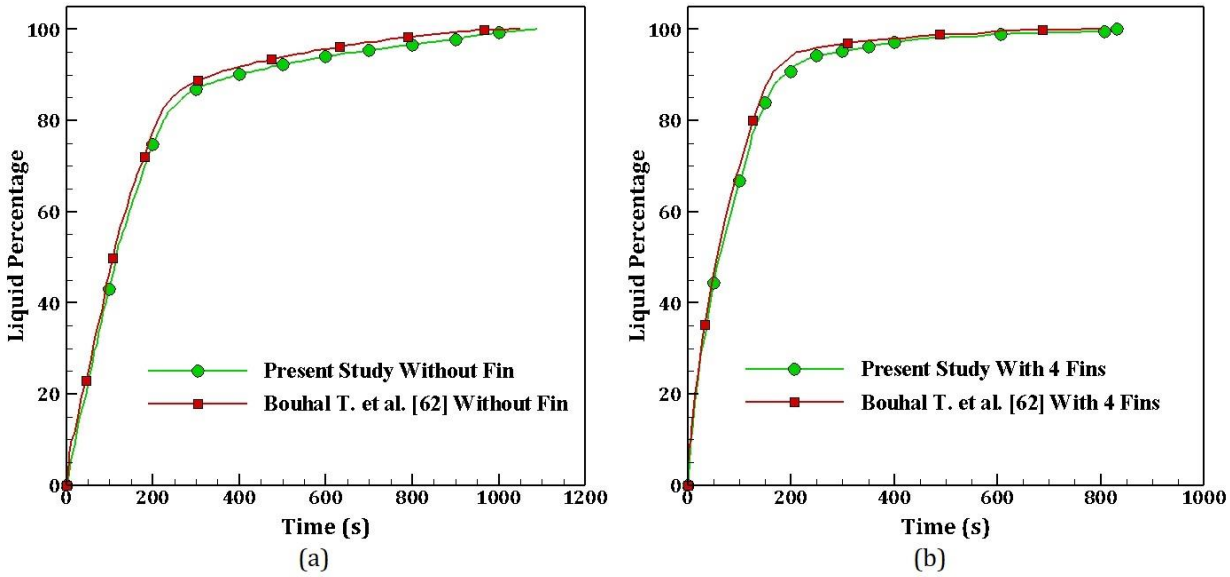

Fig 4.5 Validation of simulated model with Bouhal T. et al. [62] at 40^{o}C (a) without fin geometry (b) with 4 fins geometry

The geometry was replicated in this investigation to ensure that the findings were accurate. The melting time of PCM and development in the liquid fraction of PCM with time were two measures used to assess the study's validity. The validation study's findings are displayed in Figure 4.5 and show good agreement with Bouhal T. et al. [62] numerical data for the development of liquid fraction and melting time of PCM for both configurations without fin geometry and with four fins geometry. In this study, the overall melting time is 1090 seconds for the configuration having no fin and 835 seconds for the configuration having four fins, compared to 1050 seconds and 801 seconds respectively in the previous numerical analysis, suggesting a 3.8 percent and 4.1 percent difference.

CHAPTER 5: RESULTS & DISCUSSIONS

5 Results and Discussions

2D CFD numerical investigation of heat transfer & melting of PCM in different geometries of PCMHE has been performed in this research work. After the execution of the solution of all geometries of PCMHE has been completed, viewing and postprocessing of the results are performed in this section. The analysis of the results of different geometries of PCMHE has been performed according to the shape of the outer shell of the PCMHE.

5.1 Square Shell Geometries with Circular, Square, and Elliptical Tubes

A 2D CFD investigation for the melting of PCM and heat transfer characteristics of the square shell PCMHE having circular, square, and elliptical tubes are analyzed in this study. The variation in the shape of the tubes at a fixed temperature of 60^{o}C applied on the outer surface of the tubes has been utilized for the analysis and the effect of the shape of these tubes on the melting of PCM in terms of liquid proportion and melting time has been analyzed. The melting duration of PCM is 745 seconds for a configuration with circular tubes, 650 seconds for a configuration with square tubes, and 740 seconds for a configuration with elliptical tubes. The duration by the PCM to reach 60^{o}C from the initial temperature of 27^{o}C with a melting temperature of 30^{o}C for a configuration with circular tubes is 800 seconds, for a configuration with square tubes is 725 seconds, and for a configuration with elliptical tubes 770 seconds. Hence it is indicated by the results that the lowest melting time of PCM can be obtained by the heat exchanger having square tubes followed by elliptical tubes and circular tubes at a temperature of 60^{o}C.

The heat transfer phenomenon during PCM melting is investigated using simulation studies to see the impact of the shape of the tubes in the heat exchanger. Melting duration, liquid

proportion, and temperature distribution are all factors to consider in the effect of tube geometry on heat transmission into PCM.

Figures 5.1 and Figure 5.2 demonstrate the contours of liquid proportions evolutions and mean temperature of PCM for a geometry of PCMHE having circular tubes after 30, 85, 235, and 450 seconds. These contours show the progression of the PCM melting behavior in the PCMHE having circular tubes with a fixed temperature of 60^{o}C imposed on the outside surface of the tubes.

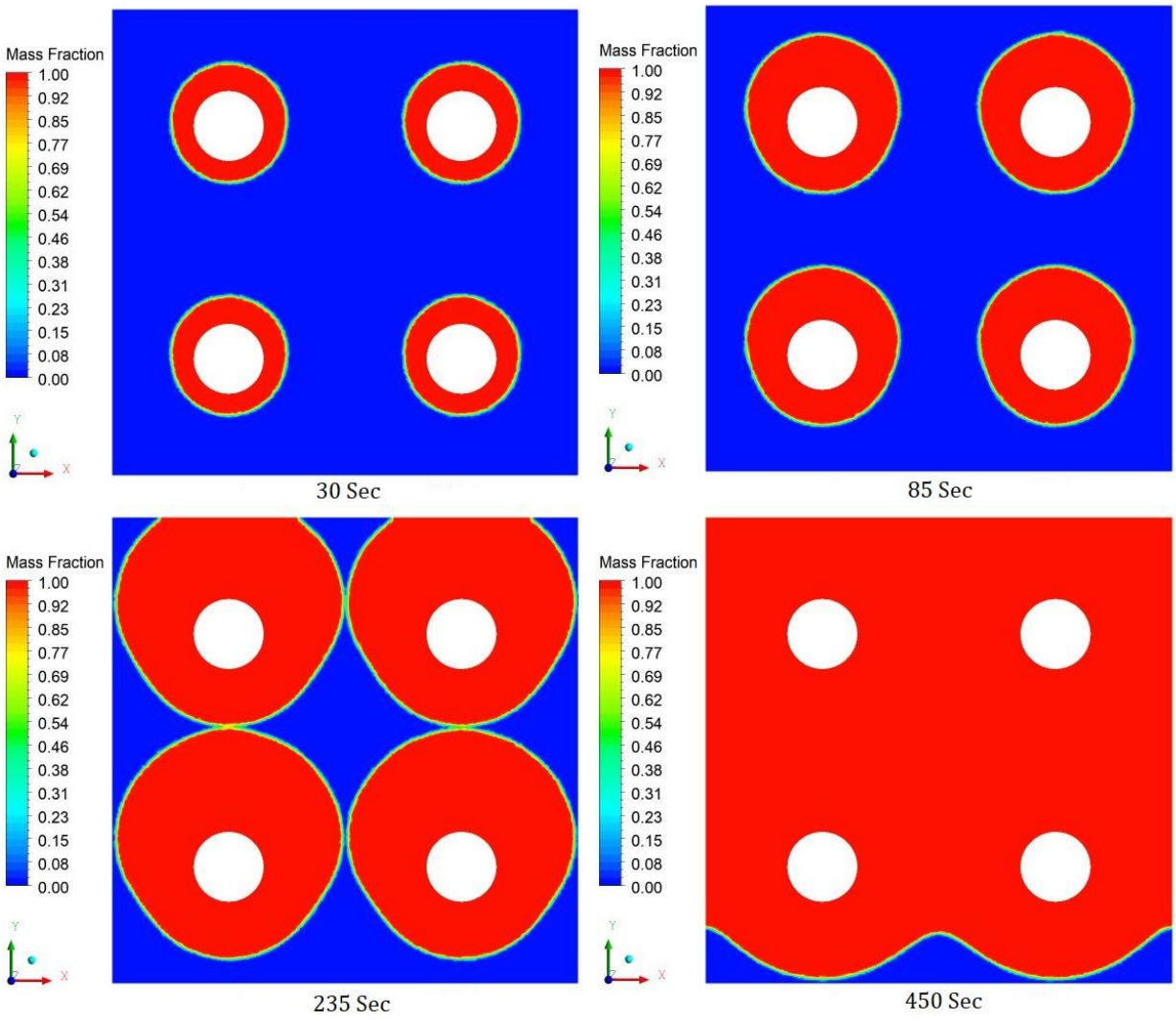

Fig 5.1 Contours of liquid proportion evolution for a configuration having circular tubes

Because of the similarity of the geometry around the axial direction, the melt regions are similar in shape around the circular tubes during the beginning of the melting process, when conduction accounts for the majority of heat exchange in PCM. Heat transmission inside PCM occurs due to free convection after 85 seconds when the majority of the melting around the circular tubes goes upward because of buoyancy effects, as seen in the contours.

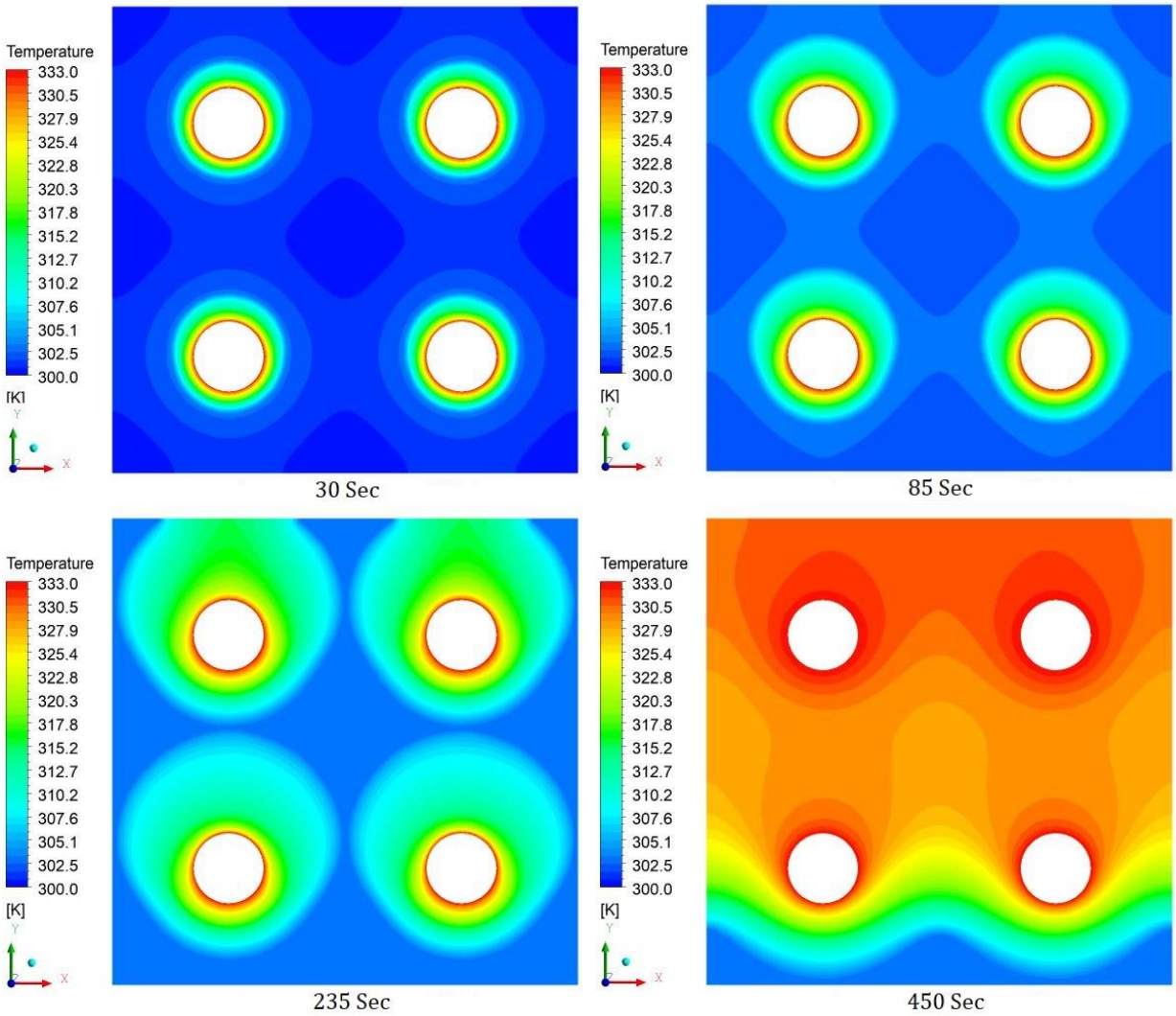

Fig 5.2 Contours of temperature progression for a configuration having circular tubes

Until the four melting regions surrounding the circular tubes haven't come together and created a single melting region having a similar solid-liquid area, each melt zone around the four tubes is initially unaffected by the existence of other melt regions.

The effect of the melting process on the liquid proportion and the solid-liquid interface several times for the configuration of PCMHE having circular tubes is presented in Figure 5.1. The total melting time is 745 seconds for this configuration.

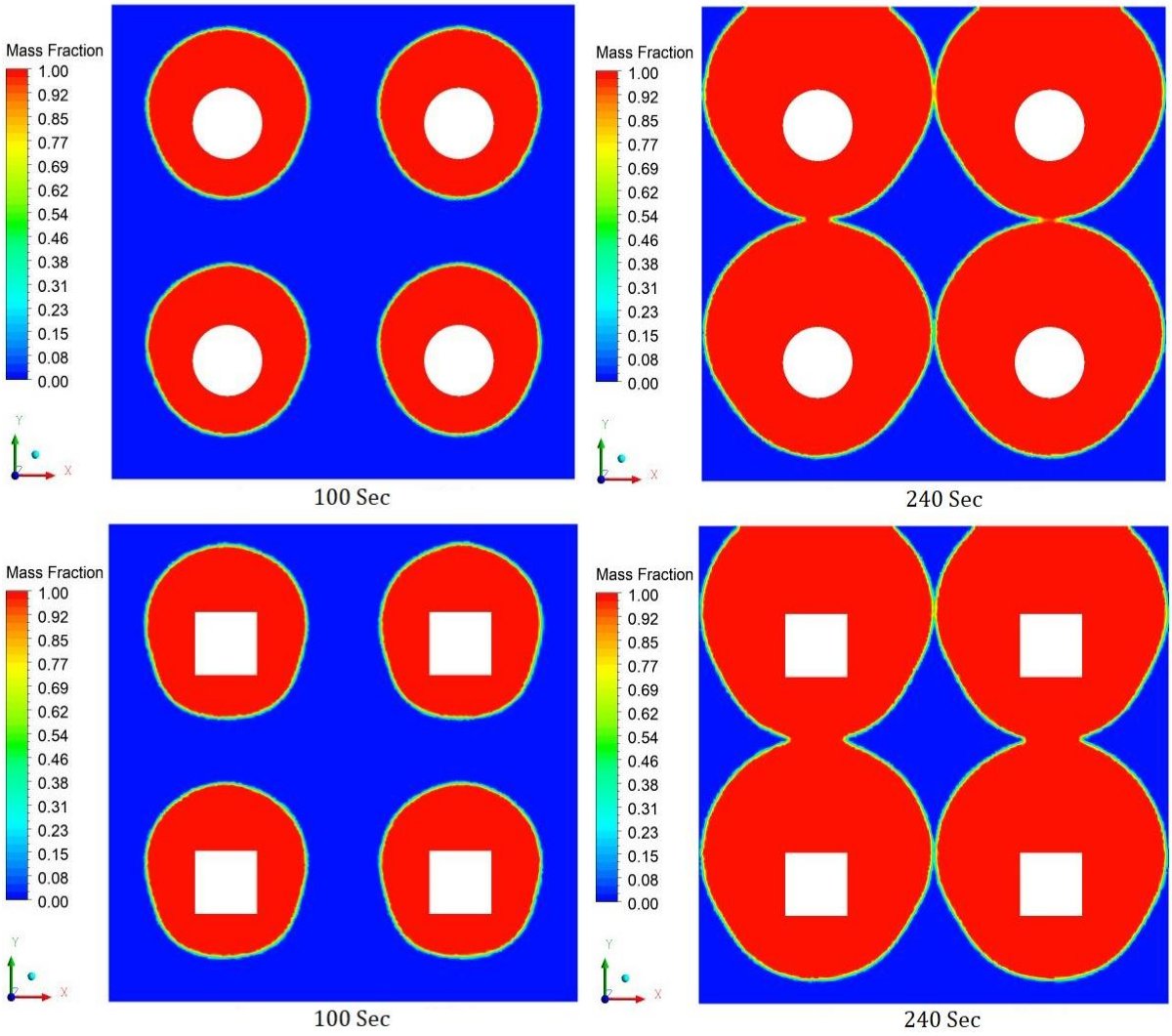

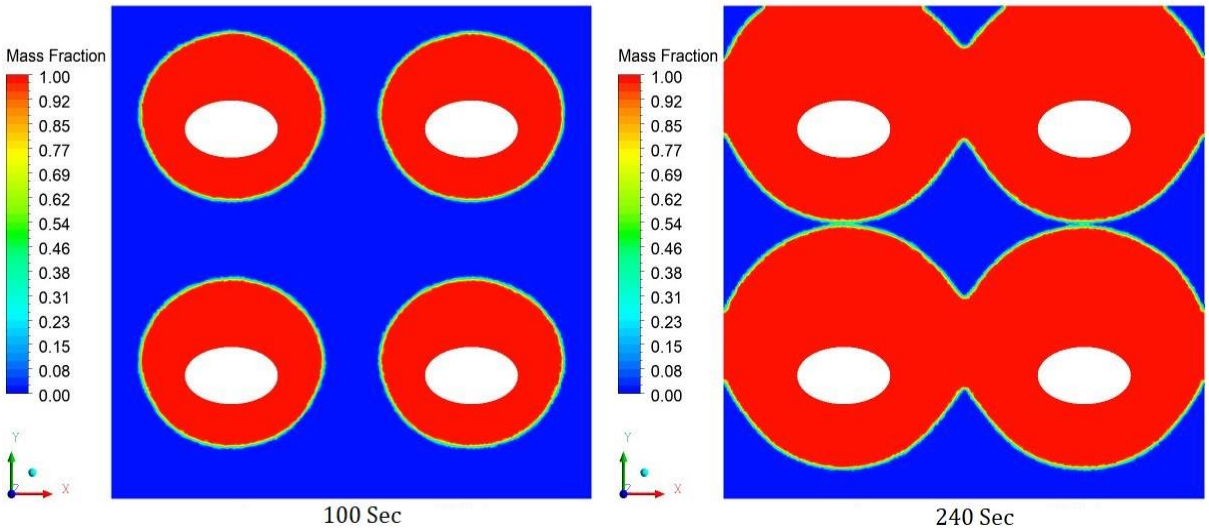

Fig 5.3 Comparison of contours of liquid proportion for all configurations at 100s & 240s

The effect of the melting process on the temperature contours for various times for the configuration of PCMHE having circular tubes is illustrated through the result depicted in Figure 5.2. The total duration by the PCM to reach 60^{o}C is 800 seconds for this configuration.

Figures 5.3 and Figure 5.4 show the comparison of liquid proportion and temperature contours of PCM for all configurations of PCMHE after 100 seconds and 240 seconds. These contour plots examine the influence of tube shape on PCM melting in terms of liquid proportion and mean temperature of PCM with a fixed temperature of 60^{o}C imposed on the external surface of tubes.

The graphs show that the quantity of PCM transformed into liquid after 100 seconds is 34.5 percent in the case of circular tubes, 35.6 percent in the case of square tubes, and 35.5 percent in the case of elliptical tubes. After 240 seconds, the liquid proportion of PCM is 71.5 percent in a circular tube configuration, 73.3 percent in a square tube configuration, and 72.7 percent in an elliptical tube configuration. The temperature of PCM after 100 seconds is 33.1^{o}C in a circular tube configuration, 33.3^{o}C in a square tube configuration, and 33.2^{o}C in an elliptical tube configuration, whereas the temperature of PCM after 240 seconds is 36.4^{o}C in a circular tube configuration, 37^{o}C in a square tube configuration, and 36.8^{o}C in an elliptical tube configuration.

As shown in Figure 5.5, the duration to entirely melt the PCM for a configuration with circular tubes is 745 seconds, with square tubes is 720 seconds, and for a configuration with elliptical tubes is 740 seconds, and the duration by the PCM to reach 60^{o}C for a configuration with circular tubes is 800 seconds, with square tubes is 760 seconds, and with elliptical tubes is 770 seconds.

Figure 5.6 shows the proportion of PCM transformed into liquid as a function of time for all geometries of PCMHE having circular, square, and elliptical tubes. The plot shows that the melting of PCM is uniform in all configurations and the configuration with square tubes has the shortest melting duration of PCM.

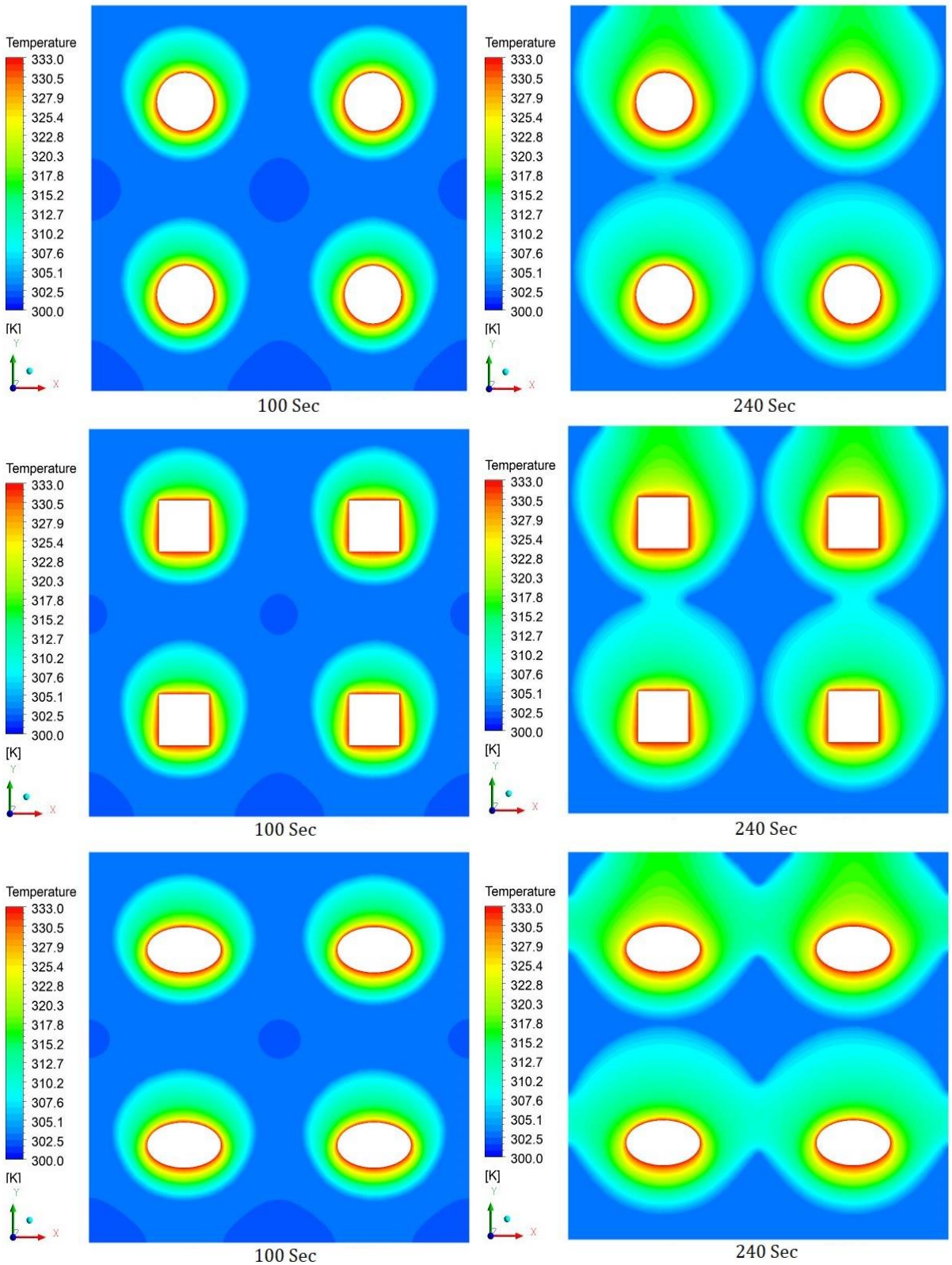

Fig 5.4 Comparison of contours of temperature evolution for all configurations at 100s & 240s

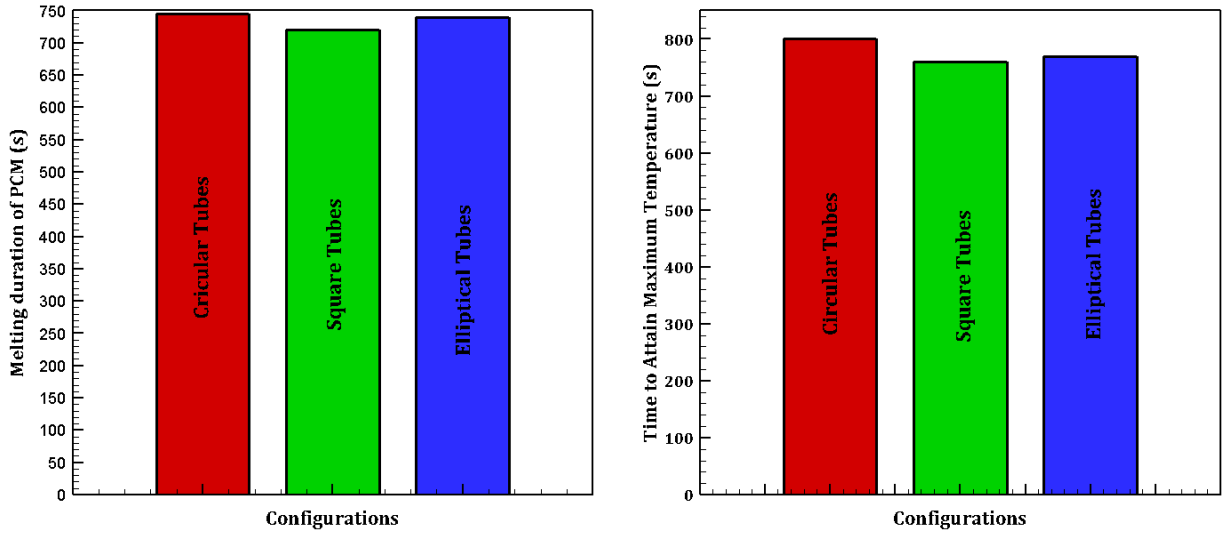

Fig 5.5 Comparison of melting duration & time taken to attain applied temperature for all geometries

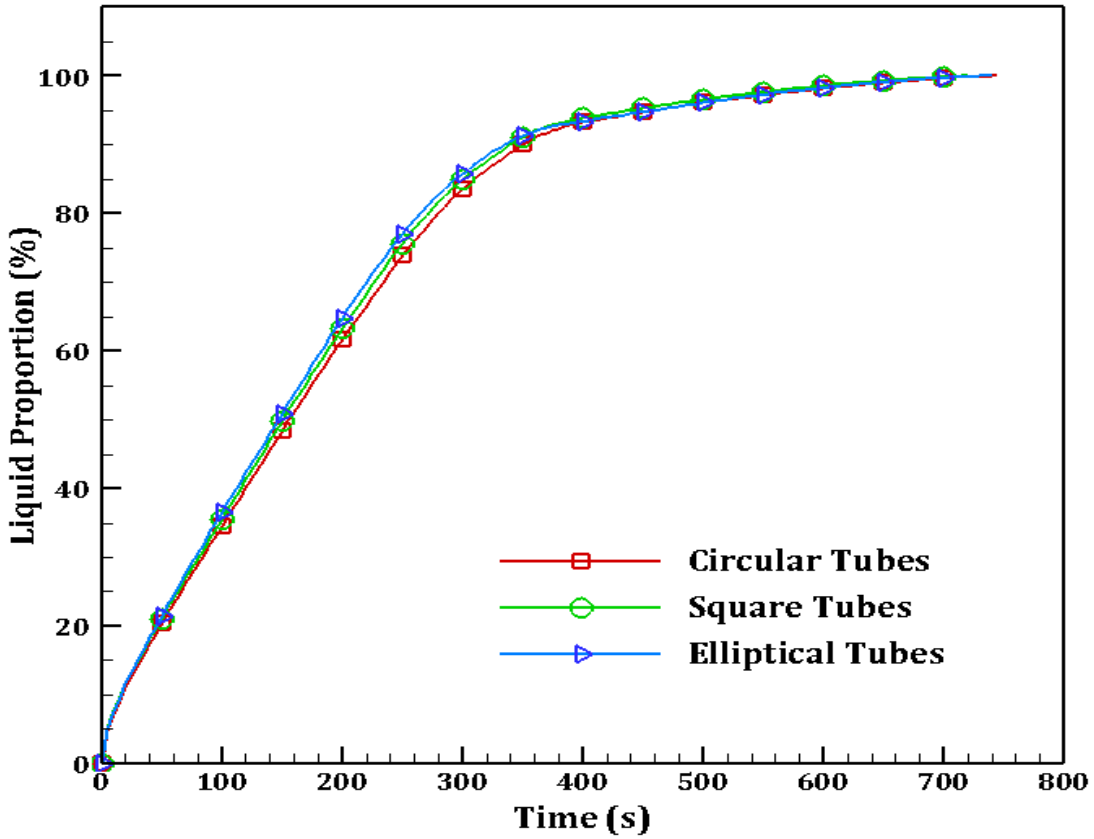

Fig 5.6 Evolution of liquid proportion of PCM with time for all configurations

The temperature evolution of PCM has been monitored inside the square shell cavity for all configurations of PCMHE having circular, square, and elliptical tubes as presented in Figure 5.7.

It has been observed from the plot that the rise in temperature of PCM between 30^{o}C and 35^{o}C near melting temperature is very slow because most of the heat has been utilized in melting the PCM rather than increasing the temperature of PCM. The increase in the mean temperature of PCM rises rapidly after that up to 55^{o}C because most of the heat after the melting of PCM is utilized to increase the temperature of PCM. After 55^{o}C the rise in temperature again goes down because of the very short temperature difference between PCM and heat source.

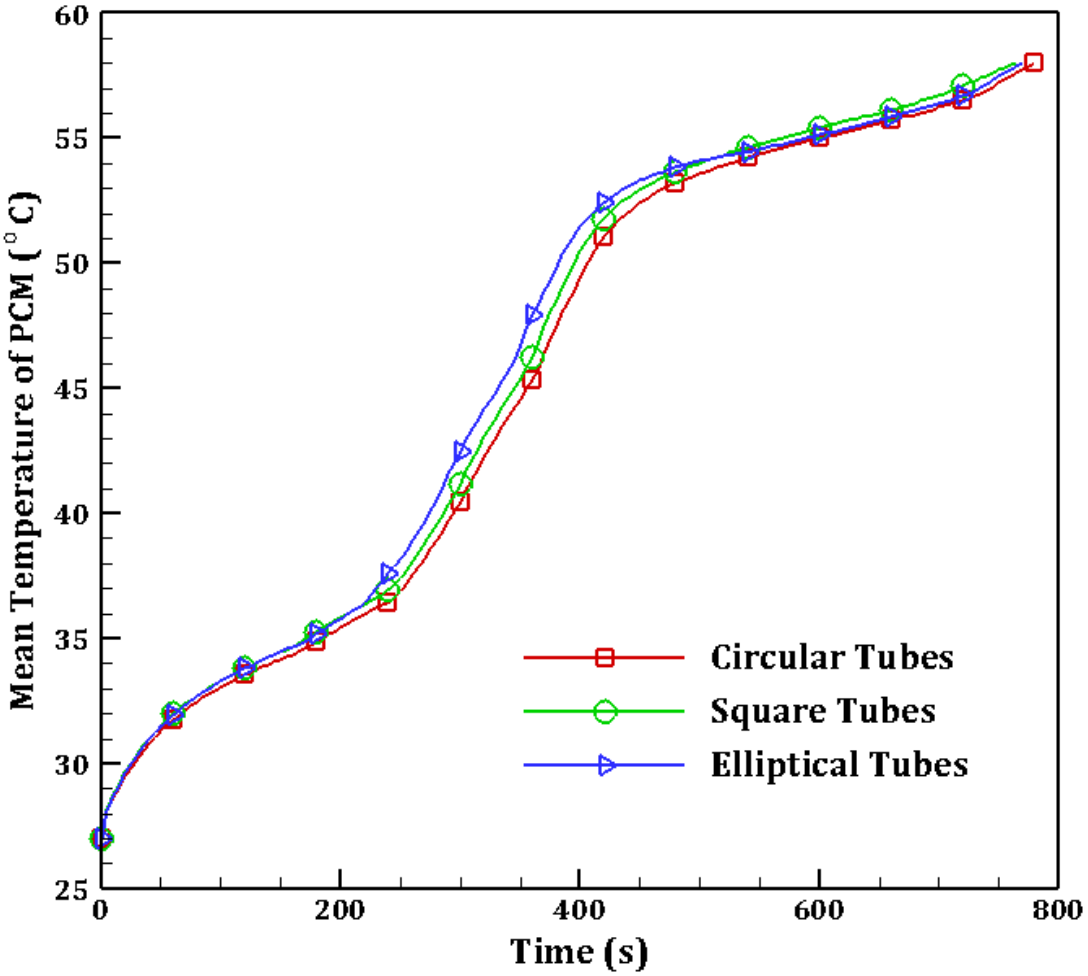

Fig 5.7 Evolution of mean temperature of PCM with time for all configurations

5.2 Square Shell Geometries having Square Tubes with & without Fins

A different investigation has also been made in square shell geometries having square tubes. In this investigation, a PCM-filled square shell heat exchanger has been selected, and four square

tubes are inserted in the shell. As a TES material, Gallium is employed as a PCM for conserving thermal energy. To investigate the PCM melting process and optimize the shape of the square tubes within the shell, a CFD simulation has been performed.

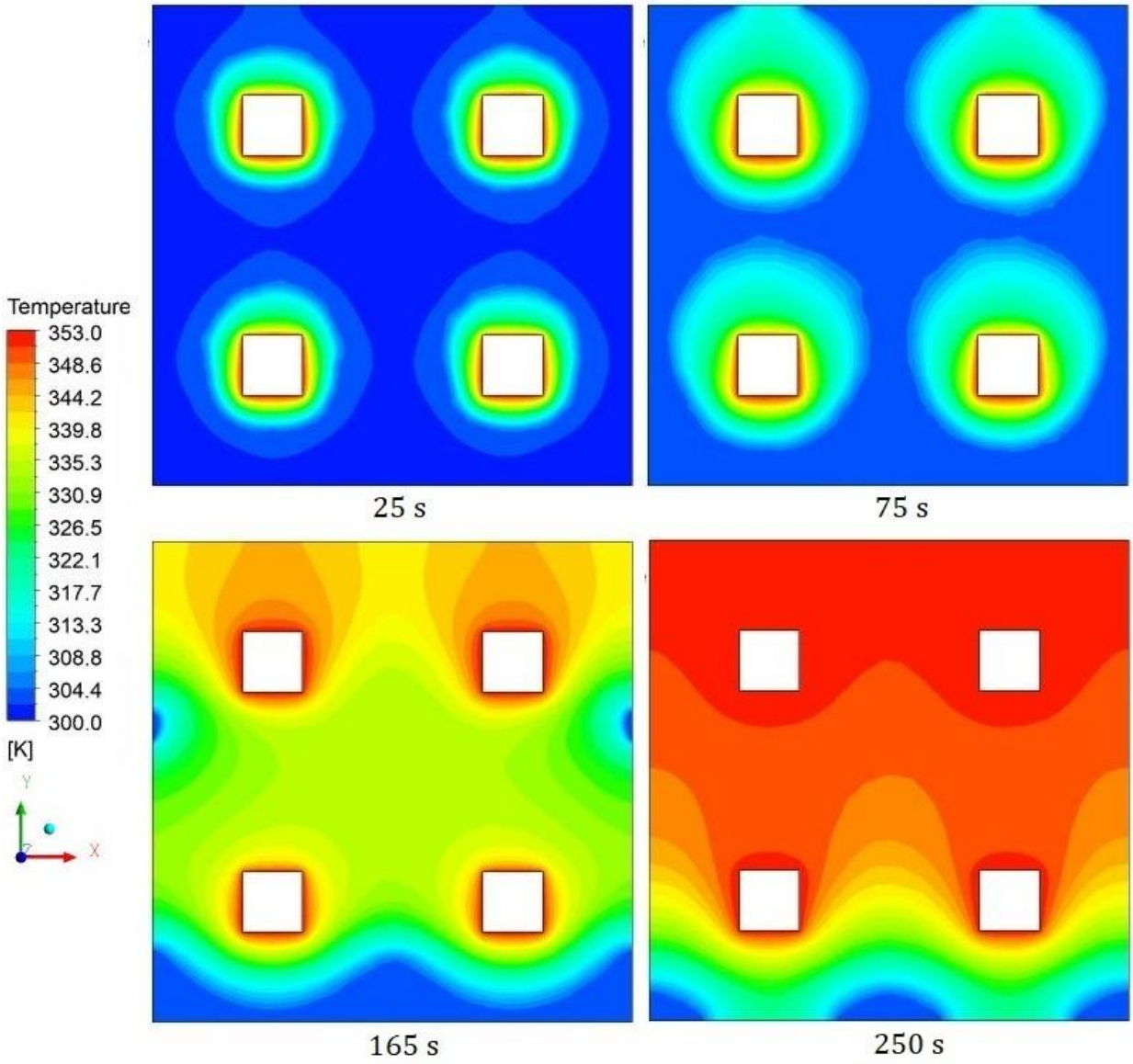

Fig 5.8 Contours of temperature evolution for a configuration having square tubes without fins

Two geometries of PCMHE having square tubes without fins and with four fins, are employed to examine the impact of the fin integration on square tubes on the transmission of heat and PCM melting. The purpose of this study is to increase heat transmission in PCM by optimizing the

geometry and to evaluate the outcomes in terms of liquid percentage at an applied tube temperature of 80^{o}C.

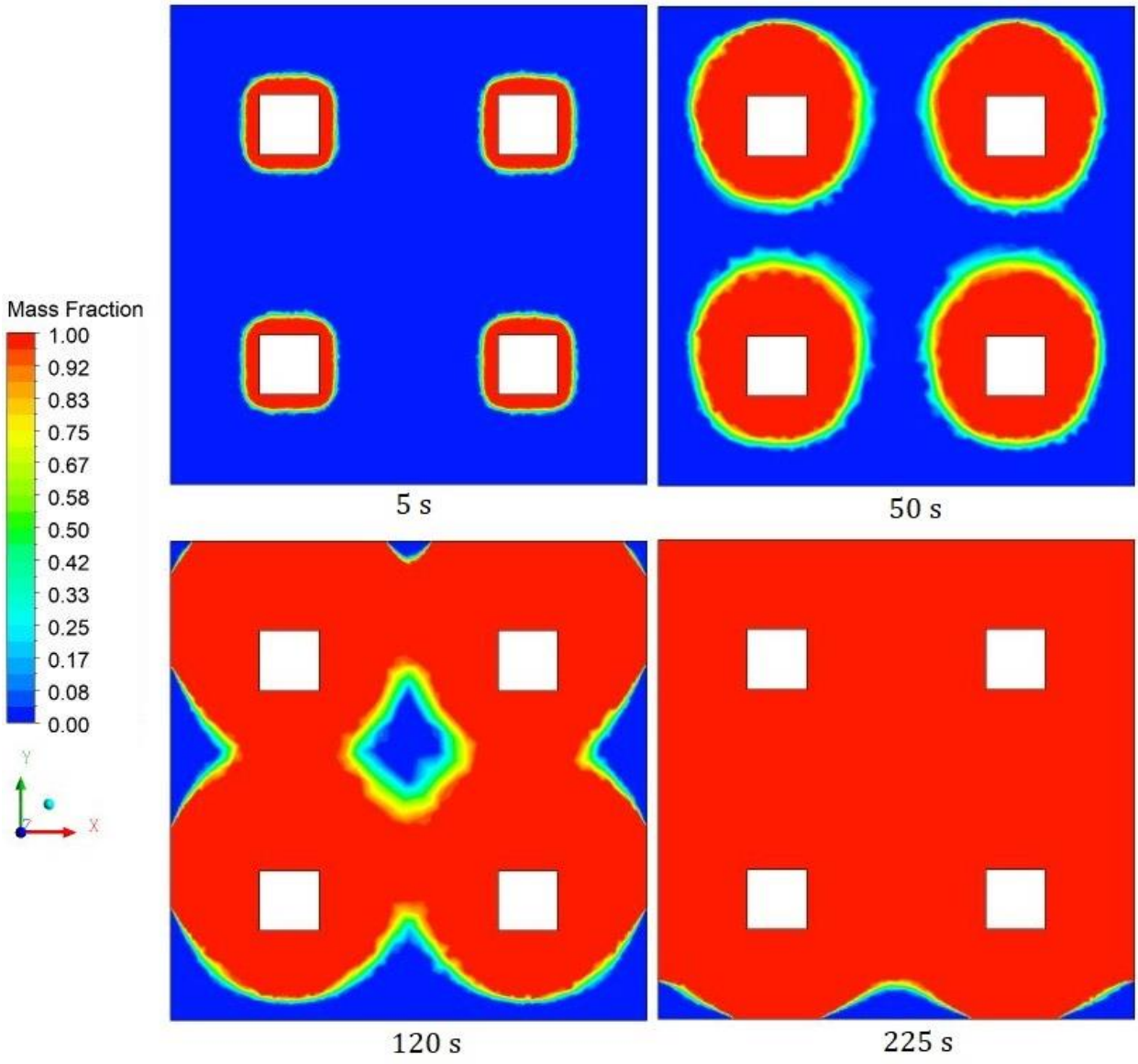

Fig 5.9 Contours of liquid proportion evolution for geometry having square tubes without fin

The contours of the temperature profile of PCM for the geometry of PCMHE having square tubes without fins for 25 seconds, 75 seconds, 165 seconds, and 250 seconds and contours of liquid proportions for the geometry of PCMHE having square tubes without fins for 5 seconds, 50 seconds, 120 seconds and 225 seconds are illustrated in Figure 5.8 and Figure 5.9. These contour plots present the evolution of the melting phenomenon of the PCM and temperature

contours for the geometry of PCMHE having square tubes without fins where a constant temperature of 80^{o}C is applied on the outer surface of the square tubes. It is clear from the contour plots that at the start of the melting of PCM when most of the heat transfer in PCM is due to conduction, the melt zones are identical in shape around the tubes because of the symmetry of the geometry of the axis.

It can be seen from the plots that after 50 seconds, heat transfer within the PCM occurs due to natural convection, and most of the melting occurs around the tubes going upward due to the gravity effect and Boussinesq approximation. Initially, each melt zones around the four tubes are not influenced by the presence of other melt zones as long as all four melt zones around the tubes have not merged and created one common melt zone with a common solid-liquid region.

The temperature contours for the melting process of PCM at several times for the geometry of PCMHE having square tubes without fins is presented in Figure 5.8 and the liquid proportion evolution contours for melting of PCM at different times for geometry without fins are shown in Figure 5.9. The time taken to completely melt the PCM for this configuration is 310 seconds.

The contours of liquid proportion for the geometry of PCMHE having square tubes with four fins are compared with the geometry without fins after 25 seconds and 100 seconds and temperature contours are compared for 50 seconds and 150 seconds and illustrated in Figure 5.10 and Figure 5.11. These contour plots compare the evolution of the melting process of PCM in terms of liquid proportion for the geometry of PCMHE having square tubes with four fins where a constant temperature of 80^{o}C is imposed on the outer surface of the tubes. In addition, these plots compare the effect of square tube geometry on the melting time of PCM. It can be seen from the plots that when the melting of PCM starts, conduction is dominant and the melt zone around the

tubes is identical. But the heat transfer in PCM due to convection starts after 50 seconds in the configuration without fins and 40 seconds in the configuration with four fins.

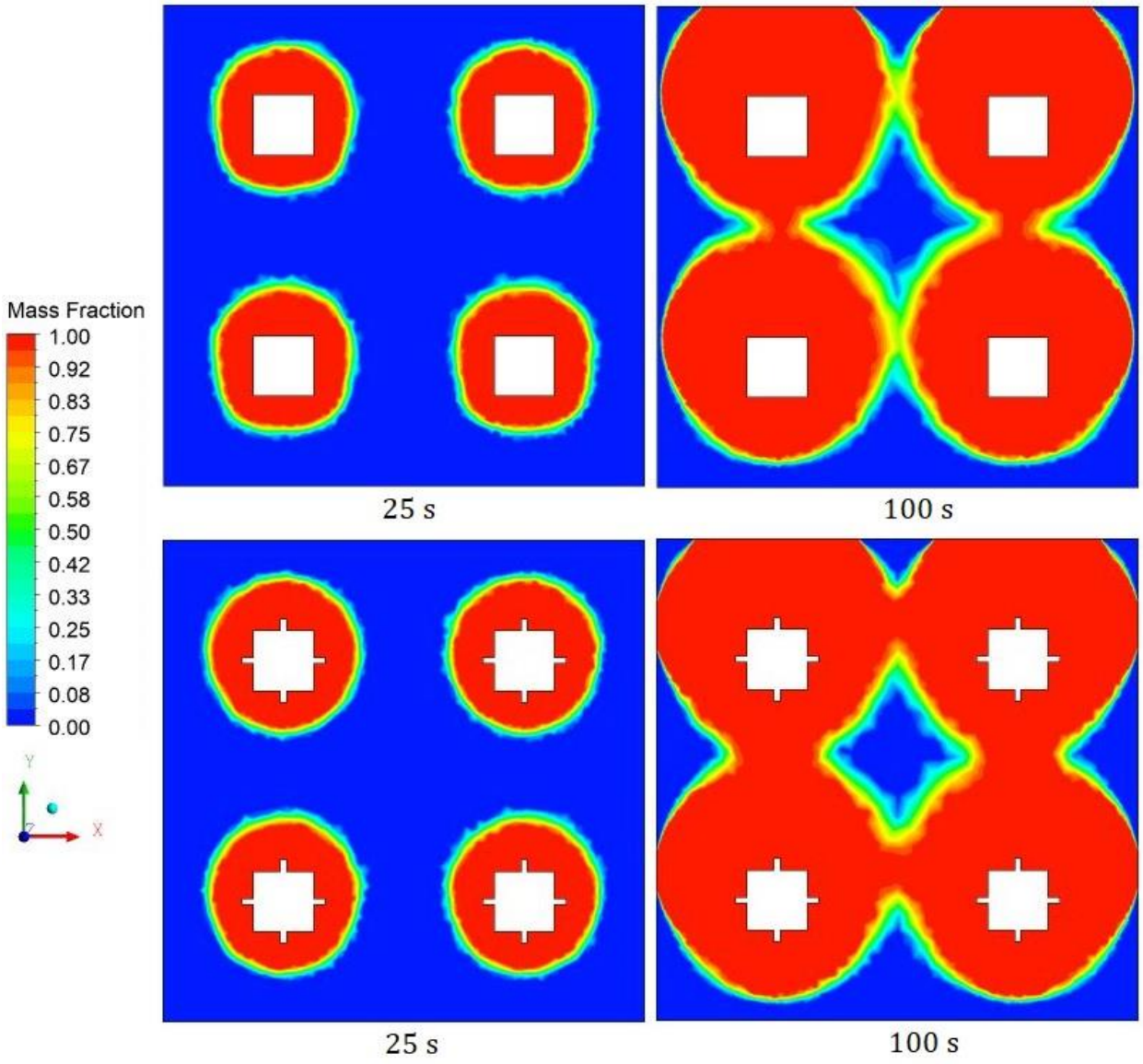

Fig 5.10 Comparison of the liquid proportion's contours for both geometries at 25s and 100s

After 25 seconds, there is a 31.4% conversion of PCM into liquid in the configuration without fins and a 43.6% conversion in the configuration with 4 fins. On the other hand, the liquid percentage of PCM is 61.1% in the geometry without fins and 72.5% with four fins after 100 seconds. The temperature of PCM after 50 seconds is 39.8^{o}C in configuration without fins and

45.7^{o}C in configuration with four fins. Whereas the temperature of PCM after 150 seconds is 54.8^{o}C in configuration without fins and 61.2^{o}C in configuration with 4 fins.

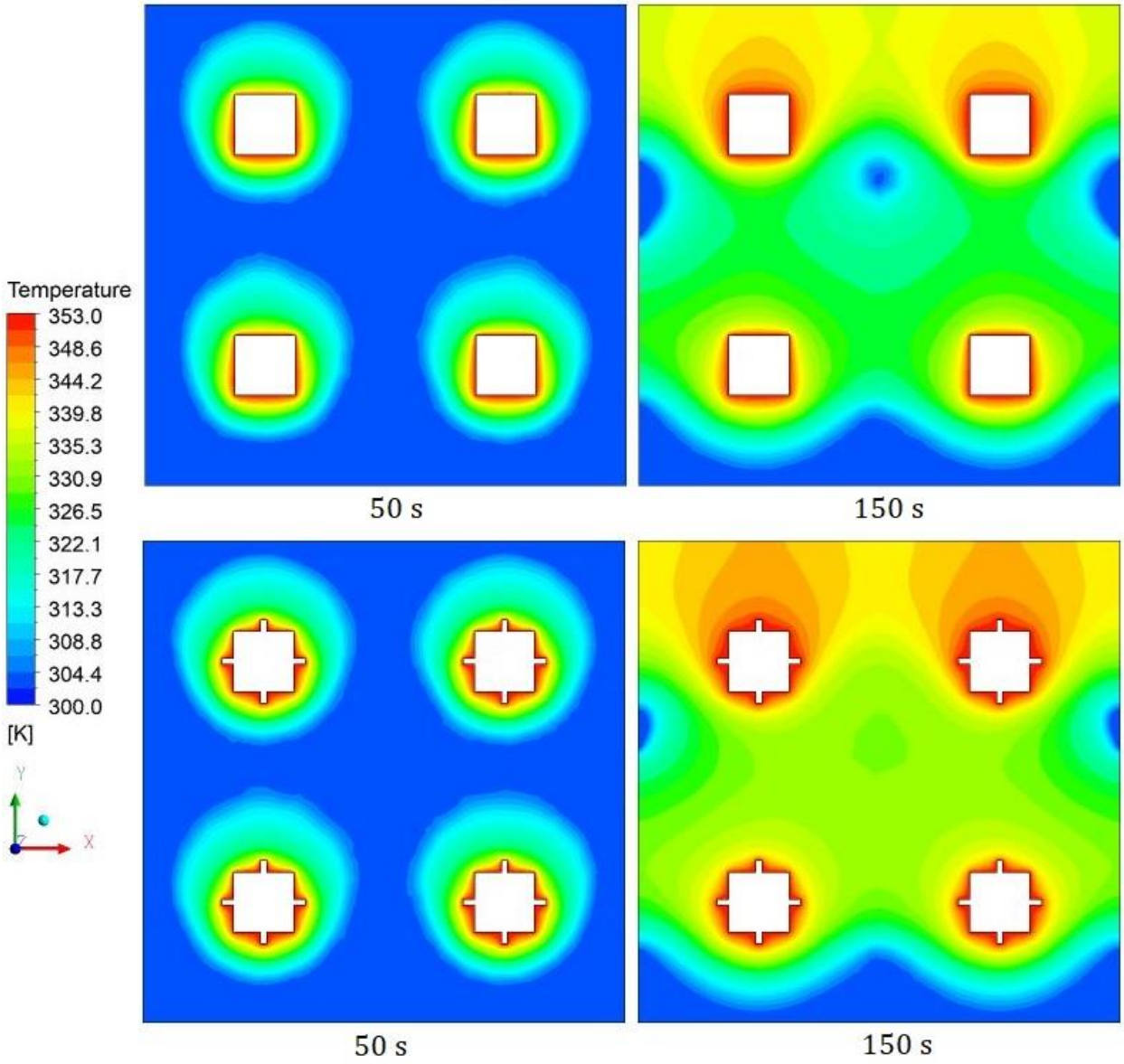

Fig 5.11 Comparison of contours of mean temperature for both geometries at 50s and 150s

The time taken to completely melt the PCM for configuration without fins is 310 seconds and for configuration with four fins is 290 seconds and the time taken by the PCM to attain the temperature of 80^{o}C for configuration without fins is 460 seconds and for configuration with four fins is 425 seconds as presented in Figure 5.12.

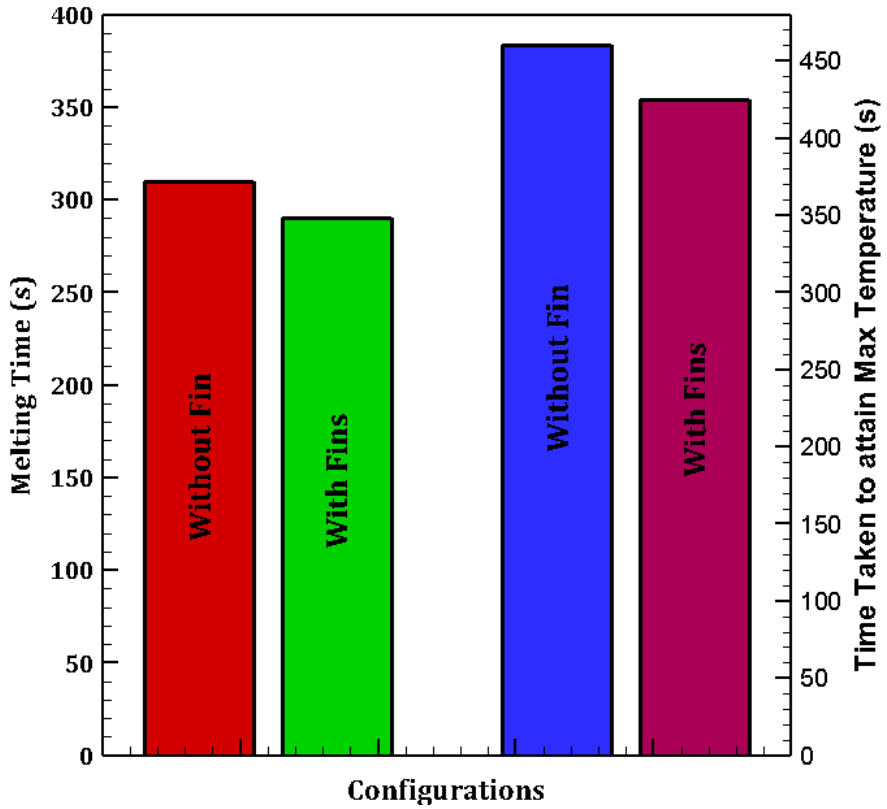

Fig 5.12 Comparison of PCM melting time and applied temperature attainment time for the two geometries

The proportion of PCM converted into the liquid with respect to time for both configurations is presented in Figure 5.13. It was observed from the plot that the minimum melting time of PCM is obtained by integrating fins on the circumference of the square tubes in STHE which enhances the heat transfer in the PCM.

The temperature evolution of PCM has been monitored inside the square shell cavity for all configurations of PCMHE having circular, square, and elliptical tubes as presented in Figure 5.14.

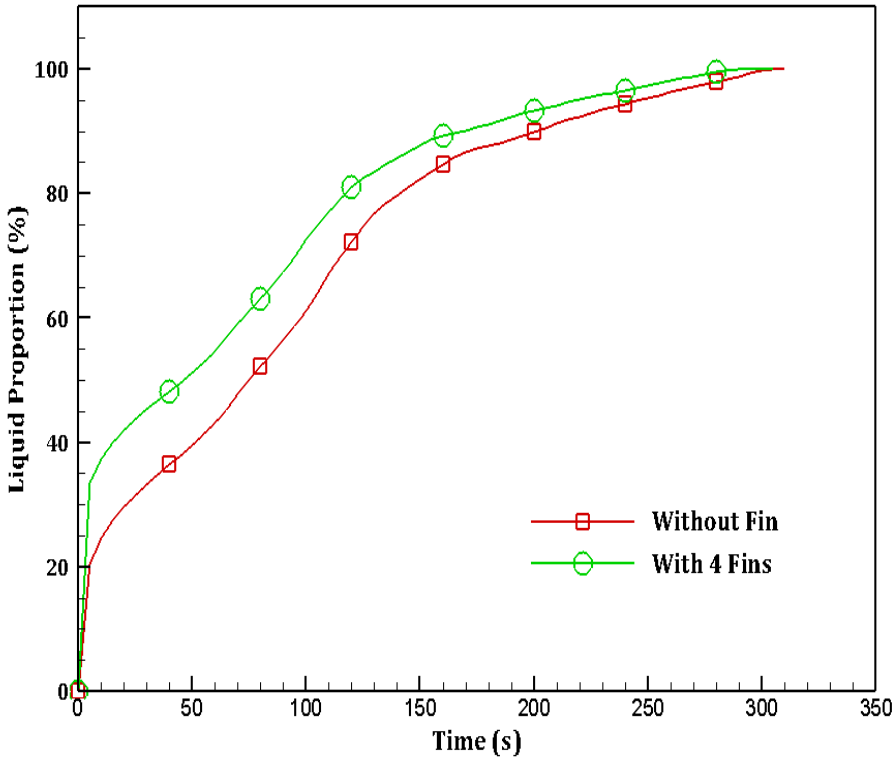

Fig 5.13 Evolution of liquid proportion with time for both configurations at 80°C

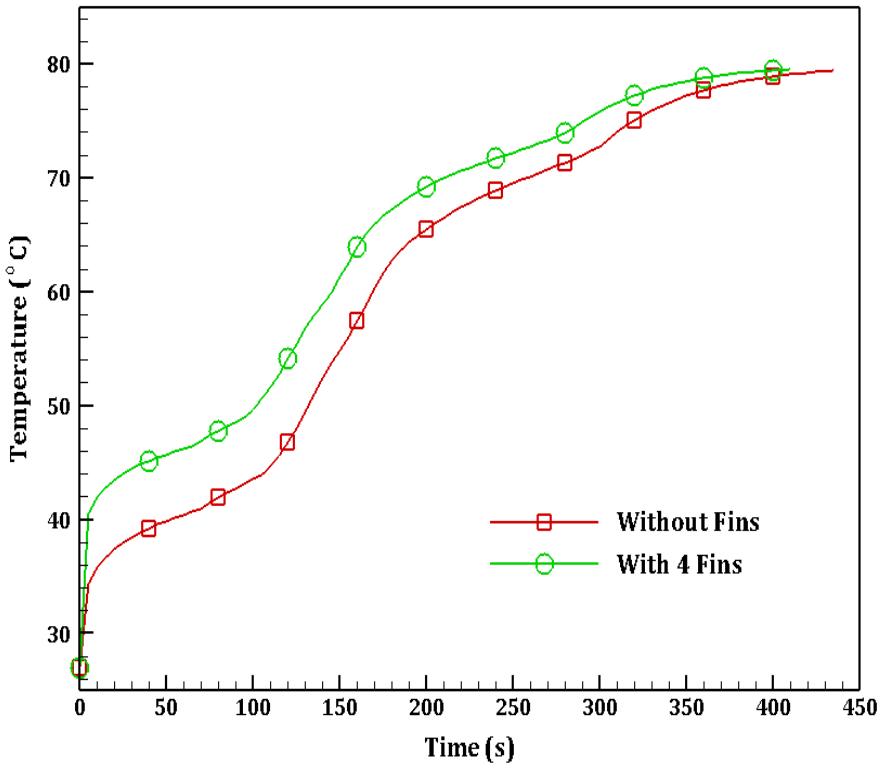

Fig 5.14 Evolution of mean temperature with time for both configurations at 80°C

It has been observed from the plot that the variation of temperature of PCM is similar for both configurations of PCMHE. The mean temperature of PCM rises rapidly up to 75^{o}C because most of the heat after the melting of PCM is utilized to increase the temperature of PCM. After 75^{o}C the rise in temperature goes down because of the very short temperature difference between PCM and heat source.

5.3 Circular Shell Geometries having Circular Tubes with & without Fins

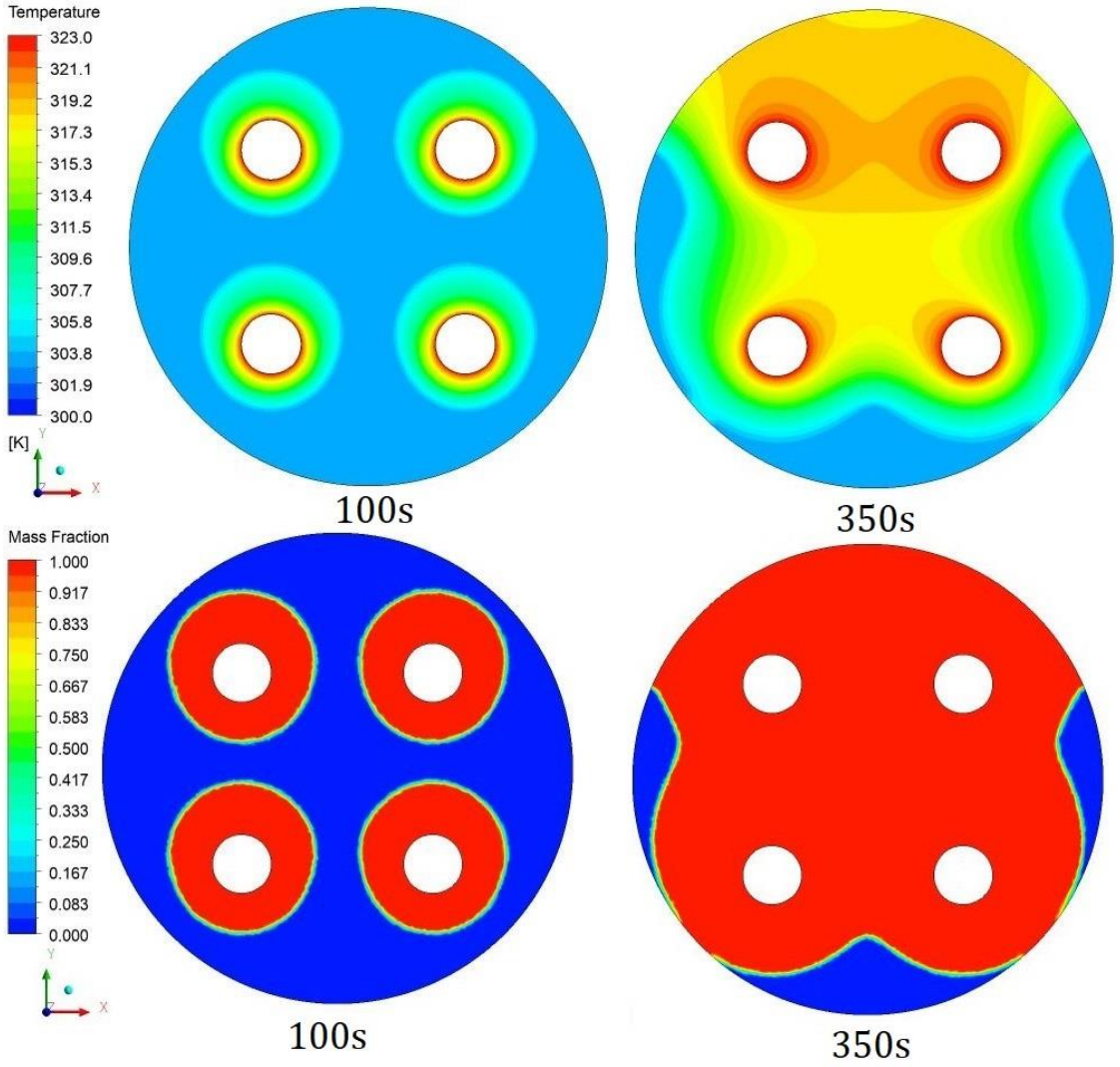

Fig 5.15 Temperature and liquid proportion evolution contours for the geometry having circular tubes without fin at 50^{o}C

In this investigation, the shape of the outer shell of PCMHE is taken as circular and the shape of the inside tubes is also taken as circular. A PCM is filled in the circular shell and a HTF is flowing in the tubes. A number of fins are incorporated into the tubes to enhance heat transmission into the PCM. In this study, a comparison has been made among the circular shell geometries of PCMHE to see the effect of the number of fins incorporated into the circular tubes on the heat transfer rate into the PCM in terms of liquid proportion and melting time. The three geometries of PCMHE include circular tubes without fins, circular tubes with three fins, and circular tubes with six fins.

Simulated numerical data are utilized to examine the melting behavior of PCM to understand how integrating fins affect the cylindrical tube geometries in PCMHE. The effects of incorporating three and six fins on the circular tubes on the liquid proportion of PCM, and temperature characteristics, as well as melting time, are analyzed at two different applied temperatures of 50^{o}C and 60^{o}C in this investigation.

Figure 5.15 illustrates the contours of the temperature profile and liquid proportion of PCM at an applied temperature of 50^{o}C on the outer surface of tubes for the geometry of PCMHE having circular tubes without fins at time steps of 100 and 350 seconds. It can be seen from the contours that the melt zones surrounding the cylindrical tubes are similar in shape at the start of melting up to 80 seconds when the majority of the heat is transferred in the PCM due to conduction alone, because of the symmetry of the geometry about the axis. Heat transfer occurs within PCM due to natural convection after 100 seconds at 50^{o}C, and the majority of the melting takes place near the cylindrical tubes rising upward due to density changes and gravitation influence by Boussinesq approximation. All melting zone surrounding the tubes is initially unaffected by the existence of other melting zones as long as all melting regions over the tubes have not combined

at 200 seconds and produced one homogeneous melting region with a common solid-liquid interface. For this configuration, it takes 13 minutes to completely melt the PCM, and 17 minutes and 20 seconds for the PCM to reach the temperature of 50^{o}C.

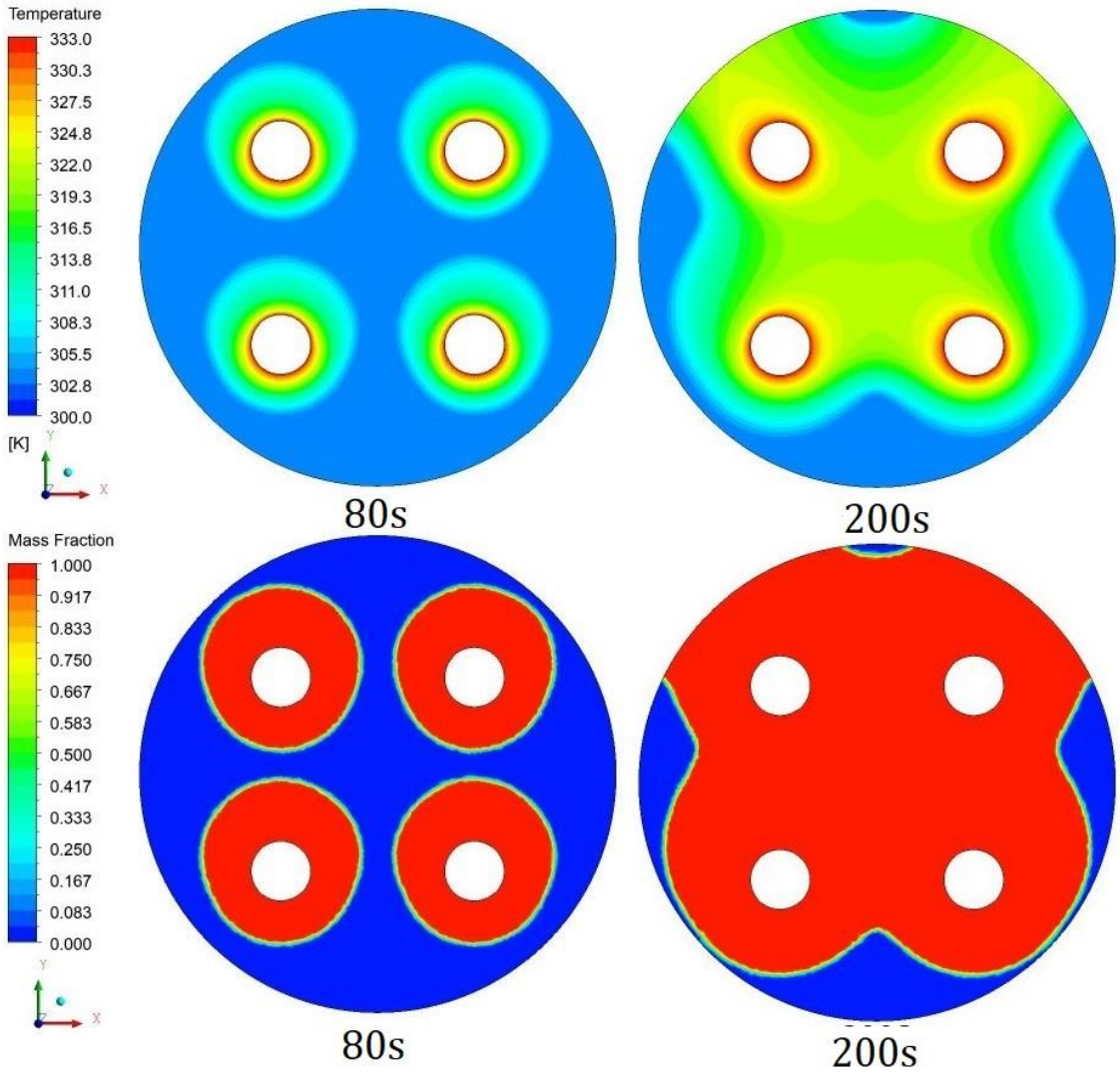

Fig 5.16 Temperature and liquid proportion evolution contours for the geometry having circular tubes without fin at 60^{o}C

Figure 5.16 shows the contours of the temperature profile and liquid proportion evolution of PCM for the geometry of PCMHE having circular tubes without fins at 80 and 200 seconds at a temperature of 60^{o}C. At the beginning of melting up to 60 seconds, conduction accounts for the majority of heat transmission in PCM only because of the symmetry of the configuration around

the axis, and melt zones have a similar shape around the circular tubes. Heat transmission occurs within PCM due to natural convection after 80 seconds at 60^{o}C, and the majority of melting takes place near the cylindrical tubes moving upward because of density changes and gravitational impact by Boussinesq approximation. All melting zone around the tubes is initially unaffected by the existence of another melting region as long as all melting region over the tubes have not combined at 130 seconds and produced one homogeneous melting zone with a common solid-liquid interface. For this arrangement, it takes 9 minutes to completely melt the PCM, and 13 minutes and 20 seconds for the PCM to attain the temperature of 60^{o}C.

Figure 5.17 shows the contours of the liquid percentage of PCM for geometries of PCMHE having circular tubes with three and six fins compared to the geometry of PCMHE having circular tubes without fins after 60 seconds and 180 seconds at 50^{o}C. These contour graphs show how the PCM melting phenomenon has evolved over time in terms of liquid proportion for three and six fins geometry with a constant temperature of 50^{o}C applied to the outside face of tubes. Furthermore, the graphs evaluate the impact of cylindrical tube design on PCM melting duration. The graphs show that when PCM melting begins, conduction is predominant around the tubes, and the melt zones are similar. However, convection heat transmission in PCM begins after 100 seconds in a configuration without fins, 80 seconds in a configuration with three fins, and 60 seconds in a configuration with six fins at 50^{o}C. After 60 seconds, 24.6 percent of PCM is transformed into liquid in the configuration without fins, 35 percent in a configuration with three fins, and 43.3 percent in a configuration with six fins. After 180 seconds, the liquid percentage of PCM is 57.4 percent in the configuration without fins, 71.3 percent in the configuration with 3 fins, and 79.6 percent in the configuration with 6 fins.

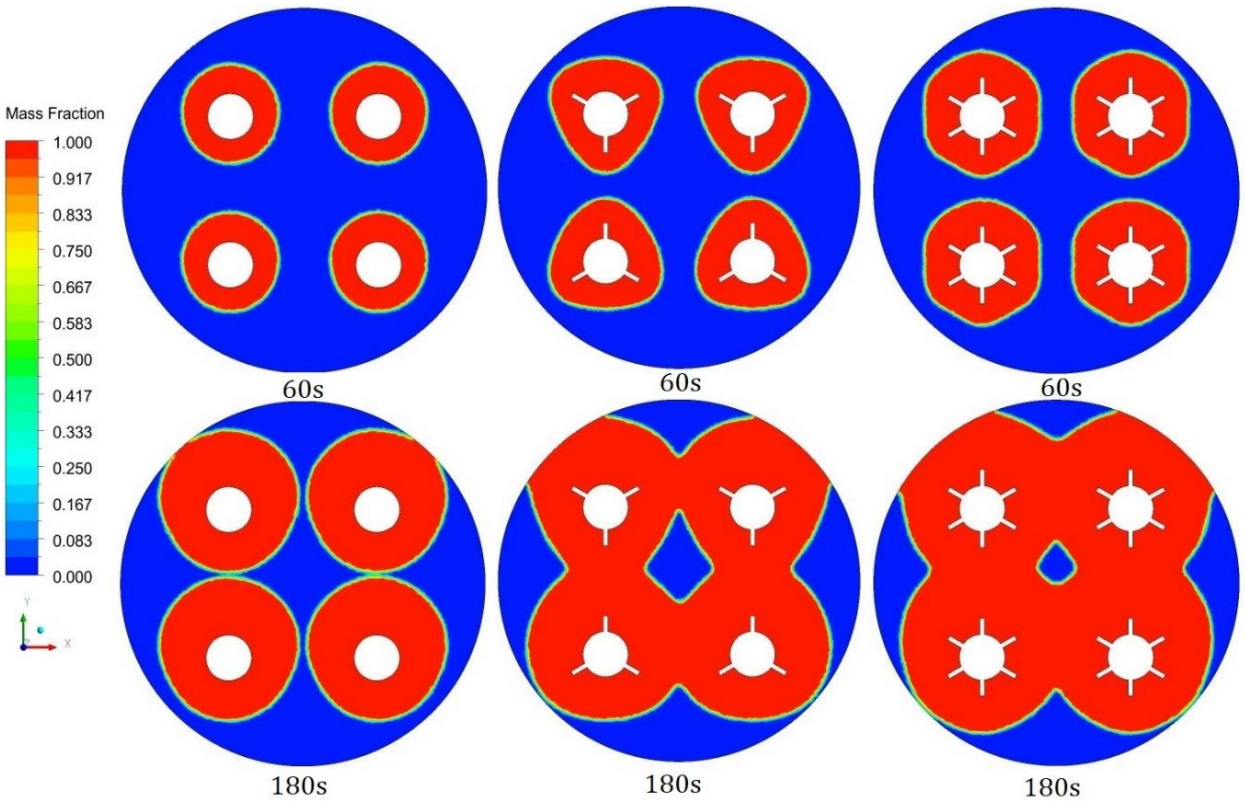

Fig 5.17 Comparison of liquid proportion evolution among all geometries at 60s & 180s at 50^{o}C

Figure 5.18 illustrates the contours of the average temperature of PCM for geometries of PCMHE with three and six fins compared to the geometry without fins after 80 seconds and 190 seconds at 50^{o}C applied to the outside tube surface. These contour plots evaluate the impact of the geometry of cylindrical tubes on the average temperature of PCM. The graphs show that after 80 seconds, the average temperature of PCM is 31.9^{o}C in a configuration without fins, 33.3^{o}C in a configuration with three fins, and 34.6^{o}C in a configuration with six fins. Also, after 190 seconds, the temperature of PCM is 33.5^{o}C in a configuration without fins, 36.5^{o}C in a configuration with 3 fins, and 38.8^{o}C in a configuration with 6 fins.

Figure 5.19 shows the contours of the liquid proportions of PCM for geometries of PCMHE having circular tubes with three and six fins compared to the geometry without fins after 40 seconds and 120 seconds at 60^{o}C applied to the outside tube surface. These graphs evaluate the impact of cylindrical tube design on PCM melting duration at 60^{o}C. The graphs show that

convection heat transfer in PCM begins after 80 seconds in a configuration without fins, 60 seconds in a configuration with three fins, and 40 seconds in a configuration with six fins. After 40 seconds, 25.2 percent of PCM is transformed into liquid in a configuration without fins, 35.8 percent in a configuration with three fins, and 44.3 percent in a configuration with six fins. After 120 seconds, the liquid percentage of PCM is 59.6 percent in the configuration without fins, 73.2 percent in the configuration with 3 fins, and 81.3 percent in the configuration with 6 fins.

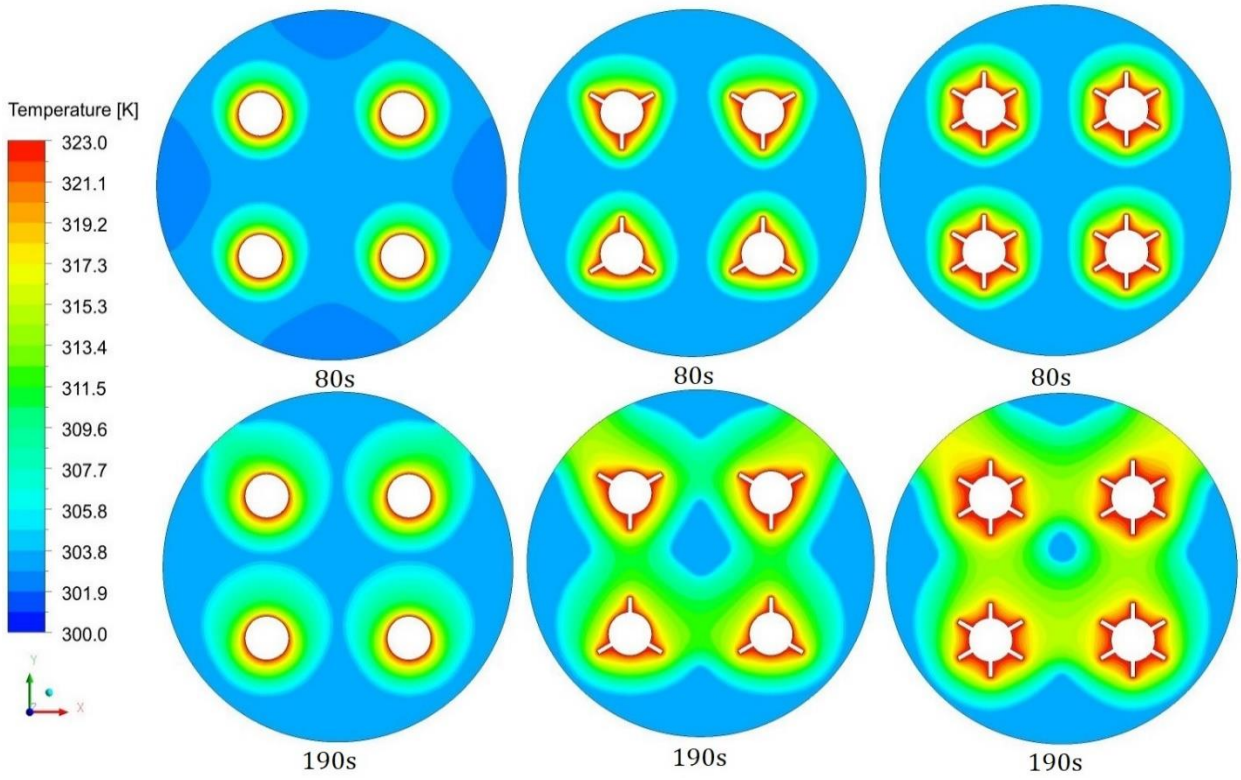

Fig 5.18 Comparison of temperature evolution among all geometries at 80s & 190s at 50^{o}C

Figure 5.20 illustrates the contours of the average temperature of PCM for geometries with three and six fins compared to the geometry without fins after 50 seconds and 120 seconds at a temperature of 60^{o}C applied to the outside tube surface. These contour plots evaluate the impact of the design of cylindrical tubes on the average temperature of PCM. The graphs show that after 50 seconds, the average temperature of PCM is 32.7^{o}C in a configuration without fins, 34.9^{o}C in a configuration with three fins, and 36.8^{o}C in a configuration with six fins. Also, after 120

seconds, the temperature of PCM is 35.3^{o}C in a configuration without fins, 39.5^{o}C in a configuration with 3 fins, and 43^{o}C in a configuration with 6 fins.

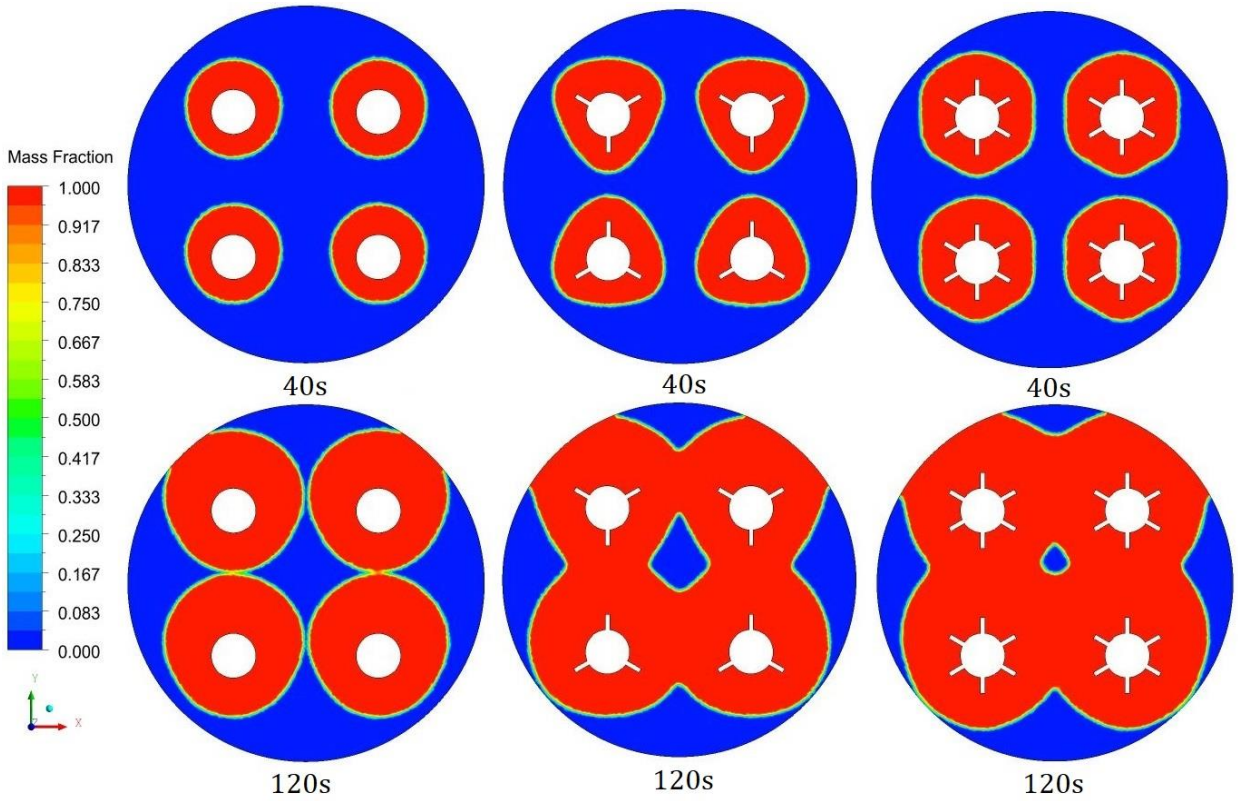

Fig 5.19 Comparison of liquid proportion evolution among all geometries at 40s & 120s at 60^{o}C

Figure 5.21 illustrates the comparison of the time taken for melting the PCM for all geometries of PCMHE at 50^{o}C and 60^{o}C applied to the outer surface of tubes. The amount of time it takes to melt the PCM at 50^{o}C for the configuration having no fin is 780 seconds, for the configuration having three fins is 645 seconds, and for the configuration having six fins is 580 seconds. And the amount of time it takes to melt the PCM at 60^{o}C for the configuration having no fin is 530 seconds, for the configuration having three fins is 440 seconds, and for the configuration having six fins is 390 seconds.

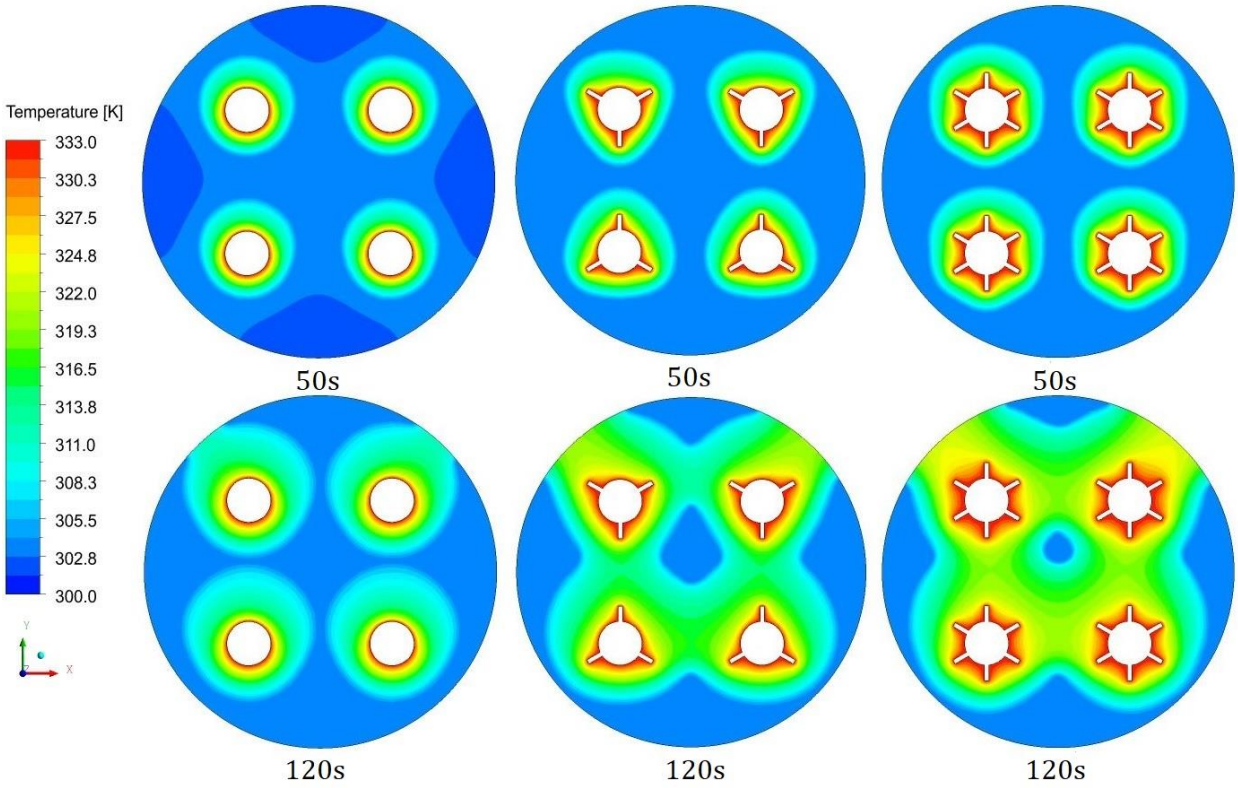

Fig 5.20 Comparison of temperature evolution among all geometries at 50s & 120s at 60^{o}C

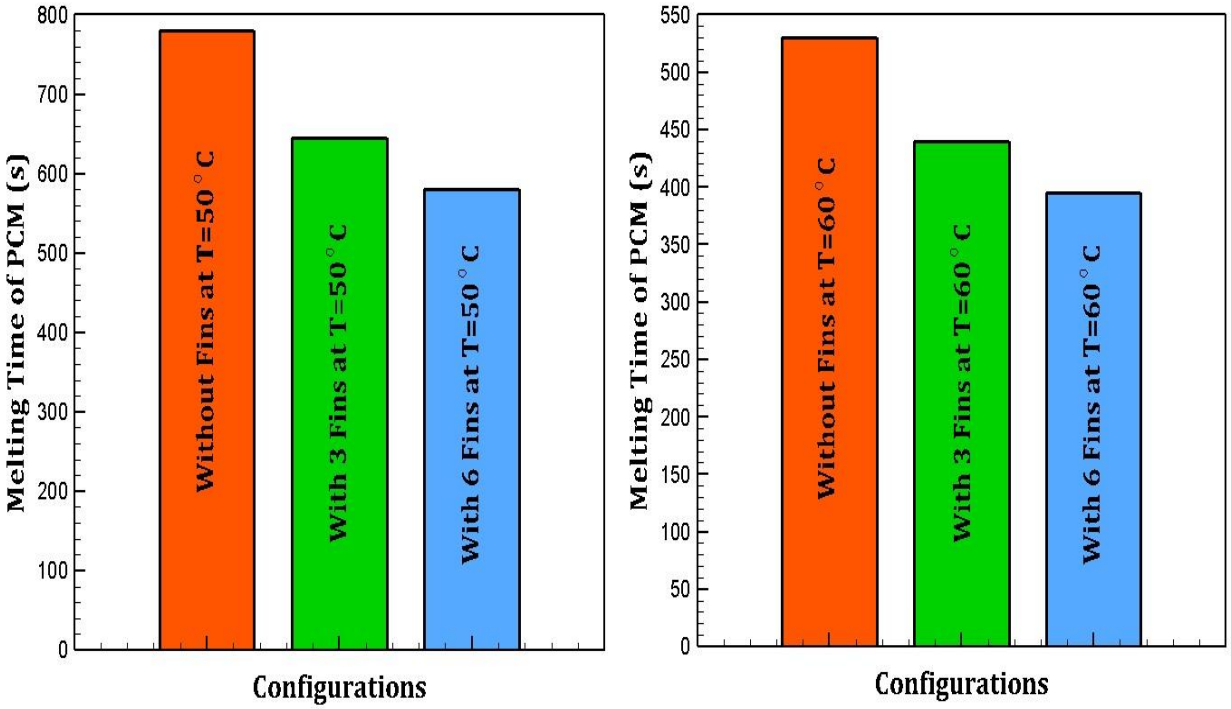

Fig 5.21 Comparison of melting time of PCM for all geometries at 50^{o}C and 60^{o}C

Figure 5.22 shows the comparison of time taken to attain the maximum temperature (Applied temperature at the outer surface of tubes) of PCM for all geometries of PCMHE at 50^{o}C and 60^{o}C. The time taken to attain maximum temperature at 50^{o}C for the configuration having no fin is 1040 seconds, for configuration having three fins is 830 seconds, and for configuration having six fins is 735 seconds. And the time taken to attain maximum temperature at 60^{o}C for the configuration having no fin is 800 seconds, for configuration having three fins is 715 seconds, and for configuration having six fins is 565 seconds.

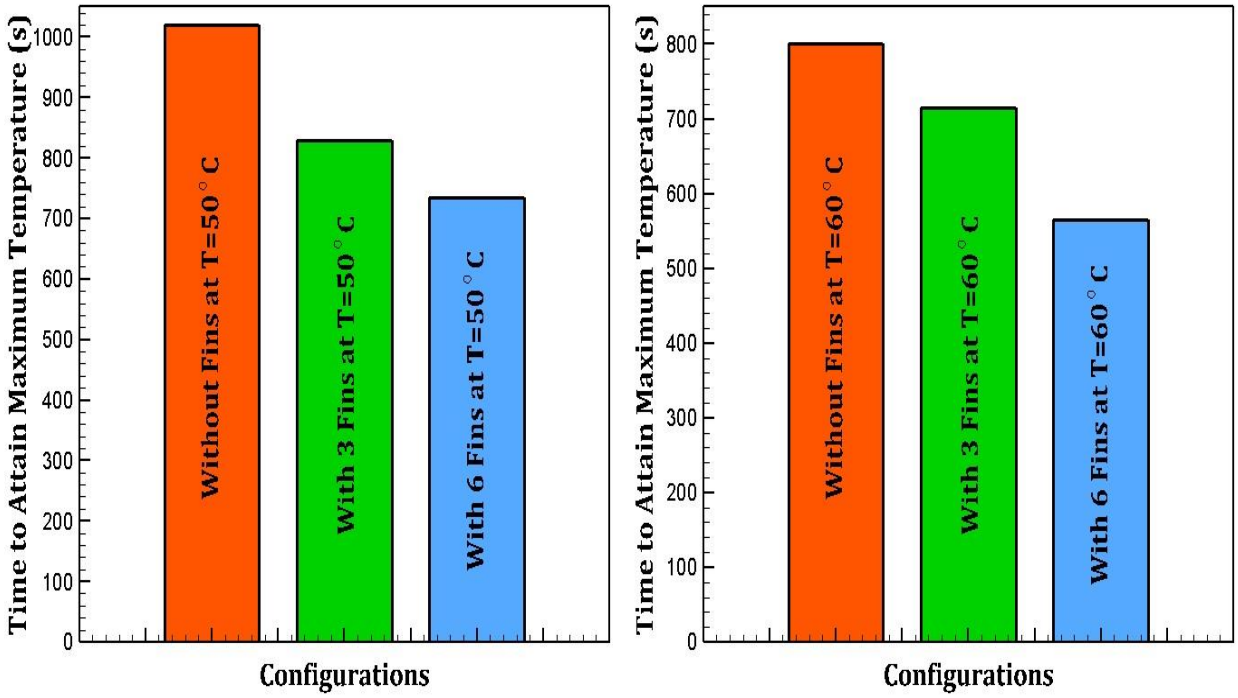

Fig 5.22 Comparison of maximum temperature attainment time of PCM for all geometries at 50^{o}C and 60^{o}C

Figure 5.23 and Figure 5.24 shows the proportion of PCM converted to liquid as a function of time for all configurations at 50^{o}C and 60^{o}C. The plot shows that incorporating six fins around the circumference of cylindrical tubes in STHE results in the fastest melting time of PCM at both the applied temperatures. That means the rate of heat transfer increases by integrating six fins on the circumference of tubes compared to integrating three fins and without fin configurations.

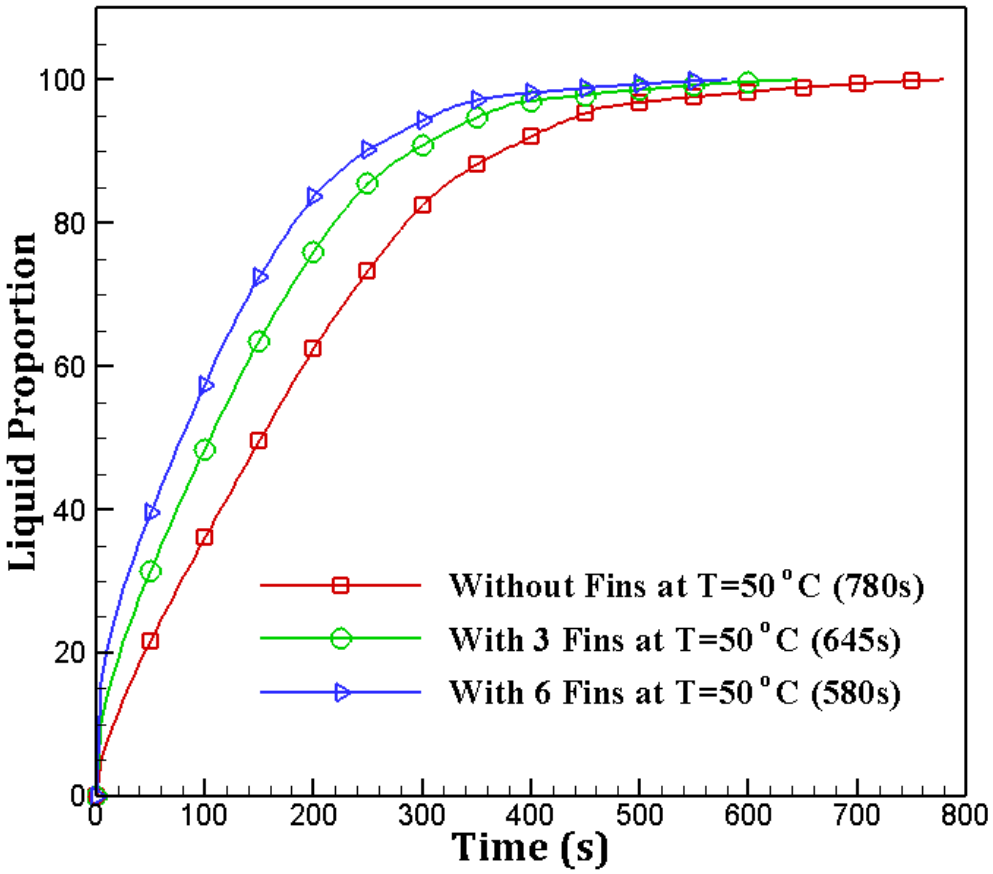

Fig 5.23 Evolution of liquid proportion of PCM with time for all configurations at 50°C

Figure 5.25 and Figure 5.26 shows the PCM temperature development within the PCMHE at 50°C and 60°C, and as may be observed from the graph, the temperature fluctuation with time is not uniform. The temperature curves are more uniform at a higher applied temperature of 60°C than at 50°C. It can be seen from the plots that the rise in temperature is more up to 45°C at an applied temperature of 50°C & then become slower because the difference in temperature between PCM and tubes becomes very low. Also, the minimum time taken to reach the applied temperature is obtained with the geometry of six fins at both applied temperatures.

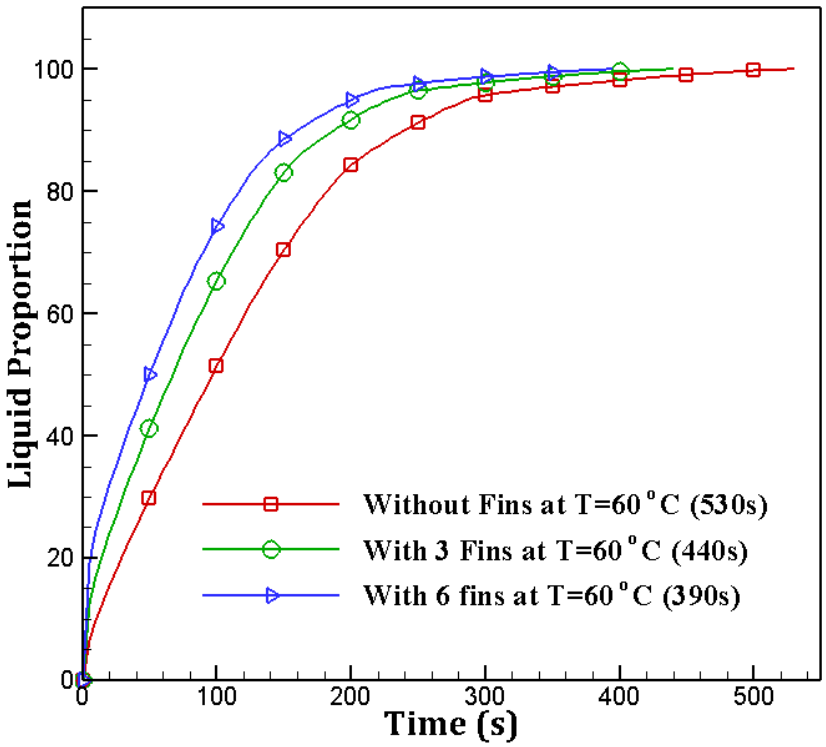

Fig 5.24 Evolution of liquid proportion of PCM with time for all configurations at 60°C

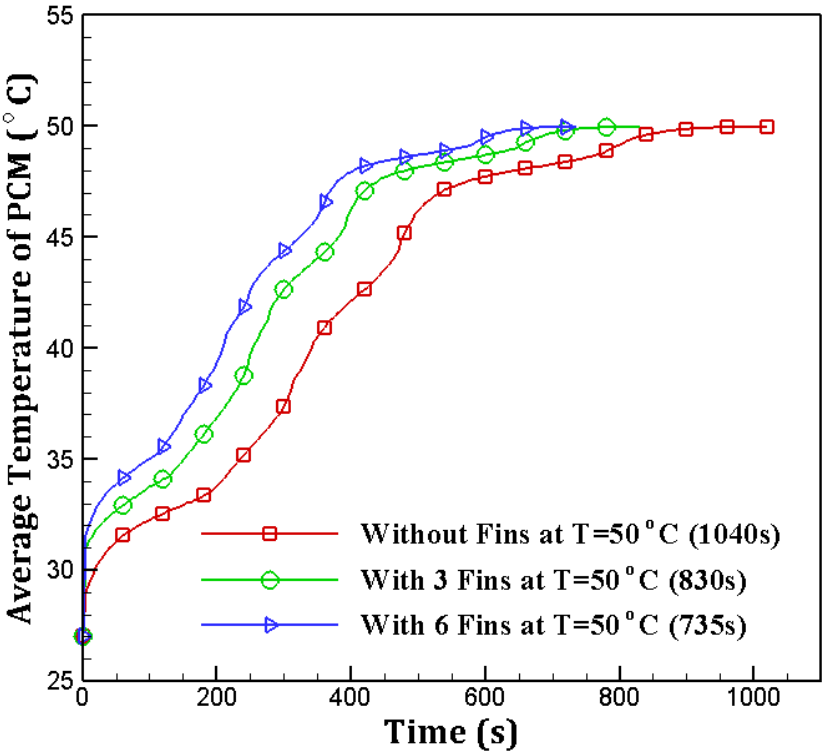

Fig 5.25 Evolution of average temperature of PCM with time for all configurations at 50°C

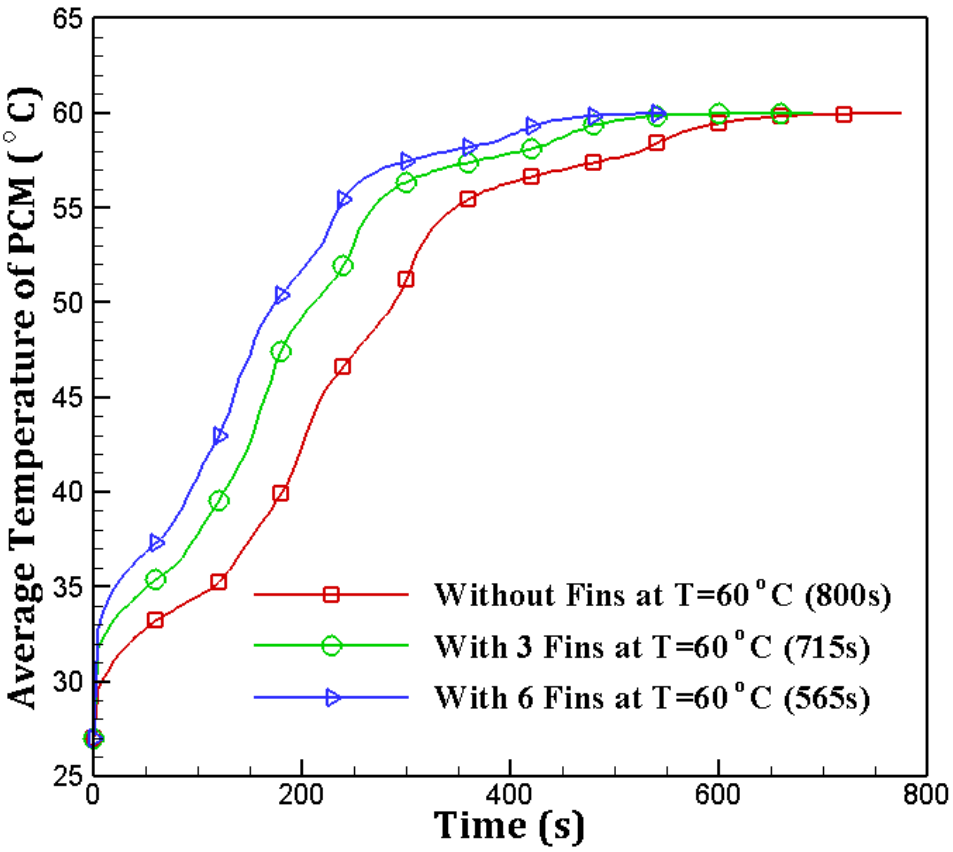

Fig 5.26 Evolution of average temperature of PCM with time for all configurations at 60°C

5.4 Circular Shell Geometries having Circular & Elliptical Tubes with & without Fins

A different investigation has also been made with circular shell geometries having circular and elliptical tubes. To enhance the heat transmission rate and to reduce the melting time of PCM rectangular fins are incorporated on the outer surface of the circular and elliptical tubes. The number of fins is also varied to investigate the effect of a number of fins on the circular and elliptical tubes. Six configurations of PCMHE with circular shell geometry are investigated in this work. The geometries of PCMHE include circular tubes without a fin, circular tubes with two fins, and circular tubes with four fins as well as elliptical tubes without a fin, elliptical tubes with two fins, and elliptical tubes with four fins.

Investigating the thermal performance of a PCMHE using multiple elliptical tubes and a PCM placed in the heat exchanger's cylindrical container is the primary objective of this investigation.

Two and four fins have been added to the outer surface of the elliptical tubes to increase heat transfer from the tubes to the PCM. A novel method for enhancing heat transmission in investigations of the thermal performance of a TES system involves the installation of elliptical tubes having fins. The configurations of heat exchangers with elliptical tubes without a fin, two fins, and four fins have been compared to the configuration of PCMHE having circular tubes without a fin, two fins, and four fins, respectively. In this research study, the phase transformation of the solid PCM is explored using a 2D CFD simulation employing a physical enthalpy-porosity approach. In addition, the results of elliptical and circular tube designs in terms of PCM average temperature and liquid proportion at two distinct temperatures of 50°C and 60°C are being compared. The impact of adding a number of fins on heat transmission has also been investigated.

Results indicate that at 50°C, the PCM melting period reduces to 550 seconds in PCMHE configuration with elliptical tubes having four fins as compared to 585 seconds and 665 seconds for the same heat exchanger having two fins & no fin, respectively. This represents a 12% and 17% decrease in melting duration. While the PCM melting period is 515 seconds with PCMHE configuration with circular tubes having four fins, it decreases to 560 seconds for heat exchangers with two fins and 655 seconds for those without fins, resulting in melting times that are reduced by 14.5% and 21%, respectively, when two and four fins are used. It is observed that introducing fins to the perimeter of elliptical and circular tubes improves heat transmission and minimizes the melting duration. Additionally, circular tube heat exchanger configurations may transmit more heat than elliptical tube heat exchanger configurations. Using numerical simulations, the melting behavior of PCM inside a heat exchanger with elliptical and circular tubes with and without fins has been compared. On PCM liquid percentage, temperature

properties, and melting duration, the impacts of including both two and four fins in elliptical and circular tubes are examined.

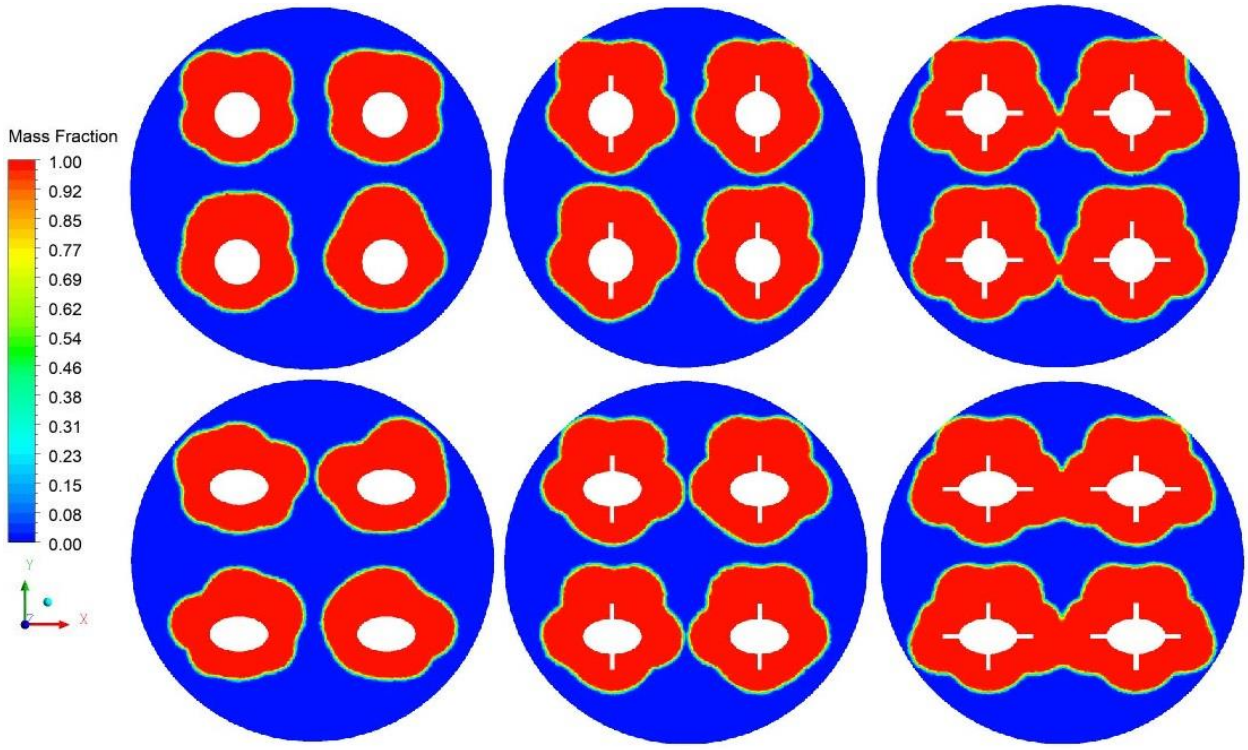

Fig 5.27 Evolution of liquid proportion contours of all geometries after 100s at 50^{o}C

Figure 5.27 illustrates a comparison of the contours of PCM proportion in liquid form at a constant temperature of 50^{o}C in a configuration of PCMHE having circular and elliptical tubes at time steps of 100 seconds. The liquid proportion contours in a configuration having no fin on circular tubes are compared with a configuration having no fin on elliptical tubes, as well as liquid proportion contours for geometries having two and four fins on the circular tubes are compared with the geometry having two and four fins on the elliptical tubes. At the start of melting, when the PCM transmits the majority of the heat only by conduction, the melting regions around the tubes are identical in shape. Natural convection causes heat transmission inside PCM after 60 seconds in the geometry having circular tubes without fins whereas it occurs after 70 seconds in the geometry having elliptical tubes without fins at 50^{o}C, and most of the

melting occurring around the tubes rises upward due to Boussinesq approximation owing to density variations and gravitational effect. Until all of the melting zones around the tubes are not merged and generated one homogenous melting region with a common solid-liquid interface, the existence of another melting region does not affect the melting zone around the tubes. The percentage of PCM converted into liquid (liquid proportion) after 100 seconds at 50^{o}C is 39.84% for a circular tube without fin geometry whereas the liquid proportion of PCM is 39.58% for an elliptical tube without fin geometry. The liquid proportion of PCM is 49% for circular tubes with two fins geometry whereas the liquid percentage of PCM is 48.74% for elliptical tubes with two fins geometry. The liquid percentage of PCM is 56.18% for circular tubes with four fins geometry whereas the liquid percentage of PCM is 55.64% for elliptical tubes with four fins geometry.

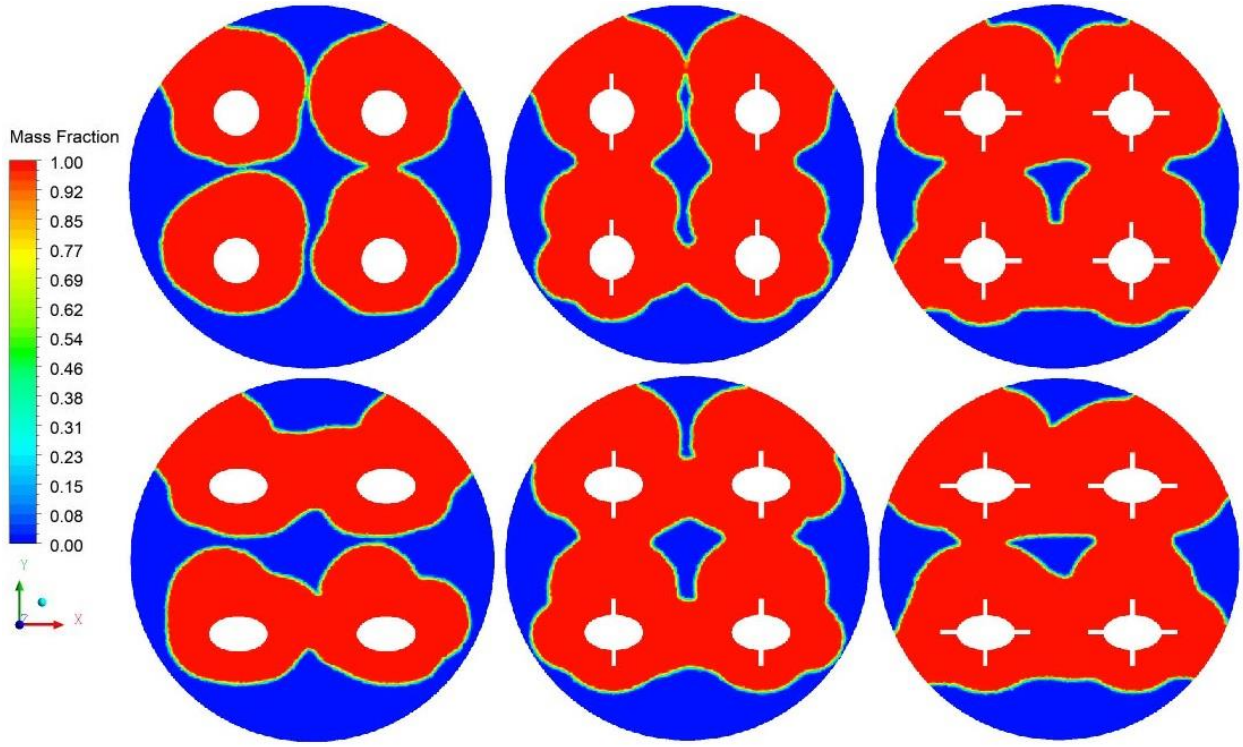

Fig 5.28 Evolution of liquid proportion contours of all geometries after 100s at 60^{o}C

Figure 5.28 illustrates the comparison of contours of the PCM proportion in liquid form at an applied temperature of 60^{o}C in the configuration of PCMHE having circular and elliptical tubes at time steps of 100 seconds. Heat transmission takes place in PCM due to natural convection after 40 seconds in the geometry having circular tubes without fins whereas it occurs after 45 seconds in the geometry having elliptical tubes without fins at 60^{o}C. The liquid proportion after 100 seconds at 60^{o}C is 60.11% for a circular tube without fin geometry whereas the liquid proportion of PCM is 59.96% for an elliptical tube without fin geometry. The liquid proportion of PCM is 70.75% for circular tubes with two fins geometry whereas the liquid proportion of PCM is 70.11% for elliptical tubes with two fins geometry. The liquid proportion of PCM is 76.66% for circular tubes with four fins geometry whereas the liquid proportion of PCM is 76.36% for elliptical tubes with four fins geometry.

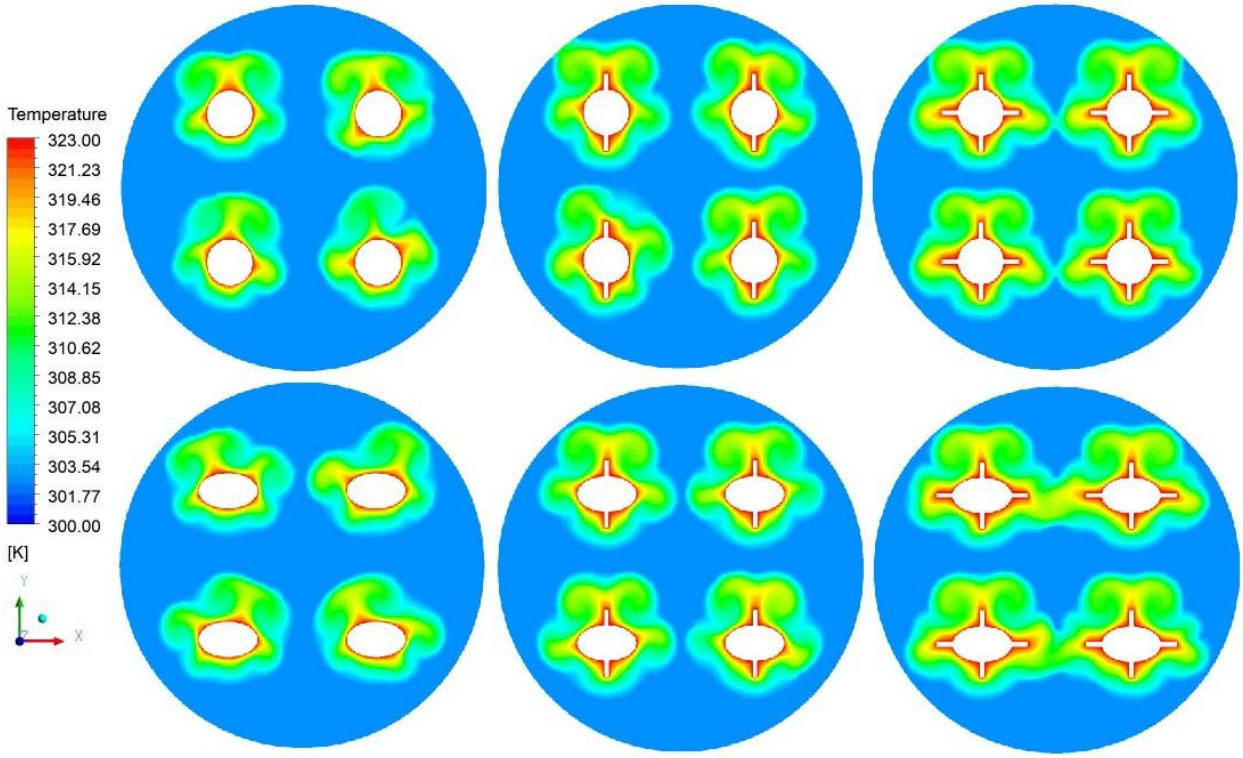

Fig 5.29 Evolution of temperature contours of all geometries after 100s at 50^{o}C

Figure 5.29 shows a comparison of contours of the average temperature of PCM after 100 seconds between the circular tube geometries and the elliptical tube geometries at 50^{o}C. These contour graphs examine the effect of tube shape on PCM's mean temperature. After 100 seconds, the mean temperature of PCM in a configuration with circular tubes having no fin is 32.9^{o}C, whereas the mean temperature of PCM in a configuration with elliptical tubes having no fin is 32.4^{o}C. PCM's mean temperature is 33.6^{o}C in a configuration having circular tubes with two fins whereas it is 33.5^{o}C in a configuration having elliptical tubes with two fins and the mean temperature of PCM is 34.8^{o}C in a configuration having circular tubes with four fins whereas the mean temperature is 34.7^{o}C in a configuration having elliptical tubes with four fins.

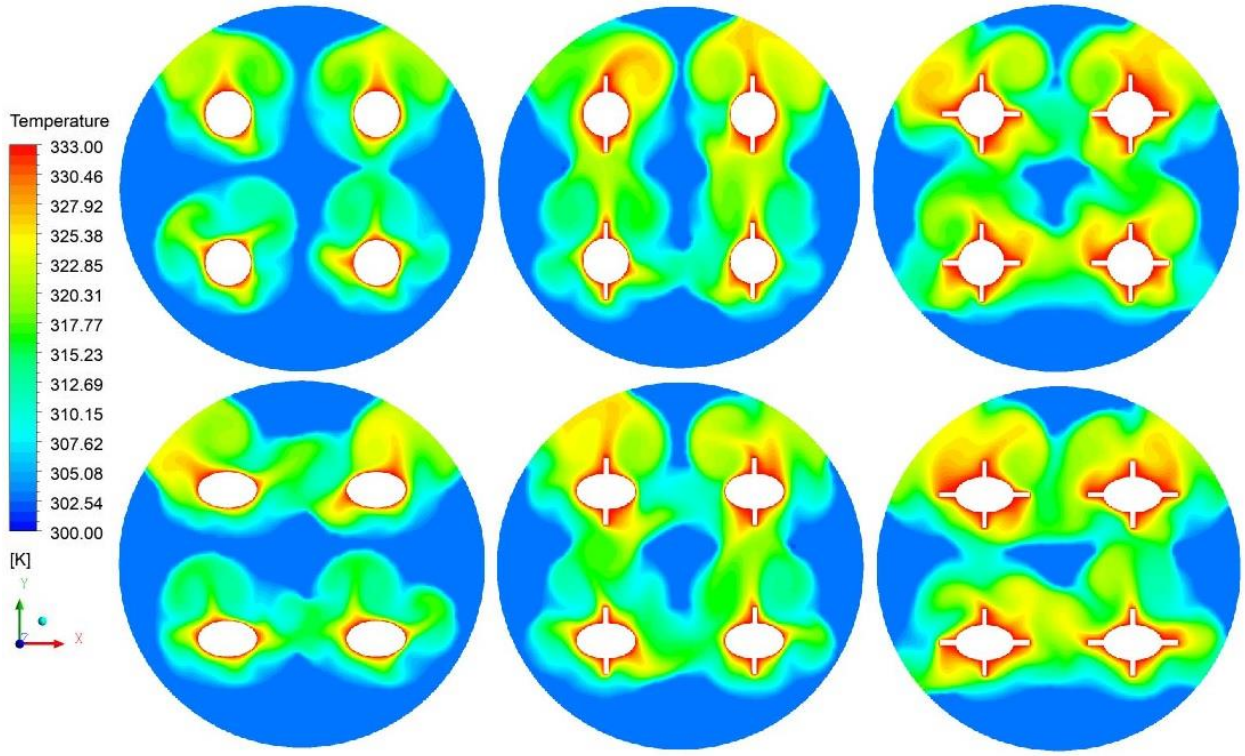

Fig 5.30 Evolution of temperature contours of all geometries after 100s at 60^{o}C

Figure 5.30 shows a comparison of the contours of the average temperature of PCM after 100 seconds between the circular tube geometries and the elliptical tube geometries at 60^{o}C. After 100 seconds, PCM's mean temperature is 36.7^{o}C in a configuration having circular tubes without

fins whereas PCM's mean temperature is 36.3^{o}C in a configuration having elliptical tubes without fins. The mean temperature of PCM is 39.3^{o}C in a configuration having circular tubes with two fins whereas it is 39.2^{o}C in a configuration having elliptical tubes with two fins and the mean temperature of PCM is 41.7^{o}C in a configuration having circular tubes with four fins whereas the average temperature is 41.6^{o}C in a configuration having elliptical tubes with four fins.

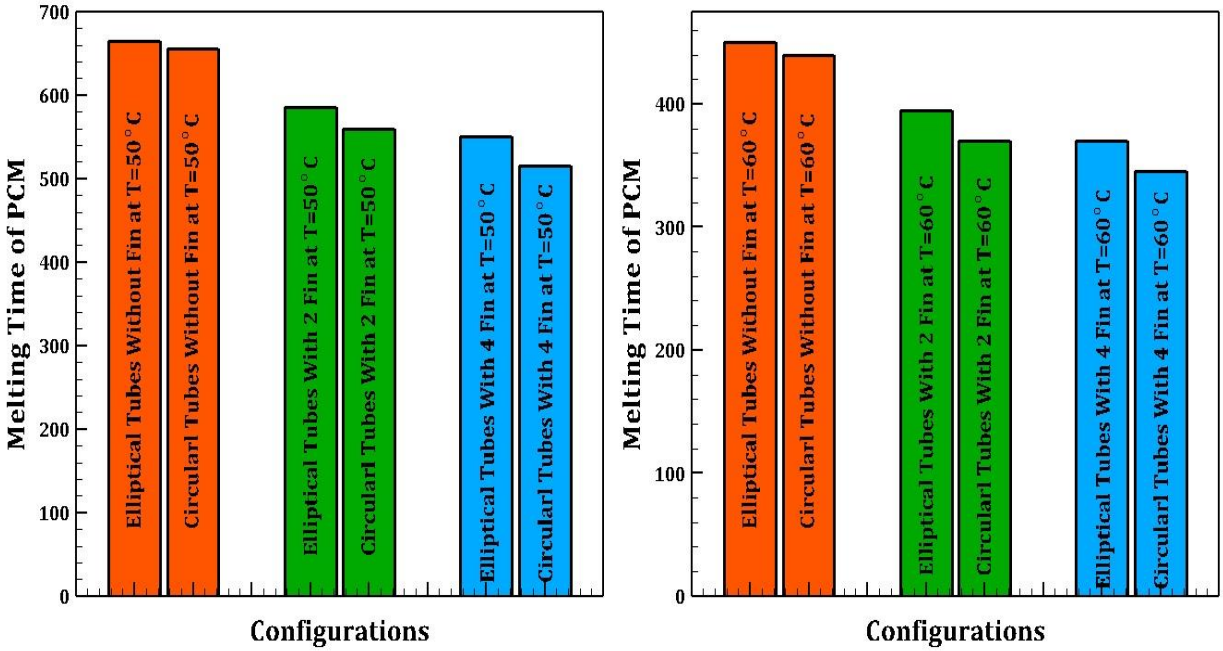

Fig 5.31 Comparison of melting time of PCM for all configurations at 50^{o}C and 60^{o}C

Figure 5.31 compares the time required to melt the PCM in all configurations at 50°C and 60°C applied at the external wall of the circular and elliptical tubes. The time required for the PCM to melt at 50^{o}C is 655 seconds for a circular tube without fin geometry whereas the melting time of PCM is 665 seconds for an elliptical tube without fin geometry. The melting time of PCM is 560 seconds for a circular tube with two fins geometry whereas the melting time of PCM is 585 seconds for an elliptical tube with two fins geometry. The melting time of PCM is 515 seconds

for a circular tube with four fins geometry whereas the melting time of PCM is 550 seconds for an elliptical tube with four fins geometry.

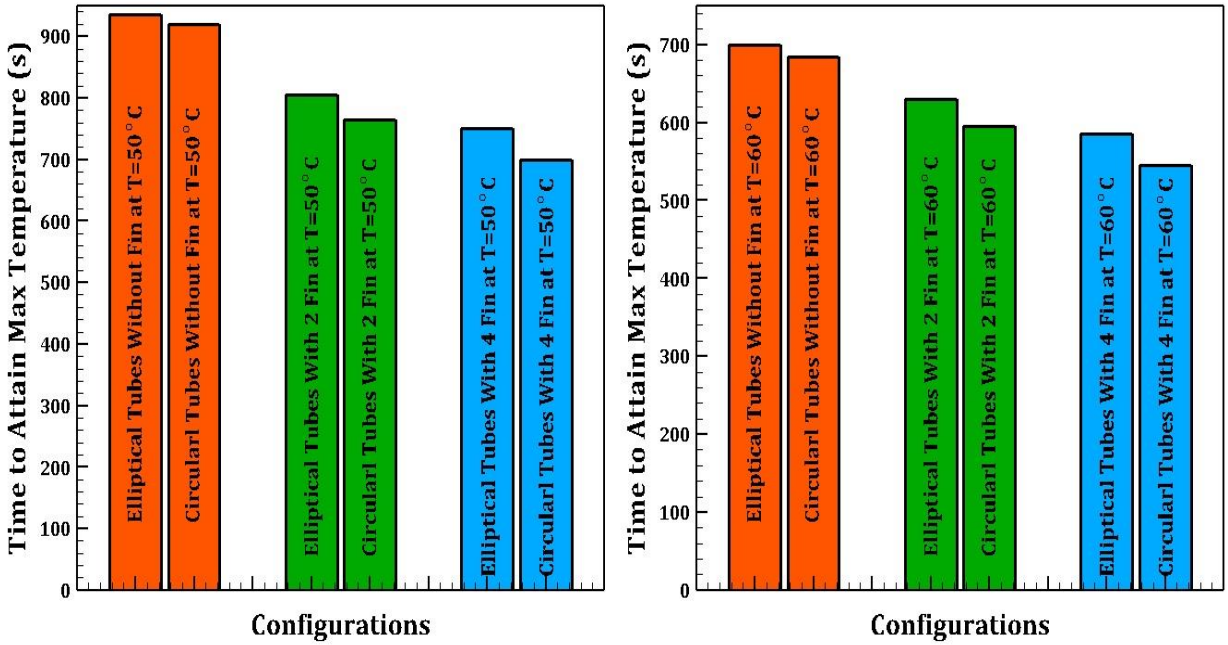

Fig 5.32 Comparison of applied temperature attainment time of PCM for all configurations at 50^{o}C and 60^{o}C

The time required for the PCM to melt at 60^{o}C is 440 seconds for a circular tube without fin geometry whereas the melting time of PCM is 450 seconds for an elliptical tube without fin geometry. The melting time of PCM is 370 seconds for a circular tube with two fins geometry whereas the melting time of PCM is 395 seconds for an elliptical tube with two fins geometry. The melting time of PCM is 345 seconds for a circular tube with four fins geometry whereas the melting time is 370 seconds for an elliptical tube with four fins geometry.

Figure 5.32 compares the time it takes for PCM to reach the applied temperature at the external wall of tubes at 50°C and 60°C for all configurations of PCMHE. The time PCM takes to reach the highest temperature of 50°C in a configuration having circular tubes with no fin is 920 seconds whereas the time PCM takes to reach the highest temperature of 50°C in a configuration having elliptical tubes with no fin is 935 seconds. The time it takes to reach the highest

temperature in a configuration having circular tubes with two fins is 765 seconds whereas it is 805 seconds in a configuration having elliptical tubes with two fins and the time it takes to reach the highest temperature in configuration having circular tubes with four fins is 700 seconds whereas it is 750 seconds in a configuration having elliptical tubes with four fins

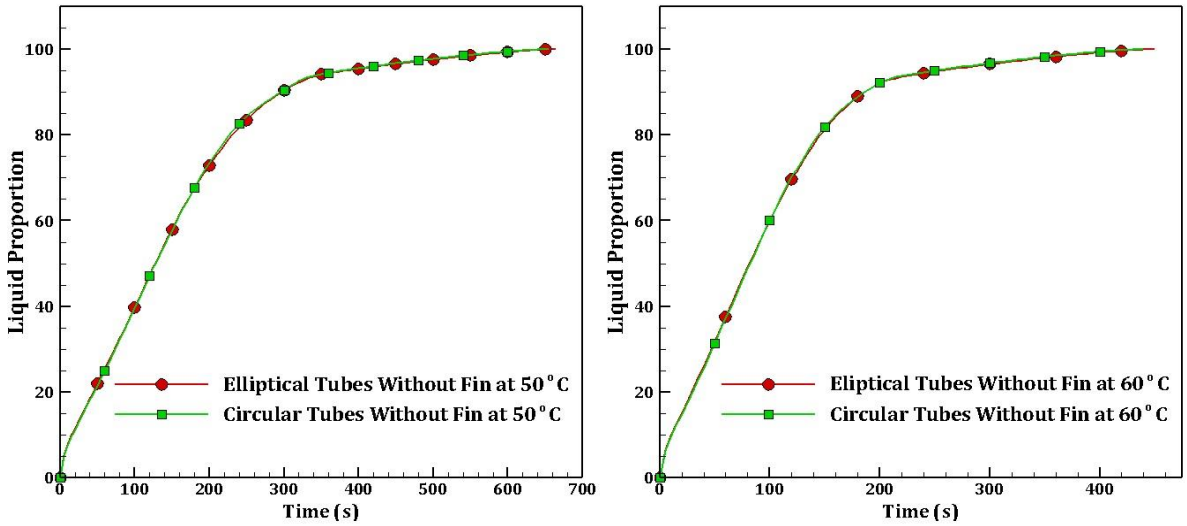

Fig 5.33 Evolution of liquid proportion of the geometries having circular and elliptical tubes without fin at 50°C & 60°C

The time PCM takes to reach the highest temperature of 60°C in a configuration having circular tubes with no fin is 685 seconds whereas the time PCM takes to reach the highest temperature of 60°C in a configuration having elliptical tubes with no fin is 700 seconds. The time it takes to reach the highest temperature in a configuration having circular tubes with two fins is 595 seconds whereas it is 630 seconds in a configuration having elliptical tubes with two fins and the time it takes to reach the highest temperature in a configuration having circular tubes with four fins is 545 seconds whereas it is 585 seconds in a configuration having elliptical tubes with four fins.

Figure 5.33, Figure 5.34, and Figure 5.35 show the comparison of the proportion of PCM transformed into the liquid with respect to time in all configurations at 50°C and 60°C. The plot shows a similar melting pattern for both circular and elliptical tube geometries of PCMHE in all

three cases i.e. without a fin, with two fins, and with four fins as well as for both applied temperatures. Plots also show that the melting rate is very high in the initial phase which is 5% liquid fraction in a configuration having no fin, 10% in a configuration having two fins and 15% in a configuration having four fins at both applied temperatures. After that, the slope of the curve changes slightly and becomes almost a straight line up to 80% liquid fraction in all configurations. After that the melting rate slows down as most of the PCM converted into liquid increases its temperature and hence the temperature difference between PCM and tube surface decreases, taking half of the total melting time to convert the remaining liquification. In all three cases, the minimum time has been taken by incorporating circular tubes in the heat exchanger for both applied temperatures.

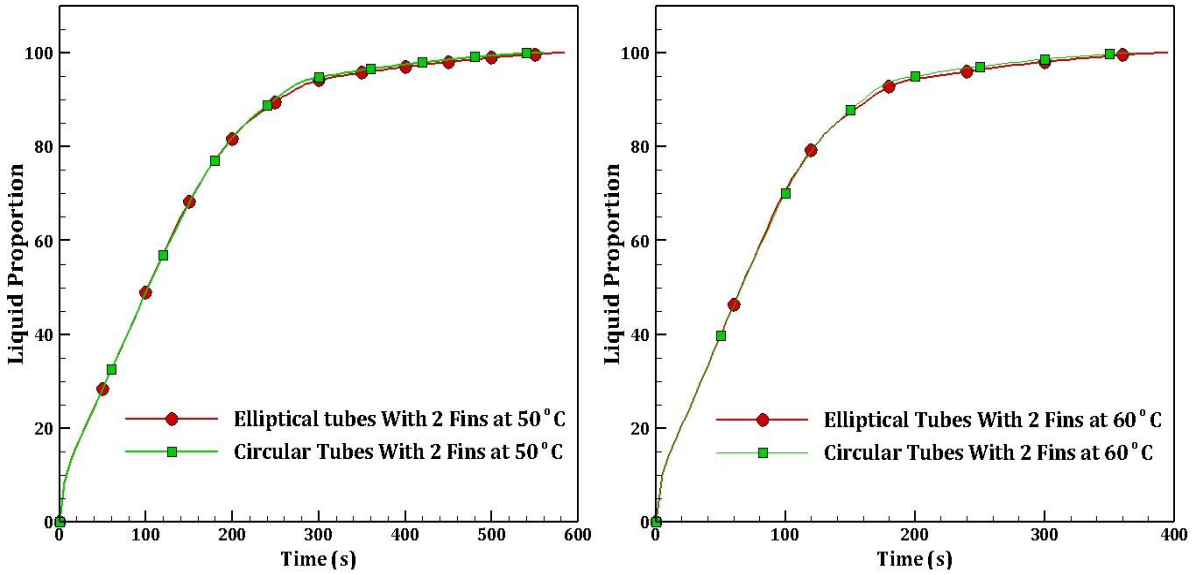

Fig 5.34 Evolution of liquid proportion of the geometries having circular and elliptical tubes with 2 fins at 50^{o}C & 60^{o}C

The proportion of PCM converted into a liquid for the geometries of PCMHE having elliptical and circular tubes without fin at both applied temperatures of 50^{o}C and 60^{o}C on the outer surface of the tubes is illustrated in Figure 5.33.

The proportion of PCM converted into a liquid for the geometries of PCMHE having elliptical and circular tubes with two fins at both applied temperatures of 50^{o}C and 60^{o}C is shown in Figure 5.34.

The proportion of PCM converted into a liquid for the geometries of PCMHE having elliptical and circular tubes with four fins at both applied temperatures of 50^{o}C and 60^{o}C is illustrated in Figure 5.35.

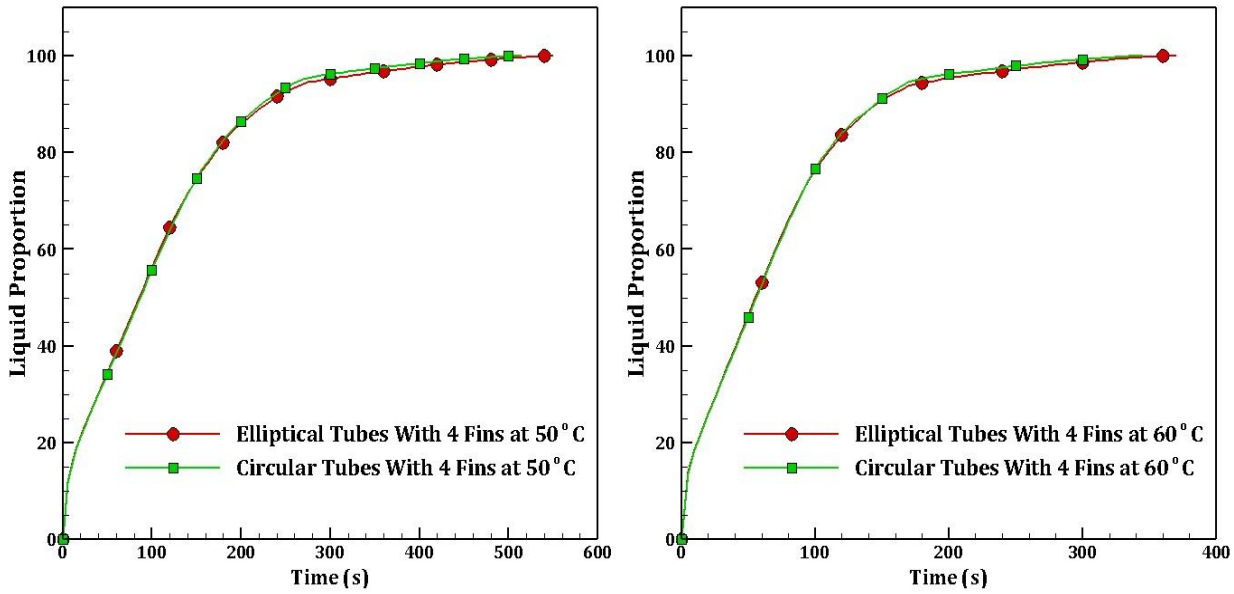

Fig 5.35 Evolution of liquid proportion of the geometries having circular and elliptical tubes with 4 fins at 50^{o}C & 60^{o}C

Figure 5.36, Figure 5.37, and Figure 5.38 represent the temperature evolution of the PCM inside the PCMHE at 50°C and at 60°C. At the start of the melting of PCM, the temperature difference between PCM and tube surface is high hence more heat transfer takes place leading to a higher temperature rise. As the temperature of PCM rises, the heat transfer rate decreases & the increase in temperature becomes very slow. PCM takes half of the time to reach a maximum temperature from 47^{o}C at an applied temperature of 50^{o}C. The plots show that the PCM takes the least amount of time to attain the applied temperature with the geometry of circular tubes having no

fins, having two fins, and having four fins compared to elliptical tubes having no fins, having two fins, and having four fins respectively.

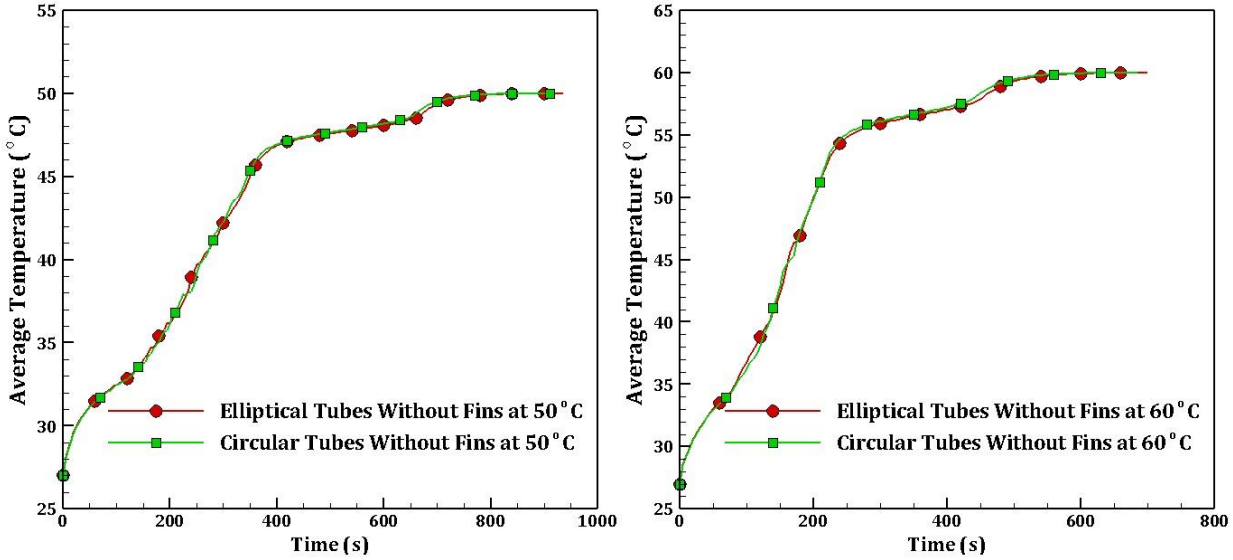

Fig 5.36 Evolution of mean temperature of PCM for geometries having circular & elliptical tubes without fin at 50°C & 60°C

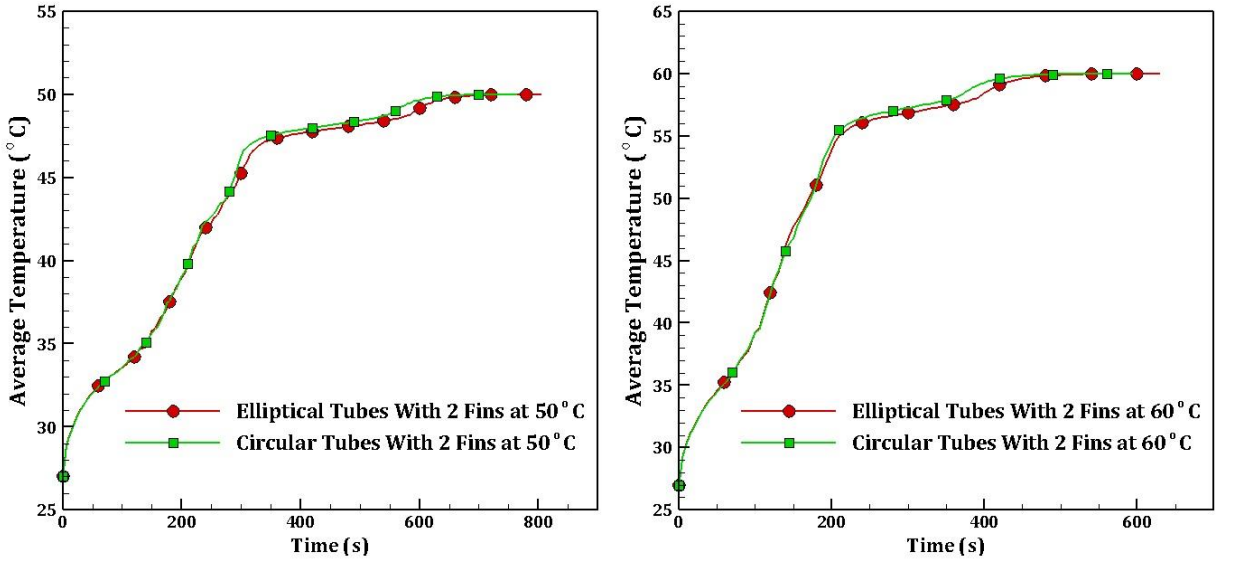

Fig 5.37 Evolution of mean temperature of PCM for geometries having circular & elliptical tubes with 2 fins at 50°C & 60°C

The average temperature of PCM for the geometries of PCMHE having elliptical and circular tubes without fin at both applied temperatures of 50°C and 60°C on the tubes is illustrated in Figure 5.36.

The average temperature of PCM for the geometries of PCMHE having elliptical and circular tubes with two fins at both applied temperatures of 50^{o}C and 60^{o}C on the tubes is illustrated in Figure 5.37.

The average temperature of PCM for the geometries of PCMHE having elliptical and circular tubes with four fins at both applied temperatures of 50^{o}C and 60^{o}C is illustrated in Figure 5.38.

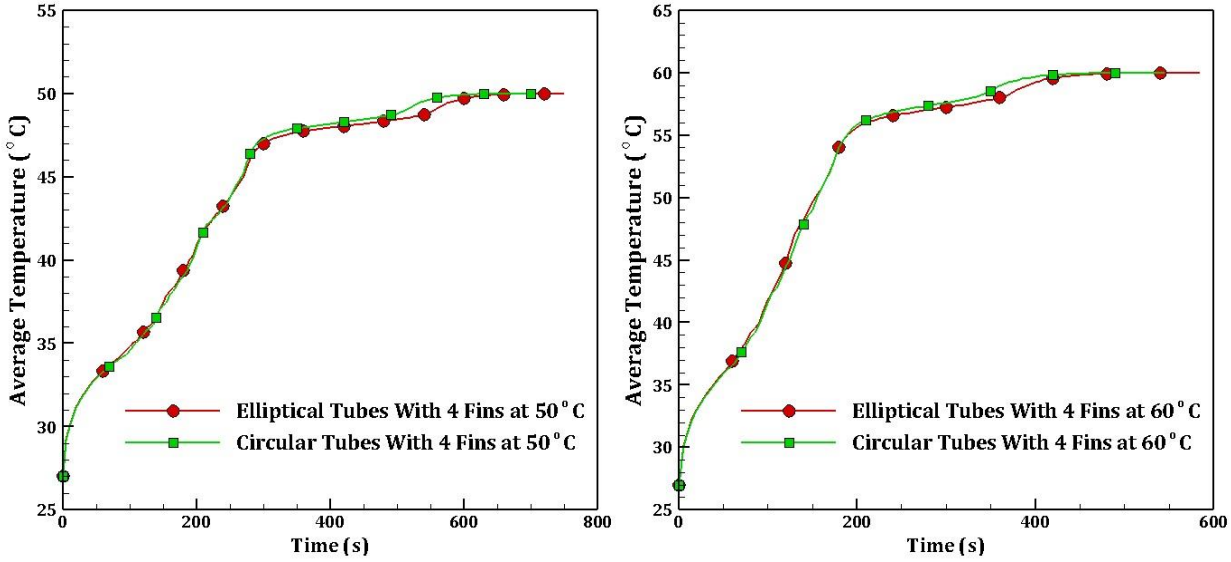

Fig 5.38 Evolution of mean temperature of PCM for geometries having circular & elliptical tubes with 4 fins at 50^{o}C & 60^{o}C

CHAPTER 6: CONCLUSIONS AND FUTURE SCOPE

6 Conclusions and Future Scope

6.1 Conclusions

This research work is conducted with the objective of enhancing the performance of a PCMHE by using such a configuration that gives a maximum heat transfer rate with the minimum melting time of PCM. To find such a type of best-suited configurations numerical investigations are carried out.

Different configurations of PCMHE have been modelled with two shapes of outer shell i.e. Square shell and circular shell in which a solid PCM is filled. Pure Gallium as PCM filled in the square and circular shell of PCMHE is used to analyze the phenomenon of melting. Two-dimensional CFD models of PCMHE of the square and circular shell having four tubes of different shapes (circular, square, and elliptical) with and without fins on the outer surface of the tubes have been generated. The effects of the shape of tubes, the introduction of fins on the outer surface of the tubes, and the number of fins on the heat transfer rate at different temperatures applied on the outer surface of the tubes have been analyzed and discussed in detail with the help of various contours available from simulations. The thermal performance data with different configurations of PCMHE is compared to choose a configuration that gives the best thermal performance having minimum melting time.

The significant findings of the numerical simulation studies are as follows:

1. At the beginning of the melting process, the melt regions are similar in shape around the tubes, when conduction accounts for the majority of heat exchange, because of the similarity of the geometry around the axis.

2. Until the four melting regions surrounding the circular tubes haven't merged and created a single melting region having a common solid-liquid interface, each melt zone around the four tubes is initially unaffected by the existence of other melt regions.
3. For all three types of inner tubes (circular, square, and elliptical) in square shell PCMHE geometries, the heat transfer rate is higher for the geometry of PCMHE having square tubes.
4. Enhancement in heat transfer is observed due to the introduction of a number of fins on the outer surface of the square tubes. An increment in heat transfer and a decrement in the melting time of PCM is observed with an increase in the number of fins.
5. A decrease in the time taken by PCM to attain the temperature applied on the outer surface of the square tubes has also been observed with the introduction of fins in square shell PCMHE geometry.
6. In circular shell geometries of PCMHE, it is observed that the heat transfer rate is higher in the configuration having circular tubes compared to the elliptical tubes configuration.
7. A decrement in melting time and time taken by PCM to attain the temperature applied on the outer surface of the tubes is observed due to the introduction of a number of fins on the outer surface of both circular and elliptical tubes.
8. The rate of increment of heat transfer increases with an increase in applied temperature on the outer surface of the tubes, and this increment is observed more in the case of geometries having a higher number of fins.
9. When circular tube geometries are compared, it is observed that the minimum melting time of PCM is obtained by using six fins configuration on each tube as compared to three fins or without fins configuration.

10. PCM melting time reduces by 1.5% by using circular tube geometry compared to elliptical tube geometry without a fin. Whereas the reduction in melting time of PCM is 4.3% comparing the geometries with two fins and 6.3% with four fins at 50^{o}C.
11. The reduction in melting time of PCM is 2.2% in circular tube geometry compared to elliptical tube geometries without a fin, 6.3% with two fins, and 6.8% with four fins at 60^{o}C.
12. Based on the results of the simulation studies, it is observed that the PCM melting time is the shortest possible by using circular tubes when compared to elliptical tube geometries without fin, with two fins, and four fins.
13. The reduction in time taken to reach the applied temperature is 1.6% in circular tube geometry compared to elliptical tubes configuration having no fin, 5% for configurations having two fins, and 6.6% for configurations having four fins.
14. It is observed from the simulation studies that the geometries having similar shapes of tubes and shells (square tubes with square shell or circular tubes with circular shell) provide maximum heat transmission from tubes to PCM and have minimum melting time.

Numerical simulation results reveal that applying fins on the outer surface of the tubes enhances the heat transmission rate from tubes to PCM, leading to maximum heat storage in domestic solar water heating systems. Since the availability of hot water at night using a solar water heating system is the main challenge, a high-efficiency TES system is desired for improving the overall performance of solar water heating systems. Among all types of configurations of PCMHE investigated in this study, a circular shell with circular tubes having six fins on the outer surface gives the highest thermal performance at a minimum melting time, requiring a small-size

solar water heating system. Hence, the solar water heating system with this configuration will be cost-effective and energy-efficient. The PCM and geometry of the PCMHE are the influential factors of the heat conversion efficiency of solar water heating systems. However, the configuration of PCMHE of the square shell with square tubes having fins on the outer surface also gives better thermal performance and can be used in solar water heating systems depending on the space available for installing solar water heating systems.

6.2 Future Scope of Present Work

Here in the present analysis, CFD modeling and simulation of PCMHE of shell & tube type filled with PCM having square, circular, and elliptical tubes with and without fins for Gallium as a PCM has been studied and the best suitable geometry of PCM heat exchanger has been selected for the thermal energy storage for domestic solar water heating system. The recommendations for future work are as follows.

- The study can be performed with the other shape of tubes and can be optimized for the best one.
- The analysis can be performed with the other shapes of fins on the tubes of PCMHE.
- The study can be utilized for other types of PCMs like organic, inorganic, and salt hydrates.
- The study can be used with the mixing of higher thermal conductivity materials with the PCM to increase the heat transfer rate.

References

[1] A.F. Regin, S.C. Solanki, J.S. Saini, Heat transfer characteristics of thermal energy storage system using PCM capsules: A review, Renew. Sustain. Energy Rev. 12 (2008) 2438–2458. https://doi.org/10.1016/J.RSER.2007.06.009.

[2] I. Purohit, P. Purohit, Performance assessment of grid-interactive solar photovoltaic projects under India's national solar mission, Appl. Energy. 222 (2018) 25–41. https://doi.org/10.1016/j.apenergy.2018.03.135.

[3] A. Sharma, V. V. Tyagi, C.R. Chen, D. Buddhi, Review on thermal energy storage with phase change materials and applications, Renew. Sustain. Energy Rev. 13 (2009) 318–345. https://doi.org/10.1016/J.RSER.2007.10.005.

[4] L.F. Cabeza, Thermal energy storage, Elsevier Ltd., 2012. https://doi.org/10.1016/B978-0-08-087872-0.00307-3.

[5] H. Mehling, L.F. Cabeza, Heat and Cold Storage with PCM: An Up to Date Introduction Into Basics and Applications, 2008. https://doi.org/10.1007/978-3-540-68557-9.

[6] F.P. Incropera, D.P. DeWitt, Fundamentals of Heat and Mass Transfer, 1996. https://doi.org/10.1016/j.applthermaleng.2011.03.022.

[7] S.M. Hasnain, Review on sustainable thermal energy storage technologies, Part I: heat storage materials and techniques, Energy Convers. Manag. 39 (1998) 1127–1138. https://doi.org/10.1016/S0196-8904(98)00025-9.

[8] A.I. Fernandez, M. Martnez, M. Segarra, I. Martorell, L.F. Cabeza, Selection of materials with potential in sensible thermal energy storage, Sol. Energy Mater. Sol. Cells. 94 (2010) 1723–1729. https://doi.org/10.1016/J.SOLMAT.2010.05.035.

[9] A.M. Khudhair, M.M. Farid, A review on energy conservation in building applications with thermal storage by latent heat using phase change materials, Energy Convers. Manag. 45 (2004) 263–275. https://doi.org/10.1016/S0196-8904(03)00131-6.

[10] M.F. Demirbas, Thermal Energy Storage and Phase Change Materials: An Overview, Energy Sources, Part B Econ. Planning, Policy. 1 (2006) 85–95. https://doi.org/10.1080/009083190881481.

[11] L.F. Cabeza, I. Martorell, L. Miró, A.I. Fernández, C. Barreneche, Introduction to thermal energy storage (TES) systems, Woodhead Publishing Limited, 2015. https://doi.org/10.1533/9781782420965.1.

[12] B. Michel, N. Mazet, S. Mauran, D. Stitou, J. Xu, Thermochemical process for seasonal storage of solar energy: Characterization and modeling of a high density reactive bed, Energy. 47 (2012) 553–563. https://doi.org/10.1016/J.ENERGY.2012.09.029.

[13] J. Cot-Gores, A. Castell, L.F. Cabeza, Thermochemical energy storage and conversion: A-state-of-the-art review of the experimental research under practical conditions, Renew. Sustain. Energy Rev. 16 (2012) 5207–5224. https://doi.org/10.1016/J.RSER.2012.04.007.

[14] A. Haselbacher, An Overview of Thermal Energy Storage, (2015).

[15] M.M. Farid, A.M. Khudhair, S.A.K. Razack, S. Al-Hallaj, A review on phase change energy storage: materials and applications, Energy Convers. Manag. 45 (2004) 1597–1615. https://doi.org/10.1016/J.ENCONMAN.2003.09.015.

[16] E. Assis, L. Katsman, G. Ziskind, R. Letan, Numerical and experimental study of melting in a spherical shell, Int. J. Heat Mass Transf. 50 (2007) 1790–1804. https://doi.org/10.1016/J.IJHEATMASSTRANSFER.2006.10.007.

[17] A. Fallahi, G. Guldentops, M. Tao, S. Granados-Focil, S. Van Dessel, Review on solid-solid phase change materials for thermal energy storage: Molecular structure and thermal properties, Appl. Therm. Eng. 127 (2017) 1427–1441. https://doi.org/10.1016/j.applthermaleng.2017.08.161.

[18] M. Mhadhbi, Introductory Chapter: Phase Change Material, Phase Chang. Mater. Their Appl. (2018) 3–6. https://doi.org/10.5772/intechopen.79432.

[19] W.D. Li, E.Y. Ding, Preparation and characterization of cross-linking PEG/MDI/PE copolymer as solid–solid phase change heat storage material, Sol. Energy Mater. Sol. Cells. 91 (2007) 764–768. https://doi.org/10.1016/J.SOLMAT.2007.01.011.

[20] H. Nazir, M. Batool, F.J. Bolivar Osorio, M. Isaza-Ruiz, X. Xu, K. Vignarooban, P. Phelan, Inamuddin, A.M. Kannan, Recent developments in phase change materials for energy storage applications: A review, Int. J. Heat Mass Transf. 129 (2019) 491–523. https://doi.org/10.1016/j.ijheatmasstransfer.2018.09.126.

[21] A.A. Aydn, H. Okutan, High-chain fatty acid esters of myristyl alcohol with odd carbon number: Novel organic phase change materials for thermal energy storage—2, Sol. Energy Mater. Sol. Cells. 95 (2011) 2417–2423. https://doi.org/10.1016/J.SOLMAT.2011.04.018.

[22] V. V. Tyagi, S.C. Kaushik, S.K. Tyagi, T. Akiyama, Development of phase change materials based microencapsulated technology for buildings: A review, Renew. Sustain. Energy Rev. 15 (2011) 1373–1391. https://doi.org/10.1016/J.RSER.2010.10.006.

[23] N. Xie, Z. Huang, Z. Luo, X. Gao, Y. Fang, Z. Zhang, Inorganic salt hydrate for thermal energy storage, Appl. Sci. 7 (2017). https://doi.org/10.3390/app7121317.

[24] S.D. Sharma, K. Sagara, Latent Heat Storage Materials and Systems: A Review, Int. J. Green Energy. 2 (2005) 1–56. https://doi.org/10.1081/GE-200051299.

[25] S. Khare, M. Dell'Amico, C. Knight, S. McGarry, Selection of materials for high temperature latent heat energy storage, Sol. Energy Mater. Sol. Cells. 107 (2012) 20–27. https://doi.org/10.1016/J.SOLMAT.2012.07.020.

[26] M.K.R.E.-M. Mhadhbi, Thermal Stability of Phase Change Material, (2018) Ch. 3. https://doi.org/10.5772/intechopen.75923.

[27] A.A. El-Sebaii, S. Al-Heniti, F. Al-Agel, A.A. Al-Ghamdi, F. Al-Marzouki, One thousand thermal cycles of magnesium chloride hexahydrate as a promising PCM for indoor solar cooking, Energy Convers. Manag. 52 (2011) 1771–1777. https://doi.org/10.1016/J.ENCONMAN.2010.10.043.

[28] R. Al-Shannaq, J. Kurdi, S. Al-Muhtaseb, M. Dickinson, M. Farid, Supercooling elimination of phase change materials (PCMs) microcapsules, Energy. 87 (2015) 654–662. https://doi.org/10.1016/J.ENERGY.2015.05.033.

[29] G. Wei, G. Wang, C. Xu, X. Ju, L. Xing, X. Du, Y. Yang, Selection principles and thermophysical properties of high temperature phase change materials for thermal energy storage: A review, Renew. Sustain. Energy Rev. 81 (2018) 1771–1786. https://doi.org/10.1016/J.RSER.2017.05.271.

[30] T. Yan, J. Gao, X. Xu, T. Xu, Z. Ling, J. Yu, Dynamic simplified PCM models for the pipe-encapsulated PCM wall system for self-activated heat removal, Int. J. Therm. Sci. 144 (2019) 27–41. https://doi.org/10.1016/j.ijthermalsci.2019.05.015.

[31] M. Ahmed, O. Meade, M.A. Medina, Reducing heat transfer across the insulated walls of

refrigerated truck trailers by the application of phase change materials, Energy Convers. Manag. 51 (2010) 383–392. https://doi.org/10.1016/j.enconman.2009.09.003.

[32] P. Ping, R. Peng, D. Kong, G. Chen, J. Wen, Investigation on thermal management performance of PCM-fin structure for Li-ion battery module in high-temperature environment, Energy Convers. Manag. 176 (2018) 131–146. https://doi.org/10.1016/j.enconman.2018.09.025.

[33] S. Ahmadi Atouei, A.A. Ranjbar, A. Rezania, Experimental investigation of two-stage thermoelectric generator system integrated with phase change materials, Appl. Energy. 208 (2017) 332–343. https://doi.org/10.1016/j.apenergy.2017.10.032.

[34] S. Khot, Comparative Performance of Phase Change Materials for Solar Thermal Storage System, J. Altern. Energy Sources Technol. 2011. 2 (2011).

[35] V.D. Bhatt, K. Gohi, A. Mishra, Thermal energy storage capacity of some phase changing materials and ionic liquids, Int. J. ChemTech Res. 2 (2010) 1771–1779.

[36] N. Ukrainczyk, S. Kurajica, J. Šipušić, Thermophysical comparison of five commercial paraffin waxes as latent heat storage materials, Chem. Biochem. Eng. Q. 24 (2010) 129–137.

[37] R. Velraj, R. V. Seeniraj, B. Hafner, C. Faber, K. Schwarzer, Heat transfer enhancement in a latent heat storage system, Sol. Energy. 65 (1999) 171–180. https://doi.org/10.1016/S0038-092X(98)00128-5.

[38] B. Zalba, J.M. Marín, L.F. Cabeza, H. Mehling, Review on thermal energy storage with phase change: materials, heat transfer analysis and applications, Appl. Therm. Eng. 23 (2003) 251–283. https://doi.org/10.1016/S1359-4311(02)00192-8.

[39] D. Zhou, C.Y. Zhao, Y. Tian, Review on thermal energy storage with phase change materials (PCMs) in building applications, Appl. Energy. 92 (2012) 593–605. https://doi.org/10.1016/j.apenergy.2011.08.025.

[40] A. Kürklü, Energy storage applications in greenhouses by means of phase change materials (PCMs): A review, Renew. Energy. 13 (1998) 89–103. https://doi.org/10.1016/S0960-1481(97)83337-X.

[41] A.F. Regin, S.C. Solanki, J.S. Saini, Latent heat thermal energy storage using cylindrical capsule: Numerical and experimental investigations, Renew. Energy. 31 (2006) 2025–2041. https://doi.org/10.1016/j.renene.2005.10.011.

[42] J.P. Bédécarrats, J. Castaing-Lasvignottes, F. Strub, J.P. Dumas, Study of a phase change energy storage using spherical capsules. Part II: Numerical modelling, Energy Convers. Manag. 50 (2009) 2537–2546. https://doi.org/10.1016/j.enconman.2009.06.003.

[43] M. Veerappan, S. Kalaiselvam, S. Iniyan, R. Goic, Phase change characteristic study of spherical PCMs in solar energy storage, Sol. Energy. 83 (2009) 1245–1252. https://doi.org/10.1016/j.solener.2009.02.006.

[44] F.L. Tan, S.F. Hosseinizadeh, J.M. Khodadadi, L. Fan, International Journal of Heat and Mass Transfer Experimental and computational study of constrained melting of phase change materials (PCM) inside a spherical capsule, Int. J. Heat Mass Transf. 52 (2009) 3464–3472. https://doi.org/10.1016/j.ijheatmasstransfer.2009.02.043.

[45] J.M. Khodadadi, Y. Zhang, E € ects of buoyancy-driven convection on melting within spherical containers, 44 (2001) 1605–1618.

[46] L. Bilir, Z. Ilken, Total solidification time of a liquid phase change material enclosed in

cylindrical/spherical containers, Appl. Therm. Eng. 25 (2005) 1488–1502. https://doi.org/10.1016/j.applthermaleng.2004.10.005.

[47] D. Vikram, S. Kaushik, V. Prashanth, N. Nallusamy, An Improvement in the Solar Water Heating Systems by Thermal Storage Using Phase Change Materials, 2006. https://doi.org/10.1115/ISEC2006-99090.

[48] G. Murali, K. Mayilsamy, T. V Arjunan, An Experimental Study of PCM-Incorporated Thermosyphon Solar Water Heating System, Int. J. Green Energy. 12 (2015) 978–986. https://doi.org/10.1080/15435075.2014.888663.

[49] H.M. Teamah, M.F. Lightstone, J.S. Cotton, Potential of cascaded phase change materials in enhancing the performance of solar domestic hot water systems, Sol. Energy. 159 (2018) 519–530. https://doi.org/10.1016/j.solener.2017.11.034.

[50] Y. Lin, Y. Jia, G. Alva, G. Fang, Review on thermal conductivity enhancement, thermal properties and applications of phase change materials in thermal energy storage, Renew. Sustain. Energy Rev. 82 (2018) 2730–2742. https://doi.org/10.1016/J.RSER.2017.10.002.

[51] K. Hariharan, G.S.S. Kumar, G. Kumaresan, R. Velraj, Investigation on Phase Change Behavior of Paraffin Phase Change Material in a Spherical Capsule for Solar Thermal Storage Units, Heat Transf. Eng. 39 (2018) 775–783. https://doi.org/10.1080/01457632.2017.1341227.

[52] Y.M. Liu, K.M. Chung, K.C. Chang, T.S. Lee, Performance of thermosyphon solar water heaters in series, Energies. 5 (2012) 3266–3278. https://doi.org/10.3390/en5093266.

[53] A. De Gracia, E. Oró, M.M. Farid, L.F. Cabeza, Thermal analysis of including phase change material in a domestic hot water cylinder, Appl. Therm. Eng. 31 (2011) 3938–

3945. https://doi.org/10.1016/j.applthermaleng.2011.07.043.

[54] M. Mazman, L.F. Cabeza, H. Mehling, M. Nogues, H. Evliya, H.Ö. Paksoy, Utilization of phase change materials in solar domestic hot water systems, Renew. Energy. 34 (2009) 1639–1643. https://doi.org/10.1016/j.renene.2008.10.016.

[55] A.J.N. Khalifa, K.H. Suffer, M.S. Mahmoud, A storage domestic solar hot water system with a back layer of phase change material, Exp. Therm. Fluid Sci. 44 (2013) 174–181. https://doi.org/10.1016/j.expthermflusci.2012.05.017.

[56] P. Bhagyalakshmi, K. Rajan, K. Senthil Kumar, Preperation and Characterization Study of Phase Change Materials for Thermal Energy Storage Applications, Appl. Mech. Mater. 787 (2015) 77–81. https://doi.org/10.4028/www.scientific.net/amm.787.77.

[57] G. Murali, K. Mayilsamy, Effect of Latent Thermal Energy storage and inlet locations on enhancement of stratification in a solar water heater under discharging mode, Appl. Therm. Eng. 106 (2016) 354–360. https://doi.org/10.1016/j.applthermaleng.2016.06.030.

[58] I. Al-Hinti, A. Al-Ghandoor, A. Maaly, I. Abu Naqeera, Z. Al-Khateeb, O. Al-Sheikh, Experimental investigation on the use of water-phase change material storage in conventional solar water heating systems, Energy Convers. Manag. 51 (2010) 1735–1740. https://doi.org/10.1016/j.enconman.2009.08.038.

[59] S. Jegadheeswaran, S.D. Pohekar, Performance enhancement in latent heat thermal storage system: A review, Renew. Sustain. Energy Rev. 13 (2009) 2225–2244. https://doi.org/10.1016/j.rser.2009.06.024.

[60] Y. Zhang, A. Faghri, Heat transfer enhancement in latent heat thermal energy storage system by using the internally finned tube, Int. J. Heat Mass Transf. 39 (1996) 3165–3173.

https://doi.org/10.1016/0017-9310(95)00402-5.

[61] J.C. Kurnia, A.P. Sasmito, S. V. Jangam, A.S. Mujumdar, Improved design for heat transfer performance of a novel phase change material (PCM) thermal energy storage (TES), Appl. Therm. Eng. 50 (2013) 896–907. https://doi.org/10.1016/j.applthermaleng.2012.08.015.

[62] T. Bouhal, S. ed-Dîn Fertahi, T. Kousksou, A. Jamil, CFD thermal energy storage enhancement of PCM filling a cylindrical cavity equipped with submerged heating sources, J. Energy Storage. 18 (2018) 360–370. https://doi.org/10.1016/j.est.2018.05.015.

[63] F. Agyenim, P. Eames, M. Smyth, A comparison of heat transfer enhancement in a medium temperature thermal energy storage heat exchanger using fins, Sol. Energy. 83 (2009) 1509–1520. https://doi.org/10.1016/J.SOLENER.2009.04.007.

[64] A.A. Al-Abidi, S. Mat, K. Sopian, M.Y. Sulaiman, A.T. Mohammad, Internal and external fin heat transfer enhancement technique for latent heat thermal energy storage in triplex tube heat exchangers, Appl. Therm. Eng. 53 (2013) 147–156. https://doi.org/10.1016/J.APPLTHERMALENG.2013.01.011.

[65] K. Chen, H.I. Mohammed, J.M. Mahdi, A. Rahbari, A. Cairns, P. Talebizadehsardari, Effects of non-uniform fin arrangement and size on the thermal response of a vertical latent heat triple-tube heat exchanger, J. Energy Storage. 45 (2022) 103723. https://doi.org/10.1016/j.est.2021.103723.

[66] Y. Cao, H. Ayed, H. Togun, H. Alias, S.M. Bouzgarrou, M. Wae-hayee, R. Marzouki, Observation the melting process of the phase change material inside a half-cylindrical with thermal non-equilibrium porous media: CFD simulation, Case Stud. Therm. Eng. 28

(2021) 101496. https://doi.org/10.1016/j.csite.2021.101496.

[67] J.M. Mahdi, F.T. Najim, I.M.A. Aljubury, H.I. Mohammed, N. Ben Khedher, N.K. Alshammari, A. Cairns, P. Talebizadehsardari, Intensifying the thermal response of PCM via fin-assisted foam strips in the shell-and-tube heat storage system, J. Energy Storage. 45 (2022) 103733. https://doi.org/10.1016/j.est.2021.103733.

[68] M. Iten, S. Liu, A. Shukla, Experimental validation of an air-PCM storage unit comparing the effective heat capacity and enthalpy methods through CFD simulations, Energy. 155 (2018) 495–503. https://doi.org/10.1016/J.ENERGY.2018.04.128.

[69] H.M. Teamah, M.F. Lightstone, J.S. Cotton, An alternative approach for assessing the benefit of phase change materials in solar domestic hot water systems, Sol. Energy. 158 (2017) 875–888. https://doi.org/10.1016/j.solener.2017.10.033.

[70] M. Esen, Thermal performance of a solar-aided latent heat store used for space heating by heat pump, Sol. Energy. 69 (2000) 15–25. https://doi.org/10.1016/S0038-092X(00)00015-3.

[71] M.E. Zayed, J. Zhao, A.H. Elsheikh, F.A. Hammad, L. Ma, Y. Du, A.E. Kabeel, S.M. Shalaby, Applications of cascaded phase change materials in solar water collector storage tanks: A review, Sol. Energy Mater. Sol. Cells. 199 (2019) 24–49. https://doi.org/10.1016/j.solmat.2019.04.018.

[72] Fluent INC 2016; Fluent User Guide 17.0., 2009.

[73] T. Zhou, X. Liu, Y. Li, Z. Sun, J. Zhou, Dynamic measurement of the thermal conductivity of phase change materials in the liquid phase near the melting point, Int. J. Heat Mass Transf. 111 (2017) 631–641.

https://doi.org/10.1016/j.ijheatmasstransfer.2017.04.020.

[74] W. Youssef, Y.T. Ge, S.A. Tassou, Effects of latent heat storage and controls on stability and performance of a solar assisted heat pump system for domestic hot water production, Sol. Energy. 150 (2017) 394–407. https://doi.org/10.1016/j.solener.2017.04.065.

[75] N.I. Ibrahim, F.A. Al-Sulaiman, S. Rahman, B.S. Yilbas, A.Z. Sahin, Heat transfer enhancement of phase change materials for thermal energy storage applications: A critical review, Renew. Sustain. Energy Rev. 74 (2017) 26–50. https://doi.org/10.1016/j.rser.2017.01.169.

[76] S.S. Yogesh, A.S. Selvaraj, D.K. Ravi, T.K.R. Rajagopal, Heat transfer and pressure drop characteristics of inclined elliptical fin tube heat exchanger of varying ellipticity ratio using CFD code, Int. J. Heat Mass Transf. 119 (2018) 26–39. https://doi.org/10.1016/j.ijheatmasstransfer.2017.11.094.

[77] Z.A. Qureshi, H.M. Ali, S. Khushnood, Recent advances on thermal conductivity enhancement of phase change materials for energy storage system: A review, Int. J. Heat Mass Transf. 127 (2018) 838–856. https://doi.org/10.1016/j.ijheatmasstransfer.2018.08.049.

[78] J.M. Mahdi, E.C. Nsofor, Multiple-segment metal foam application in the shell-and-tube PCM thermal energy storage system, J. Energy Storage. 20 (2018) 529–541. https://doi.org/10.1016/j.est.2018.09.021.

[79] W. Youssef, Y.T. Ge, S.A. Tassou, CFD modelling development and experimental validation of a phase change material (PCM) heat exchanger with spiral-wired tubes, Energy Convers. Manag. 157 (2018) 498–510.

https://doi.org/10.1016/j.enconman.2017.12.036.

[80] F. Ahmad, S. Hussain, I. Ahmad, T.S. Hassan, A.O. Almatroud, W. Ali, I.E. Farooq, Successive melting of a phase change material bounded in a finned trapezoidal domain, Case Stud. Therm. Eng. 28 (2021) 101419. https://doi.org/10.1016/j.csite.2021.101419.

[81] X.H. Yang, J. Liu, A novel method for determining the melting point, fusion latent heat, specific heat capacity and thermal conductivity of phase change materials, Int. J. Heat Mass Transf. 127 (2018) 457–468. https://doi.org/10.1016/j.ijheatmasstransfer.2018.07.117.

[82] E. Meng, J. Wang, H. Yu, R. Cai, Y. Chen, B. Zhou, Experimental study of the thermal protection performance of the high reflectivity-phase change material (PCM) roof in summer, Build. Environ. 164 (2019) 106381. https://doi.org/10.1016/j.buildenv.2019.106381.

[83] G. Diarce, Á. Campos-Celador, K. Martin, A. Urresti, A. García-Romero, J.M. Sala, A comparative study of the CFD modeling of a ventilated active façade including phase change materials, Appl. Energy. 126 (2014) 307–317. https://doi.org/10.1016/j.apenergy.2014.03.080.

[84] K. Kumarasamy, J. An, J. Yang, E.H. Yang, Novel CFD-based numerical schemes for conduction dominant encapsulated phase change materials (EPCM) with temperature hysteresis for thermal energy storage applications, Energy. 132 (2017) 31–40. https://doi.org/10.1016/j.energy.2017.05.054.

[85] N.S. Bondareva, M.A. Sheremet, Flow and heat transfer evolution of PCM due to natural convection melting in a square cavity with a local heater, Int. J. Mech. Sci. 134 (2017)

610–619. https://doi.org/10.1016/j.ijmecsci.2017.10.031.

[86] F. Mohammadnejad, S. Hossainpour, A CFD modeling and investigation of a packed bed of high temperature phase change materials (PCMs) with different layer configurations, J. Energy Storage. 28 (2020) 101209. https://doi.org/10.1016/j.est.2020.101209.

[87] S. Almsater, A. Alemu, W. Saman, F. Bruno, Development and experimental validation of a CFD model for PCM in a vertical triplex tube heat exchanger, Appl. Therm. Eng. 116 (2017) 344–354. https://doi.org/10.1016/j.applthermaleng.2017.01.104.

[88] A. Chaube, P.K. Sahoo, S.C. Solanki, Analysis of heat transfer augmentation and flow characteristics due to rib roughness over absorber plate of a solar air heater, Renew. Energy. 31 (2006) 317–331. https://doi.org/10.1016/j.renene.2005.01.012.

[89] H. Hu, S.A. Argyropoulos, Mathematical modelling of solidification and melting: A review, Model. Simul. Mater. Sci. Eng. 4 (1996) 371–396. https://doi.org/10.1088/0965-0393/4/4/004.

[90] V.R. Voller, A.D. Brent, C. Prakash, The modelling of heat, mass and solute transport in solidification systems, Int. J. Heat Mass Transf. 32 (1989) 1719–1731. https://doi.org/10.1016/0017-9310(89)90054-9.

[91] K.A.R. Ismail, J.R. Henríquez, Solidification of pcm inside a spherical capsule, Energy Convers. Manag. 41 (2000) 173–187. https://doi.org/10.1016/S0196-8904(99)00101-6.

[92] R.S. Gupta, D. Kumar, Variable time step methods for one-dimensional stefan problem with mixed boundary condition, Int. J. Heat Mass Transf. 24 (1981) 251–259. https://doi.org/10.1016/0017-9310(81)90033-8.

[93] Z. Ma, Y. Zhang, Solid velocity correction schemes for a temperature transforming model

for convection phase change, Int. J. Numer. Methods Heat Fluid Flow. 16 (2006) 204–225. https://doi.org/10.1108/09615530610644271.

[94] Y. Cao, A. Faghri, A Numerical Analysis of Phase-Change Problems Including Natural Convection, J. Heat Transfer. 112 (1990) 812–816. https://doi.org/10.1115/1.2910466.

[95] V.R. Voller, C.R. Swaminathan, General source-based method for solidification phase change, Numer. Heat Transf. Part B Fundam. 19 (1991) 175–189. https://doi.org/10.1080/10407799108944962.

[96] K. Morgan, A numerical analysis of freezing and melting with convection, Comput. Methods Appl. Mech. Eng. 28 (1981) 275–284. https://doi.org/10.1016/0045-7825(81)90002-5.

[97] S. Liu, Y. Li, Y. Zhang, Mathematical solutions and numerical models employed for the investigations of PCMs′ phase transformations, Renew. Sustain. Energy Rev. 33 (2014) 659–674. https://doi.org/10.1016/J.RSER.2014.02.032.

[98] V.R. Voller, C. Prakash, A fixed grid numerical modelling methodology for convection-diffusion mushy region phase-change problems, Int. J. Heat Mass Transf. 30 (1987) 1709–1719. https://doi.org/10.1016/0017-9310(87)90317-6.

[99] C.R. Swaminathan, V.R. Voller, A general enthalpy method for modeling solidification processes, Metall. Trans. B. 23 (1992) 651–664. https://doi.org/10.1007/BF02649725.

[100] V.R. Voller, M. Cross, N.C. Markatos, An enthalpy method for convection/diffusion phase change, Int. J. Numer. Methods Eng. 24 (1987) 271–284. https://doi.org/https://doi.org/10.1002/nme.1620240119.

[101] Y. Dutil, D.R. Rousse, N. Ben Salah, S. Lassue, L. Zalewski, A review on phase-change

materials: Mathematical modeling and simulations, Renew. Sustain. Energy Rev. 15 (2011) 112–130. https://doi.org/10.1016/J.RSER.2010.06.011.

[102] D.K. Gartling, Finite element analysis of convective heat transfer problems with change of phase, United States, 1978. http://inis.iaea.org/search/search.aspx?orig_q=RN:09418245.

[103] B. Ghasemi, M. Molki, Melting of unfixed solids in square cavities, Int. J. Heat Fluid Flow. 20 (1999) 446–452. https://doi.org/10.1016/S0142-727X(99)00025-9.

[104] R.R. Kasibhatla, A. König-Haagen, F. Rösler, D. Brüggemann, Numerical modelling of melting and settling of an encapsulated PCM using variable viscosity, Heat Mass Transf. Und Stoffuebertragung. 53 (2017) 1735–1744. https://doi.org/10.1007/s00231-016-1932-0.

[105] J.H.N. Ehms, R. De Césaro Oliveski, L.A.O. Rocha, C. Biserni, M. Garai, Fixed grid numerical models for solidification and melting of phase change materials (PCMs), Appl. Sci. 9 (2019). https://doi.org/10.3390/app9204334.

[106] N. Sharifi, A. Faghri, T.L. Bergman, C.E. Andraka, Simulation of heat pipe-assisted latent heat thermal energy storage with simultaneous charging and discharging, Int. J. Heat Mass Transf. 80 (2015) 170–179. https://doi.org/10.1016/J.IJHEATMASSTRANSFER.2014.09.013.

[107] N.H.S. Tay, F. Bruno, M. Belusko, Experimental validation of a CFD model for tubes in a phase change thermal energy storage system, Int. J. Heat Mass Transf. 55 (2012) 574–585. https://doi.org/10.1016/J.IJHEATMASSTRANSFER.2011.10.054.

[108] A.D. Brent, V.R. Voller, K.J. Reid, Enthalpy-porosity technique for modeling convection-di_usion phase change: Application to the melting of a pure metal, Numer. Heat Transf.

13 (1988) 297–318. https://doi.org/10.1080/10407788808913615.

[109] D. Pal, Y.K. Joshi, Melting in a side heated tall enclosure by a uniformly dissipating heat source, Int. J. Heat Mass Transf. 44 (2001) 375–387. https://doi.org/10.1016/S0017-9310(00)00116-2.

[110] M. Longeon, A. Soupart, J.F. Fourmigué, A. Bruch, P. Marty, Experimental and numerical study of annular PCM storage in the presence of natural convection, Appl. Energy. 112 (2013) 175–184. https://doi.org/10.1016/J.APENERGY.2013.06.007.

[111] O. Saro, A. De Angelis, S. D'Elia, G. Lorenzini, Utilization of phase change materials (PCM) for energy recovery in the steelmaking industry, J. Eng. Thermophys. 22 (2013) 93–110. https://doi.org/10.1134/S1810232813020021.

[112] J.H. Nazzi Ehms, R. De Césaro Oliveski, L.A. Oliveira Rocha, C. Biserni, Theoretical and numerical analysis on phase change materials (PCM): A case study of the solidification process of erythritol in spheres, Int. J. Heat Mass Transf. 119 (2018) 523–532. https://doi.org/10.1016/J.IJHEATMASSTRANSFER.2017.11.124.

[113] A.A. Al-Abidi, S. Mat, K. Sopian, M.Y. Sulaiman, A.T. Mohammad, Numerical study of PCM solidification in a triplex tube heat exchanger with internal and external fins, Int. J. Heat Mass Transf. 61 (2013) 684–695. https://doi.org/10.1016/J.IJHEATMASSTRANSFER.2013.02.030.

[114] E. Assis, G. Ziskind, R. Letan, Numerical and Experimental Study of Solidification in a Spherical Shell, J. Heat Transfer. 131 (2008). https://doi.org/10.1115/1.2993543.

[115] A.R. Archibold, M.M. Rahman, J.G. Aguilar, D.Y. Goswami, E.K. Stefanakos, M. Romero, Phase Change and Heat Transfer Numerical Analysis during Solidification on an

Encapsulated Phase Change Material, Energy Procedia. 57 (2014) 653–661. https://doi.org/10.1016/J.EGYPRO.2014.10.220.

[116] Y.T. Lee, S.W. Hong, J.D. Chung, Effects of capsule conduction and capsule outside convection on the thermal storage performance of encapsulated thermal storage tanks, Sol. Energy. 110 (2014) 56–63. https://doi.org/10.1016/J.SOLENER.2014.08.034.

[117] M.J. Hosseini, A.A. Ranjbar, K. Sedighi, M. Rahimi, A combined experimental and computational study on the melting behavior of a medium temperature phase change storage material inside shell and tube heat exchanger, Int. Commun. Heat Mass Transf. 39 (2012) 1416–1424. https://doi.org/10.1016/J.ICHEATMASSTRANSFER.2012.07.028.

[118] S.F. Hosseinizadeh, F.L. Tan, S.M. Moosania, Experimental and numerical studies on performance of PCM-based heat sink with different configurations of internal fins, Appl. Therm. Eng. 31 (2011) 3827–3838. https://doi.org/10.1016/J.APPLTHERMALENG.2011.07.031.

[119] S.F. Hosseinizadeh, A.A. Rabienataj Darzi, F.L. Tan, J.M. Khodadadi, Unconstrained melting inside a sphere, Int. J. Therm. Sci. 63 (2013) 55–64. https://doi.org/10.1016/J.IJTHERMALSCI.2012.07.012.

[120] J.M. Khodadadi, Y. Zhang, Effects of buoyancy-driven convection on melting within spherical containers, Int. J. Heat Mass Transf. 44 (2001) 1605–1618. https://doi.org/10.1016/S0017-9310(00)00192-7.

[121] F.L. Tan, S.F. Hosseinizadeh, J.M. Khodadadi, L. Fan, Experimental and computational study of constrained melting of phase change materials (PCM) inside a spherical capsule, Int. J. Heat Mass Transf. 52 (2009) 3464–3472.

https://doi.org/10.1016/J.IJHEATMASSTRANSFER.2009.02.043.

[122] A.R. Archibold, M.M. Rahman, D.Y. Goswami, E.K. Stefanakos, Analysis of heat transfer and fluid flow during melting inside a spherical container for thermal energy storage, Appl. Therm. Eng. 64 (2014) 396–407. https://doi.org/10.1016/J.APPLTHERMALENG.2013.12.016.

[123] A.R. Archibold, J. Gonzalez-Aguilar, M.M. Rahman, D. Yogi Goswami, M. Romero, E.K. Stefanakos, The melting process of storage materials with relatively high phase change temperatures in partially filled spherical shells, Appl. Energy. 116 (2014) 243–252. https://doi.org/10.1016/J.APENERGY.2013.11.048.

[124] S.F. Hosseinizadeh, A.A.R. Darzi, F.L. Tan, Numerical investigations of unconstrained melting of nano-enhanced phase change material (NEPCM) inside a spherical container, Int. J. Therm. Sci. 51 (2012) 77–83. https://doi.org/10.1016/J.IJTHERMALSCI.2011.08.006.

[125] H. Shmueli, G. Ziskind, R. Letan, Melting in a vertical cylindrical tube: Numerical investigation and comparison with experiments, Int. J. Heat Mass Transf. 53 (2010) 4082–4091. https://doi.org/10.1016/J.IJHEATMASSTRANSFER.2010.05.028.

[126] V. Shatikian, G. Ziskind, R. Letan, Numerical investigation of a PCM-based heat sink with internal fins, Int. J. Heat Mass Transf. 48 (2005) 3689–3706. https://doi.org/10.1016/J.IJHEATMASSTRANSFER.2004.10.042.

[127] W.B. Ye, D.S. Zhu, N. Wang, Fluid flow and heat transfer in a latent thermal energy unit with different phase change material (PCM) cavity volume fractions, Appl. Therm. Eng. 42 (2012) 49–57. https://doi.org/10.1016/J.APPLTHERMALENG.2012.03.002.

[128] L. Solomon, A.F. Elmozughi, A. Oztekin, S. Neti, Effect of internal void placement on the heat transfer performance – Encapsulated phase change material for energy storage, Renew. Energy. 78 (2015) 438–447. https://doi.org/10.1016/J.RENENE.2015.01.035.

[129] L.W. Fan, Z.Q. Zhu, S.L. Xiao, M.J. Liu, H. Lu, Y. Zeng, Z.T. Yu, K.F. Cen, An experimental and numerical investigation of constrained melting heat transfer of a phase change material in a circumferentially finned spherical capsule for thermal energy storage, Appl. Therm. Eng. 100 (2016) 1063–1075. https://doi.org/10.1016/J.APPLTHERMALENG.2016.02.125.

[130] H. Sattari, A. Mohebbi, M.M. Afsahi, A. Azimi Yancheshme, CFD simulation of melting process of phase change materials (PCMs) in a spherical capsule, Int. J. Refrig. 73 (2017) 209–218. https://doi.org/10.1016/J.IJREFRIG.2016.09.007.

[131] W. Li, S.G. Li, S. Guan, Y. Wang, X. Zhang, X. Liu, Numerical study on melt fraction during melting of phase change material inside a sphere, Int. J. Hydrogen Energy. 42 (2017) 18232–18239. https://doi.org/10.1016/J.IJHYDENE.2017.04.136.

[132] F. Faistauer, P. Rodrigues, R. de C. Oliveski, Numerical Study of Phase Change of PCM in Spherical Cavities, Defect Diffus. Forum. 372 (2017) 21–30. https://doi.org/10.4028/www.scientific.net/DDF.372.21.

[133] P. Blanco-Rodríguez, J. Rodríguez-Aseguinolaza, A. Gil, E. Risueño, B. D'Aguanno, I. Loroño, L. Martín, Experiments on a Lab Scale TES Unit using Eutectic Metal Alloy as PCM, Energy Procedia. 69 (2015) 769–778. https://doi.org/10.1016/J.EGYPRO.2015.03.087.

[134] A. Rabinataj Darzi, H. Hassanzadeh Afrouzi, M. Khaki, M. Abbasi, Unconstrained

melting and solidification inside rectangular enclosure, J. Fundam. Appl. Sci. 7 (2015) 436. https://doi.org/10.4314/jfas.v7i3.10.

[135] X. Gui, W. Qu, B. Lin, X. Yuan, Two-dimensional transient thermal analysis of a phase-change-material canister of a heat-pipe receiver under gravity, J. Therm. Sci. 19 (2010) 160–166. https://doi.org/10.1007/s11630-010-0160-z.

[136] I. Danaila, R. Moglan, F. Hecht, S. Le Masson, A Newton method with adaptive finite elements for solving phase-change problems with natural convection, J. Comput. Phys. 274 (2014) 826–840. https://doi.org/10.1016/J.JCP.2014.06.036.

[137] R.R. Kasibhatla, A. König-Haagen, D. Brüggemann, Numerical Modelling of Wetting Phenomena During Melting of PCM, Procedia Eng. 157 (2016) 139–147. https://doi.org/10.1016/J.PROENG.2016.08.349.

[138] S. Lorente, A. Bejan, J.L. Niu, Phase change heat storage in an enclosure with vertical pipe in the center, Int. J. Heat Mass Transf. 72 (2014) 329–335. https://doi.org/10.1016/J.IJHEATMASSTRANSFER.2014.01.021.

[139] S. Lorente, A. Bejan, J.L. Niu, Constructal design of latent thermal energy storage with vertical spiral heaters, Int. J. Heat Mass Transf. 81 (2015) 283–288. https://doi.org/10.1016/J.IJHEATMASSTRANSFER.2014.09.077.

[140] S. Ziaei, S. Lorente, A. Bejan, Constructal design for convection melting of a phase change body, Int. J. Heat Mass Transf. 99 (2016) 762–769. https://doi.org/10.1016/J.IJHEATMASSTRANSFER.2016.04.022.

[141] Y. Asako, E. Gonçalves, M. Faghri, M. Charmchi, Numerical solution of melting processes for fixed and unfixed phase change material in the presence of magnetic field—

Simulation of low-gravity environmenT, Numer. Heat Transf. Part A Appl. 42 (2002) 565–583. https://doi.org/10.1080/10407780290059701.

[142] Y. Asako, M. Faghri, M. Charmchi, P.A. Bahrami, Numerical solution for melting of unfixed rectangular phase-change under low-gravity environment, Numer. Heat Transf. Part A Appl. 25 (1994) 191–208. https://doi.org/10.1080/10407789408955944.

Research Publication

International Journal Publications

1. **Sachin Rana,** Mohammad Zunaid, Rajesh Kumar (2022)**. "**CFD approach for the enhancement of thermal energy storage in phase change material charged heat exchanger**" Case Studies in Thermal Engineering, Vol. 33, 101921.** https://doi.org/10.1016/j.csite.2022.101921. (SCIE, I.F. 6.268).

2. **Sachin Rana,** Mohammad Zunaid, Rajesh Kumar (2022)**. "**Enhancement of thermal energy storage in a phase change material heat exchanger having elliptical and circular tubes with & without fins**" Journal of Energy Storage, Vol. 56, 105856.** https://doi.org/10.1016/j.est.2022.105856 (SCIE, I.F. 8.907).

International Conference Publications

3. **Sachin Rana,** Mohammad Zunaid, Rajesh Kumar (2021)**. "**CFD simulation for heat transfer enhancement in phase change materials**" Materials Today Proceedings, Vol. 46, 10915-10921.** https://doi.org/10.1016/j.matpr.2021.02.006.

4. **Sachin Rana,** Mohammad Zunaid, Rajesh Kumar (2021)**. "**CFD analysis for heat transfer comparison in circular, rectangular and elliptical tube heat exchangers filled with

PCM" **Materials Today Proceedings, Vol. 56, 637-644.** https://doi.org/10.1016/j.matpr.2021.12.412.

Biography

Sachin Rana has received his B. Tech. in Mechanical Engineering from UP Technical University, Lucknow and M. Tech in Thermal Engineering from Indian Institute of Technology Roorkee. He is currently working as an Assistant Professor in ABES Institute of Technology, Ghaziabad. His research interest includes Computational Fluid Dynamics, Heat Transfer Enhancement, Phase Change Materials and Thermal Contact Conductance. He has more than 12 years of industrial, academic and research experience. He has published many high impact papers and book chapters in various international journals and international conferences of repute.